Stability of dynamical processes on complex networks

On the assessment of the structure of basins of attraction

D I S S E R T A T I O N

zur Erlangung des akademischen Grades

d o c t o r r e r u m n a t u r a l i u m
(Dr. rer. nat.)
im Fach Physik
Spezialisierung: Theoretische Physik

eingereicht an der
Mathematisch-Naturwissenschaftlichen Fakultät
der Humboldt-Universität zu Berlin

von
M.Sc.-Phys. Chiranjit Mitra

Präsidentin der Humboldt-Universität zu Berlin:
Prof. Dr.-Ing. Dr. Sabine Kunst

Dekan der Mathematisch-Naturwissenschaftlichen Fakultät:
Prof. Dr. Elmar Kulke

Gutachter:

1. Prof. Dr. Dr. h.c. mult. Jürgen Kurths
2. Prof. Dr. Ulrich Parlitz
3. Dr. Alexander Pisarchik

Tag der mündlichen Prüfung: 16. März 2018

To my family, friends and supervisors...

Abstract

Dynamical systems exhibiting *multistability*, characterized by the coexistence of several stable states, are abundant across natural sciences and engineering. Maintaining operation of such systems in a particular stable state in the face of random perturbations, is often critical to their functionality. There has been a persistent drive towards quantifying the *stability* of the multiple stable states of such systems. A major development in this direction was that of *basin stability* (BS), which relates the volume of the basin of attraction of any stable state to the probability of returning to the same in the event of random perturbations. Many complex systems exhibiting multistability involve *complex networks* of interacting oscillators, whereby their *synchronized* dynamics often concurs with the desired operational state of the network. The application of BS to assessing the stability of synchronization and its extension to *single-node basin stability* (SNBS) constitute notable developments. Despite such recent advancements in stability theory, a comprehensive framework for quantifying multistability is still lacking. This fuels the present endeavour, comprising the development of a framework for the assessment of the stability of (multistable) complex (networked) dynamical systems, particularly in the face of random perturbations.

As a first contribution, we propose the framework of *multiple-node basin stability* (MNBS) for gauging the stability of networked dynamical systems in response to non-infinitesimal perturbations simultaneously affecting multiple nodes of the system. We then turn to the theoretical framework of *resilience* in identifying the different aspects characterizing multistability. Inspired by the concept of *ecological resilience*, we assert that the stability of the different attractors of a multistable system is determined by the overall structure of their respective basins of attraction. In particular, we identify the local dynamics of the system in the state space and the relative position of the attractor within the basin, in addition to the volume of the basin of attraction as crucial aspects determining overall stability of an attractor. We combine the aforementioned aspects in proposing the measure of *integral stability* (IS) for holistically quantifying multistability. We also draw inspiration from the concept of *engineering resilience*, which relates to the speed of return of the system to its equilibrium, following a perturbation. In the specific context of networked dynamical systems, we propose the framework of *single-node recovery time* (SNRT) for obtaining an estimate of the relative time scales underlying the transient dynamics of the nodes of a network returning to its desired operational state, following a non-infinitesimal perturbation to any specific node. The conjugation of the concepts of MNBS, IS and SNRT with those of linear stability, BS and SNBS provides a comprehensive framework for quantifying multistability.

Finally, we delve into the explicit investigation of the stability of synchronization on complex dynamical networks exhibiting *small-world* properties and of those, simultaneously displaying *scale-free* behaviour and *hierarchical* organization. The results emanating from these investigations bear important implications in the design of topologies for better synchronizability and in ensuring persistent synchronized operation of dynamical units coupled

on them. The aforementioned results open up several new avenues of research directed towards probing the robustness of the synchronized state in complex dynamical networks.

Zusammenfassung

Multistabile dynamische Systeme, die durch die Koexistenz mehrerer stabiler Zustände gekennzeichnet sind, finden sich häufig in den Naturwissenschaften und in technischen Anwendungen. Den Betrieb solcher Systeme in einem bestimmten stabilen Zustand angesichts zufälliger Störungen aufrechtzuerhalten ist oft kritisch für deren Funktionalität. Es ist somit essenziell, die *Stabilität* verschiedener stabiler Zustände solcher Systeme quantifizieren und somit vergleichen zu können. Ein wesentlicher Fortschritt in diesem Punkt war die Entwicklung der *basin stability* (BS), welche das Volumen des Einzugsgebiet eines stabilen Zustandes als Maß für die Wahrscheinlichkeit nutzt, angesichts zufälliger Störungen zu diesem zurückzukehren. Viele multistabile komplexe Systeme bestehen aus *komplexen Netzwerken* von interagierenden Oszillatoren, deren *synchrone* Dynamik häufig mit dem gewünschten Betriebszustand des Netzwerks übereinstimmt. Die Anwendung von BS zur Beurteilung der Stabilität der Synchronisation, sowie ihre Ausdehnung auf die *single-node basin stability* (SNBS), sind in diesem zusammenhang besonders bemerkenswerte Entwicklungen. Trotz jüngster Fortschritte in der Stabilitätstheorie fehlt jedoch weiterhin ein ganzheitliches Konzept zur Quantifizierung der Stabilität von (multistabilen) komplexen (vernetzten) dynamischen Systemen. Die Entwicklung eines ebensolchen Rahmenwerks, unter Einbeziehung zufälliger Störungsverteilungen, ist daher die Hauptmotivation der vorliegenden Arbeit.

Als ersten Beitrag schlagen wir die Erweiterung der BS zur *multiple-node basin stability* (MNBS) vor, um die Stabilität vernetzter dynamischer Systeme als Reaktion auf nicht-infinitesimale Störungen zu messen, die gleichzeitig mehrere Knoten des Systems beeinflussen. Weiterhin beziehen wir uns auf das Konzept der *Resilienz* zur Charakterisierung von Multistabilität. Inspiriert vom Konzept der *ökologischen Resilienz* schlussfolgern wir, dass die Stabilität der verschiedenen Attraktoren eines multistabilen Systems von der Gesamtstruktur ihrer jeweiligen Einzugsgebiet bestimmt wird. Insbesondere identifizieren wir sowohl die lokale Dynamik des Systems im Zustandsraum als auch die relative Position des Attraktors im Einzugsgebiet zusätzlich zum dessen Volumen als entscheidende Aspekte, welche die Gesamtstabilität eines Attraktors charakterisieren. Die genannten Aspekte werden im Maß der *integral stability* (IS) für die ganzheitliche Quantifizierung von Multistabilität zusammengeführt. Komplementär lässt sich auch das Konzept der *technischen Resilienz* betrachten, welches sich auf die Rückkehrgeschwindigkeit eines Systems zu seinem Gleichgewicht, in Folge einer Störung, bezieht. Im spezifischen Kontext von vernetzten dynamischen Systemen definieren wir die *single-node recovery time* (SNRT). Diese stellt ein neues Maß zur Schätzung der relativen Zeitskalen dar, die der transienten Knotendynamik eines Netzwerks zugrunde liegen, welches nach einer nicht-infinitesimalen Störung an einem Knoten in seinen gewünschten Betriebszustand zurückkehrt. Die Verbindung der Konzepte von MNBS, IS und SNRT mit denen der linearen Stabilität, BS und SNBS liefert einen vielversprechenden Ansatz zur ganzheitlichen Quantifizierung von Multistabilität.

Schliesslich befassen wir uns mit der Untersuchung der Synchronisationsstabilität in speziellen komplexen Netzwerken, welche entweder die *Kleine-Welt*-Eigenschaft aufweisen oder eine Kombination aus *skalenfreier* Knotengradverteilung und *hierarchischer* Organisation zeigen. Die aus diesen Untersuchungen resultierenden Ergebnisse haben wichtige Implikationen für die Konstruktion von Netzwerktopologien mit verbesserter Synchronisierbarkeit als auch für die Gewährleistung eines dauerhaften synchronen Betriebs entsprechender dynamischer Systeme. Wir erwarten, dass die oben genannten Ergebnisse weiterführende Forschungen motivieren werden, welche sich mit der Robustheit synchroner Zustände in komplexen Netzwerken beschäftigten.

List of Publications

This dissertation is partly based on the following publications. The identifiers given below (e.g., P1) are cited in the text to highlight passages that are connected to these studies:

Papers

P1 **Mitra, C.**, Choudhary, A., Sinha, S., Kurths, J., & Donner, R. V. (2017). Multiple-node basin stability in complex dynamical networks. *Physical Review E*, 95(3), 032317. (DOI: 10.1103/PhysRevE.95.032317)

P2 **Mitra, C.**, Kurths, J., & Donner, R. V. (2015). An integrative quantifier of multistability in complex systems based on ecological resilience. *Nature Scientific Reports*, 5, 16196. (DOI: 10.1038/srep16196)

P3 **Mitra, C.**, Kittel, T., Choudhary, A., Kurths, J., & Donner, R. V. (2017). Recovery time after localized perturbations in complex dynamical networks. *New Journal of Physics*, 19(10), 103004. (DOI: 10.1088/1367-2630/aa7fab)

P4 **Mitra, C.**, Kurths, J., & Donner, R. V. (2017). Rewiring hierarchical scale-free networks: Influence on synchronizability and topology. *EPL* (*Europhysics Letters*), 119, 30002. (DOI: 10.1209/0295-5075/119/30002)

P5 Choudhary, A., **Mitra, C.**, Kohar, V., Sinha, S., & Kurths, J. (2017). Small-world networks exhibit pronounced intermittent synchronization. *Chaos* (*Fast Track*), 27(11), 111101. (DOI: 10.1063/1.5002883)

Earlier publications of the author with topical similarities to that of this dissertation:

Earlier papers

EP1 **Mitra, C.**, Ambika, G., & Banerjee, S. (2014). Dynamical behaviors in time-delay systems with delayed feedback and digitized coupling. *Chaos, Solitons & Fractals*, 69, 188-200. (DOI: 10.1016/j.chaos.2014.10.001)

EP2 Giri, B. K., **Mitra, C.**, Panigrahi, P. K., & Iyengar, A. N. S. (2014). Multi-scale dynamics of glow discharge plasma through wavelets: Self-similar behavior to neutral turbulence and dissipation. *Chaos*, 24(4), 043135. (DOI: 10.1063/1.4903332)

Acknowledgements

Acknowledgements are probably only as good as one's experiences. The last three years of my life as a doctoral student endowed me with the most vivid range of personal and professional experiences. Besides anything, this process has been rather gradual, but the cumulative expansion of my being has been rather monumental and certainly prepared me for the life to come. Anything such phenomenal requires contributions from several entities and I would now like to thank them and recognize their support with utmost sincerity.

First of all, I would like to take this privilege to express my deepest appreciation to my supervisors, Dr. Reik V. Donner and Prof. Dr. Dr. h.c. mult. Jürgen Kurths for helping me en route to my doctorate in every possible way, for which I shall remain indebted to them. I am deeply thankful to them for giving me the freedom to explore my ideas, while showing faith in me during the process as well as constantly supporting and encouraging me. I would also like to thank them for being instrumental in finding time for fruitful discussions during the entire course of this venture.

I am deeply indebted to the German Federal Ministry of Education and Research (BMBF) via the Young Investigators Group CoSy-CC^2 (grant no. 01LN1306A) for generously supporting my work financially, which allowed me to also participate in several inspiring national and international meetings, conferences, schools, seminars, workshops, etc. I would also like to thank the Potsdam Institute for Climate Impact Research (PIK) for providing an amicable environment, copious infrastructure and an equally competent administration during my entire stay, initially in the Pappelallee campus and thereafter on the gorgeous Telegraphenberg hill. I would also like to gratefully acknowledge the European Regional Development Fund (ERDF), BMBF and the Land Brandenburg for supporting this work by providing resources on the high performance computer system at PIK.

The magnitude of my life at PIK would have only been a fraction of itself, had it not been in the presence of the CoSy group. In this regard, a special thanks goes to Jasper Franke, Julian Maluck, Marc Wiedermann, Jonatan Siegmund, Jaqueline Lekscha, Dilya Willink, Catrin Kirsch, Nikoo Ekhtiari, Pascal Klamser, Nils Harmening, Malte Ziebarth, Cordula Schwappach, Jann Launer and Eva Hauber. In addition, I would like to acknowledge the support of Dr. Bedartha Goswami, Paul Schultz, Sabine Auer, Dr. Deniz Eroglu, Merve Eroglu, Dr. Jobst Heitzig, Tim Kittel, Dr. Frank Hellmann, Dr. Niklas Boers, Ankit Agarwal, Thomas Peron, Dr. Peng Ji, Dr. Liubov Tupikina, Prof. Elena Surovyatkina, Dr. Veronika Stolbova, Michael Lindner, Dr. Jonathan Donges, Dr. Norbert Marwan, Catrin Ciemer, Dr. Carsten Grabow, Dr. Dominik Traxl, Dr. Aljoscha Rheinwalt, Maria

Jarolin and the entire research group of Prof. Kurths'. I would like to express my deepest appreciation to Dr. Anshul Choudhary and Prof. Sudeshna Sinha for many useful discussions and productive collaborations. I would also like to thank all my friends within and outside PIK as well as around the globe (too many to list here but you know who you are!) for providing constant support and encouragement. In this regard, I would like to particularly thank Tapas Deb Sharma, Sourav Sarkar, Chandan Kumar, Abhinna Kumar Behera, Avichal Vaish, Abhijit Bendre, Snehal M. Shekatkar, Ramana Gudipudi, Abhijeet Mishra and Wei Weng. I would also like to thank Gabriele Pilz, Till Hollmann, Anja Bruhn and rest of the administration at PIK for their support in bureaucratic issues and otherwise, which always facilitated my stay at PIK.

Finally, I would like to thank all my family members - my mother, father, brother, sister-in-law and niece for their unconditional love, care and support. I would have never made it this far without them.

Thank you all for making my PhD a rather inexplicable experience!

- Chiranjit Mitra

Contents

List of Figures

List of Frequently Used Mathematical Symbols and Abbreviations

Mathematical Symbols

$\mathbf{x}$	State vector
t	Time
$\mathbf{X}$	State space
$\mathbf{\Phi}_t$	Evolution operator
$\mathbf{F}$	Function determining system evolution
$\Delta\mathcal{V}$	Volume element in the state space
$\langle\cdot\rangle$	Average
S	Invariant set
O	Orbit
$\mathcal{G}$	Graph
$\mathcal{V}$	Set of nodes/vertices
$\mathcal{E}$	Set of edges/links
N	Number of nodes/vertices
E	Number of edges/links
$\mathbf{A}$	Adjacency matrix
k	Degree
$\mathbf{L}$	Laplacian matrix
$\mathcal{L}$	Average path length
bc	Betweenness centrality
$\mathcal{C}^L$	Local clustering coefficient
$\mathcal{C}^G$	Global clustering coefficient
r	Assortativity
Q_k	Probability distribution of the remaining degrees
σ_Q^2	Variance of the probability distribution of the remaining degrees
E_{jk}	Joint probability distribution of the remaining degrees of two vertices
p	Connection probability in an Erdős-Rényi random network

$\langle k \rangle$	Average degree
γ	Scaling exponent of a scale-free network
β	Rewiring probability in a Watts-Strogatz network
$\| \cdot \|$	Norm
$\mathbf{\Phi}_t^p$	p-periodic solution
Γ	Closed orbit in state space
$\mathbf{J}$	Jacobian matrix
$\mathbb{V}$	Lyapunov function
$\mathcal{A}$	Attractor
$\mathcal{B}$	Basin of attraction
S_B	Basin stability
ρ	Probability distribution
μ	Probability measure
$\mathcal{Q}$	Reference subset for estimation of basin stability
I_C	Number of initial conditions for estimation of basin stability
F_C	Number of trajectories (final conditions) approaching an attractor (for estimation of its basin stability)
$\mathbf{H}$	Coupling function
ϵ	Coupling strength
λ_2	Second smallest eigenvalue of Laplacian matrix
λ_N	Largest eigenvalue of Laplacian matrix
R	Eigenratio
P	Number of points chosen on an attractor to be perturbed (for estimation of its basin stability)
S_B^1	Single-node basin stability
m	Number of simultaneously perturbed nodes
S_B^m	Multiple-node basin stability
$\{E_j^m\}$	Ensemble of m-*node sets*, each consisting of m nodes to be simultaneously perturbed
M	Number of m-node sets for estimation of multiple-node basin stability
m_{crit}	Critical number of perturbed nodes for which multiple-node basin stability is lower than a set threshold $\langle S_B \rangle_{th}$
L	Latitude
Λ	(Local) Lyapunov exponents
R	Resistance
Pr	Precariousness

S_I	Integral stability
$\tilde{\mathbf{x}}$	Desired operational state
δ	Neighbourhood around an attractor
t_L	Last-entry time for a trajectory to enter a δ-neighbourhood around an attractor $\mathcal{A}$
T_{RR}	Regularized reaching time
$\mathbf{x}_{ref}$	Reference trajectory for calculation of regularized reaching time
$\langle T_R^1 \rangle$	Single-node recovery time
$\langle T_R \rangle$	Global relaxation time
f	Fraction of rewired edges
Z_{sync}	Synchronization error

Abbreviations

BS	Basin stability
MSF	Master stability function
SNBS	Single-node basin stability
MNBS	Multiple-node basin stability
IS	Integral stability
SNRT	Single-node recovery time
DOS	Desired operational state
RT	Recovery time
GRT	Global recovery time
DSF	Deterministic scale-free
PSF	Pseudofractal scale-free
BA	Barabási-Albert
SW	Small-world
WS	Watts-Strogatz
TLE	Transverse Lyapunov exponent

Chapter 1.

Introduction

1.1. Motivation

Stability is vital to the normal or desired functionality of real-world dynamical systems [1]. For example, the persistence of an equilibrium of relative species' abundances in a miniature ecological system with respect to disturbances (manifesting as changes in population sizes) determines its *ecological stability* [2]. Similarly, the balanced operation of a power grid is determined by its stability to *small* perturbations on account of say, a light bulb switched on/off in a household [3]. Roughly speaking, such dynamical regimes to which the system returns to following perturbations are considered to be *stable*. The discipline of *stability theory* dealing with the aforementioned issue thus plays a central role in complex systems science, particularly with regard to real-world applications in the *control* and *automation* of dynamical systems [1].

Dynamical systems often exhibit *multistability*, characterized by the coexistence of several possible final stable states/attractors [4, 5]. Real-world dynamical systems exhibiting multistability are often subject to *large* perturbations or shocks, which drive the system to an alternative stable state. For example, the Amazonian rainforest is a potential climate *tipping* element, which is suspected of exhibiting *bistability* while being at the risk of shifting from a state of forest to savanna under the pressure of drought or deforestation [6, 7]. Maintaining operation of such systems in a particular stable state in the face of random perturbations, is often critical to their functionality. The natural abundance of multistable dynamical systems calls for the development of suitable quantifiers of the respective stability of the multiple stable states of such systems.

In the above context, complex systems science draws substantially from *linear stability* theory [1]. Linear stability analysis assesses the vulnerability of a state in response to infinitesimal perturbations and subsequently classifies the state as stable or unstable. However, linear stability analysis is too local to investigate the stability of a dynamical system against large perturbations or shocks. In a related context, Wiley et al. [8] have previously suggested utilizing the volume of the basin of attraction as a measure of the likelihood of the system (when started from a random initial condition) to *arrive* at the corresponding attractor. Following this development, Menck et al. [9] have suggested a novel extension of this concept by drawing a relationship between the volume of the basin of attraction and the

likelihood of *returning* to the corresponding attractor, following non-infinitesimal perturbations. This proposal of Menck et al. culminated in the measure of *basin stability* (BS) [9], quantified in a non-local and nonlinear fashion using the volume of the basin of attraction of a stable state as an answer to the question of *how stable* an attractor of a dynamical system is, in the event of random perturbations. Thus far, linear stability analysis in conjugation with BS, constitute state of the art methods of gauging stability in dynamical systems theory, where the latter complements the former substantially. However, we here assert that the non-local stability of the different attractors of a multistable dynamical system is determined by the overall structure (besides the corresponding volume) of their respective basins of attraction.

Many complex systems (exhibiting multistability and subject to random perturbations) involve large collections of dynamical units interacting with each other on *complex networks* [10]. Such networked dynamical systems often exhibit a multitude of stable states, whereby sustained operation of the system in the desired state is of central importance. The desired operational state in such systems often concurs with the *synchronization* of the dynamical components coupled on their networked architecture [11]. It is essential to appropriately assess and quantify multistability, particularly, the robustness of the synchronized state to arbitrary perturbations of such coupled dynamical systems. In this direction, the framework of *master stability function* (MSF) [12] as an extension of the linear stability concept to assess the stability of the completely synchronized state in complex dynamical networks was a considerable development, but still locally restrictive to small perturbations. Thereafter, the application of BS to assessing the non-local stability of synchronized dynamics has been a major advancement [9].

Despite recent developments of stability concepts outlined above, wholesome measures of stability are still wanting, as we shall explicate in the following. The developments to follow in this dissertation are largely motivated by the pervasiveness of multistability in complex (networked) dynamical systems and the associated need for suitable quantifiers of the respective stability of the multiple stable states of such systems. Also, a central focus of this dissertation is on the investigation of stability of dynamical processes (particularly, synchronization) against random perturbations of complex (networked) dynamical systems. In what follows, we shall set forth on an endeavour comprising the development of a framework for the assessment of stability of (multistable) complex (networked) dynamical systems, particularly in the face of random perturbations.

1.2. Scope

The concept of BS mentioned earlier, has been extended to that of *single-node basin stability* (SNBS) [13] in quantifying the contributions of individual nodes to the overall stability of the synchronized state. More precisely, the SNBS of a particular node of a network, corresponds to the probability of the system to

return to the desired stable state in the event of random perturbations hitting the respective node. However, in general, networked dynamical systems can also be subject to perturbations simultaneously affecting several nodes of the system. In this regard, we propose the framework of *multiple-node basin stability* (MNBS) for gauging the global stability and robustness of networked dynamical systems in response to non-infinitesimal perturbations simultaneously hitting multiple nodes of the system [P1]. Subsequently, we study the MNBS of the synchronized state in a deterministic scale-free network of Rössler oscillators and a conceptual model of the United Kingdom power grid with second-order Kuramoto-type nodal dynamics.

In addition to modern developments in stability theory, the foundation of this dissertation draws substantially from the theory of *resilience* [14]. Resilience, primarily introduced in the context of ecological systems [15], has been defined in at least two different ways, namely, *ecological resilience* and *engineering resilience* [16]. Ecological resilience of the multiple stable states of a system captures the tolerance of the system to disturbances that facilitate transitions among the stable states and relates to the volume and geometry of their respective basins of attraction. On the other hand, engineering resilience of a dynamical system characterizes its resistance to disturbance and speed of return to its equilibrium, following a perturbation.

Setting the resilience concepts mentioned above as a foundation, we revisit the problem of 'appropriately' quantifying multistability. In this regard, we turn to the concept of ecological resilience and its three aspects of *latitude* (L), *resistance* (R) and *precariousness* (Pr) [14]. In particular, we redefine the aspects of L, R and Pr in the context of dynamical systems and utilize them in laying a foundation for characterizing multistability. We bring to light the inefficacy of the state of the art methods of linear and BS (as well as a combination of both) in accounting for and collectively capturing L, R and Pr of the attractors of a multistable dynamical system. We subsequently propose the measure of *integral stability* (IS) for holistically inferring stability of multistable dynamical systems [P2]. IS allows for a more comprehensive stability assessment by consolidating the different factors of the volume of the basin of attraction (L), the local dynamics at different points in the state space (R) and the relative position of the attractor within the basin (Pr). We demonstrate the potential of IS by using exemplary multistable dynamical systems such as the damped driven pendulum, a model of the Amazonian rainforest and the Daisyworld model.

The measures of BS, SNBS and IS relate to the ecological resilience of the different stable states of a multistable dynamical system. However, random perturbations may also drive multistable dynamical systems operating in their desired stable state to arbitrary states within the corresponding basin of attraction, thereby leading to epochs of transient dynamics with a priori unknown durations until the system resumes operation in the desired stable state. Thus, it is highly relevant to have an estimate of the duration of such transient phases before the

system returns to its desired operational state, following a random perturbation. This issue of *recovery time* of complex (networked) dynamical systems ensuing a random perturbation, which is a measure of how quickly the (networked) system relaxes back to the desired operational state (e.g., a synchronized state) after being perturbed from the same relates to their engineering resilience. Besides ecological resilience, we also consider the view point of engineering resilience in addressing the aforementioned problem of 'appropriately' quantifying multistability. More specifically, in the context of networked dynamical systems, we propose the framework of *single-node recovery time* (SNRT) for obtaining an estimate of the relative time scales underlying the transient dynamics of the nodes of a network returning to its desired operational state, following a non-infinitesimal perturbation to the dynamical state of any particular node of the network [P3]. Thus, the proposed engineering resilience-based architecture of SNRT complements the ecological resilience-based framework of SNBS in characterizing the overall stability and resilience of the different nodes of a networked dynamical system. We apply the framework of SNRT to deterministic and random networks of Rössler oscillators and a conceptual model of the power grid of the United Kingdom with second-order Kuramoto-type nodal dynamics, as considered earlier in the applications of MNBS.

MNBS, IS and SNRT comprise the notable stability concepts emanating from this dissertation. The above concepts in conjugation with those of linear stability, BS and SNBS provides a comprehensive framework for the quantification of multistability. Following the above developments, we delve into the explicit investigation of stability of synchronization on complex dynamical networks exhibiting *small-world* properties [17], *scale-free* behaviour [18], and *hierarchical* organization [19].

As previously underlined, synchronization of dynamical elements coupled on complex networks has been recognized as one of the most significant forms of collective behaviour in studies of complex systems [11]. The last few decades have continuously witnessed a substantial amount of inquiry probing the existence and stability of synchronized dynamics on complex networks. Many real-world complex networks simultaneously exhibit topological features of scale-free behaviour and hierarchical organization. Scale-free networks are characterized by a degree distribution which follows a power-law, at least asymptotically [18]. Hierarchical organization is characterized by small groups of nodes organizing in a stratified manner into larger groups, over multiple scales [19]. We consider deterministic network models which simultaneously capture the two aforementioned topological properties. Subsequently, we utilize the framework of MSF in investigating synchronizability of dynamical systems coupled on such network structures. Interestingly, this reveals that randomly rewired versions of such networks exhibit significantly enhanced as well as deteriorated synchronizability, as compared to that of their completely deterministic counterparts. Importantly, when a certain critical fraction of edges of the otherwise completely deterministic networks are

rewired, it optimizes the average synchronizability of the resulting topologies [P4]. These results may have potential implications in the design of complex networks (simultaneously exhibiting scale-free behaviour and hierarchical structure) for achieving better synchronizability.

Also, many real-world complex networks have been found to exhibit the small-world (SW) property characterized by surprisingly short distances between nodes of such a network, even as its overall size increases substantially [10, 17]. Interestingly, amongst various real-world topologies, those with SW properties have been found to be quite conducive for the optimal manifestation of synchronized motion [9, 17]. We revisit the above result and present a case which appears to challenge the robustness of synchronized dynamics on small-world networks. In particular, we investigate the phenomenon of *temporally intermittent* synchronized and desynchronized dynamics [20] in Watts-Strogatz (WS) networks [17] of chaotic Rössler oscillators [P5]. We specifically find that the likelihood of the system to exhibit the intermittently synchronized state becomes appreciably large in the SW regime, which is surprising, since this limit has been otherwise considered optimal for synchronized dynamics. Also, the likelihood of the system to exhibit persistent synchronized motion in the SW regime of the WS model is not much different from that observed for greater randomness ($p \sim 1$) in the respective model. This leads us to the conclusion that although the synchronized state does occur in SW networks, they are not manifested with larger likelihoods of observation in the SW regime of the WS model. In fact, we speculate that SW networks may be significantly more prone to exhibit intermittently synchronized dynamics.

1.3. Contents

In Chapter 2, we recapitulate the basic terminology of dynamical systems theory. Chapter 3 provides a description of the quantitative foundations of the study of networks as well as measures for quantifying network structure. We review the established fundamental concepts enveloping the theory of stability and resilience of (complex) dynamical systems in Chapter 4, which shall serve as a foundation for the conceptual and methodological developments to thereafter follow in this dissertation.

In Chapter 5, we propose the framework of *multiple-node basin stability* and outline its applications to complex dynamical networks. The measure of *integral stability* is introduced in Chapter 6 and its potential in quantifying multistability is illustrated using paradigmatic examples. We propose the framework of *single-node recovery time* in Chapter 7 and outline its applications to complex dynamical networks. In Chapter 8, we study the influence of rewiring edges on the synchronizability and topology of networks simultaneously exhibiting hierarchical organization and scale-free behaviour, as often observed in nature and society. We investigate the phenomenon of temporally intermittent synchronized and

desynchronized dynamics in small-world (Watts-Strogatz) networks of chaotic oscillators in Chapter 9 and illustrate that such intermittently synchronized dynamics is particularly pronounced in the small-world regime, which is otherwise known to be conducive for synchronization of complex oscillators networks.

Finally, Chapter 10 contains a summary of the main developments emanating from this dissertation and a discussion on possible directions for future research.

Part I.

Theoretical Foundations

Chapter 2.

Dynamical Systems Theory

2.1. Introduction

Nature inevitably and ubiquitously exhibits change. Almost all systems including those which appear static at the outset undergo changes with the passage of time, only at different time scales. Such systems which change and evolve with time are called *dynamical systems* and their behaviour is investigated within the framework of *dynamical systems theory* [21]. In the following, we recapitulate the basic terminology of dynamical systems theory that will be used throughout the course of this dissertation.

2.2. State of a Dynamical System and its Evolution

Typically, the *state* of a d-dimensional dynamical system at time t is captured by its *state vector* $\mathbf{x}(t) = (x_1, x_2, \ldots, x_d)^{\mathrm{T}}$ where T stands for transpose. We label the set of all possible states of a system $\mathbf{X}$. For most dynamical systems of practical interest, the state variables' components x_i only take real values, i.e., $\mathbf{x}(t) \in \mathbb{R}^d$ and $\mathbf{X} \subset \mathbb{R}^d$. Given the initial state of a system $\mathbf{x}(t_0)$ at time t_0, its subsequent evolution in time is governed by the *evolution operator* $\mathbf{\Phi}_t$ [21] such that

$$\mathbf{x}(t) = \mathbf{\Phi}_t(\mathbf{x}(t_0), t). \tag{2.1}$$

2.3. Non-autonomous and Autonomous Dynamical Systems

Systems described by Eq. (2.1), where $\mathbf{\Phi}_t$ exhibits explicit time-dependence (and/or, external inputs, forcing functions, etc.) are termed *non-autonomous* [22]. On the other hand, systems which do not exhibit explicit dependence on time such that

$$\mathbf{x}(t) = \mathbf{\Phi}_t(\mathbf{x}(t_0)), \tag{2.2}$$

are referred to as *autonomous* or *time-invariant* [22] and we shall confine ourselves to their investigation in this dissertation.

2.4. Continuous-time and Discrete-time Dynamical Systems

Dynamical systems are usually studied by employing differential equations or difference equations, depending upon whether their evolution is captured at continuous or discrete steps of time, respectively. Consequently, the former category of systems are called *continuous-time dynamical systems*, while the latter are labelled as *discrete-time dynamical systems* (or *maps*) [21].

2.5. Deterministic Dynamical Systems

The time evolution results in a *trajectory* of the system (in Eq. (2.2)) defined by the set $\{\mathbf{\Phi}_t(\mathbf{x}(t_0)) \mid t \geq t_0\}$ corresponding to the initial state $\mathbf{x}(t_0)$. The *orbit* $O(\mathbf{x}(t_0))$ comprises the infinite-time trajectory through the point $\mathbf{x}(t_0)$. Thus, an orbit refers to the totality of states that can be reached from $\mathbf{x}(t_0)$ [23].

The system is called *deterministic* when $\mathbf{\Phi}_t$ depends completely on the state of the system such that it uniquely maps a system's state to another [21]. Thus, the existence of such a definite rule of evolution associated with *almost* every state implies that the trajectories in a deterministic dynamical system cannot intersect with each other. We shall primarily focus our investigation to continuous-time deterministic dynamical systems throughout the course of this dissertation.

The evolution of a continuous-time deterministic dynamical system can be expressed by carving Eq. (2.2) into the following form of a differential equation of motion:

$$\dot{\mathbf{x}}(t) = \mathbf{F}(\mathbf{x}(t)), \tag{2.3}$$

where $\mathbf{F}$ determines the time evolution of the system such that $\mathbf{F} : \mathbb{R}^d \rightarrow \mathbb{R}^d$, $\mathbf{F}(\mathbf{x}(t)) = (F_1(\mathbf{x}(t)), F_2(\mathbf{x}(t)), \ldots, F_d(\mathbf{x}(t)))^{\mathrm{T}}$. The evolution operator $\mathbf{\Phi}_t$ is called a *flow map* for a continuous-time dynamical system [21]. Similarly, the equivalent for a discrete-time system can be written as a difference equation:

$$\mathbf{x}(t+1) = \mathbf{F}(\mathbf{x}(t)), \tag{2.4}$$

where the evolution operator is called a *time-one map* [21]. Dynamical systems are further classified as *linear* or *nonlinear* depending upon whether the function $\mathbf{F}$ is a linear or nonlinear function of the state variable $\mathbf{x}$, respectively.

2.6. State Space

The state of a system in conjugation with its dynamical evolution (described by Eq. (2.2)) can be geometrically visualized in an abstract d-dimensional space constructed with the state space variables $x_1, x_2, \ldots, x_d$ as coordinates. This space is called the *state space* or *phase space* of the system, where we utilize the former nomenclature in this text [21]. At any given instant of time, the state of the system is represented by a point in this space. Starting from any initial condition, the system moves as a point in this space resulting in a trajectory of the system as determined by its equations of motion (Eq. (2.2)). Also, note that every point in the state space of a continuous-time dynamical system (Eq. (2.3)) is associated with a velocity vector $\dot{\mathbf{x}} = \mathbf{F}(\mathbf{x})$, which taken together comprise the *vector field* of the system [21]. A trajectory of the system starting from any chosen initial condition simply follows the direction of the vectors, implying that the vectors are tangent to the respective trajectory at every point in the state space.

2.7. Conservative and Dissipative Dynamical Systems

Dynamical systems may further be classified as *conservative* or *dissipative* [24]. A system which does not dissipate energy, and thus maintains a constant amount of total energy such that $\boldsymbol{\nabla} \cdot \mathbf{F} = 0$ (where $\boldsymbol{\nabla} \cdot \mathbf{F}$ denotes the divergence of F) is called a *conservative system* [24]. On the other hand, a *dissipative system* continuously loses energy to its surroundings due to friction-like processes [24]. In practice, systems are prone to dissipation and we shall primarily consider dissipative systems in this dissertation.

Dissipative systems are characterized by $\boldsymbol{\nabla} \cdot \mathbf{F} < 0$ (on average) over the state space, which implies that volumes of initial states will contract with time and collapse onto a geometric region whose dimensionality is generally smaller than that of the original d-dimensional state space. Thus, if we start with a set of initial conditions occupying a d-dimensional volume $\Delta\mathcal{V}\,(>0)$, then it yields $\langle \frac{d\Delta\mathcal{V}}{dt} \rangle = \langle \boldsymbol{\nabla} \cdot \mathbf{F} \Delta\mathcal{V} \rangle < 0$ signifying contraction [24]. The corresponding trajectories converge to an *invariant set* of the system, which we define in the following.

2.8. Invariant Sets

An *invariant set* of a dynamical system is a subset $S \subset X$ such that $\mathbf{x}(t_0) \in S$ implies $\boldsymbol{\Phi}_t(\mathbf{x}(t_0)) \in S, \forall\, t \geq t_0$ [24]. This implies that $\boldsymbol{\Phi}_t S \subset S$. An orbit of a dynamical system is an invariant set. Also, an invariant set consists of a union of orbits of a dynamical system. The geometric dimension of an invariant set of a dynamical system is smaller than (or equal to) that of its original state space. An invariant set S must be *stable* in order to represent an observable asymptotic

state of a dynamical system [21]. Thus, invariant sets determine the long-term behaviour of dissipative dynamical systems.

We shall return to our discussion of the stability of invariant sets in Chapter 4. In the following chapter, we shall briefly recapitulate the basics of network theory, which will be useful for the subsequent developments to follow in this dissertation.

Chapter 3.

Complex Network Theory

This chapter presents the fundamental quantitative foundations of the study of complex networks as well as measures for quantifying network structure. The elements of network theory described in this chapter are requisite for the methodological developments and applications presented in the subsequent parts of this dissertation. The theoretical foundations outlined in this chapter are closely related to those of the associated publications P1, P3, P4 and P5 and some of these details follow the corresponding sections in the respective publications.

3.1. Mathematical Background

In the mathematical literature, a *network* is usually referred to as a *graph*. In the most common sense of the term, a graph $\mathcal{G}$ comprises a set $\mathcal{V}$ of *vertices* together with a set $\mathcal{E}$ of edges connecting the vertices [10]. Vertices and edges are also commonly referred to as *nodes* and *links* across different disciplines, respectively. These terms will be used synonymously during the course of this dissertation. We denote the number of nodes in a network by N and the number of edges by E. Node i of an N-node network is usually labelled with an integer such that $i \in \{1, 2, \ldots, N\}$. The label i given to each node should be unique in order to use the labels to refer to any node unambiguously.

The networks we study in this dissertation have at most a single edge between any pair of nodes and also no edges (also referred to as *self-loops*) which connect nodes to themselves. Such networks are called *simple networks* or *simple graphs* [10]. Further, links in a network can be *undirected* or *directed* [10]. In an undirected network, given that two distinct nodes i and j are connected, there is an edge representing the influence of node j on node i and vice-versa. However, a directed network allows for directionality of the links in the sense that there may be an edge representing the influence of node j on node i, but not necessarily the other way around.

A simple undirected network is usually represented by its *adjacency matrix* $\mathbf{A}$, which is a matrix with elements A_{ij} such that [10]

$$A_{ij} = \begin{cases} 1 & \text{if there is an edge connecting nodes } i \text{ and } j, \\ 0 & \text{otherwise.} \end{cases} \tag{3.1}$$

Note that the adjacency matrix in Eq. (3.1) is symmetric with respect to i and j on account of the corresponding network being undirected. Similarly, a simple directed network is represented by a non-symmetric adjacency matrix such that

$$A_{ij} = \begin{cases} 1 & \text{if there is an edge from node } j \text{ to } i, \\ 0 & \text{otherwise.} \end{cases} \tag{3.2}$$

Further, the strength of interaction from node j to i may be weighted, represented by a weight w_{ij} assigned to the respective edge between the associated nodes. This leads to a *weighted network* (and possibly directed with asymmetric weights of interactions between any pair of nodes, i.e., $w_{ij} \neq w_{ji}$) represented by an adjacency matrix with entries equal to the weights, i.e., $A_{ij} = w_{ij}$ [10].

3.2. Network Measures

We now describe some standard measures and metrics which capture particular features of the network topology and provide useful insights about its underlying structure. In particular, we discuss the topological properties of *degree*, *average path length*, *maximum betweenness centrality*, *average local clustering coefficient*, *global clustering coefficient* and *assortativity coefficient* of a network [10].

3.2.1. Degree

The connectivity of a node i is described by its *degree* $k_i = \sum_j A_{ij}$ (where $\mathbf{A}$ again is the adjacency matrix of the respective network) [10]. The probability distribution of the degree of all nodes of a network termed as its *degree distribution* P_k represents the probability that a node chosen at random has a degree k. P_k is effectively given by the expected proportion of nodes in the network having a degree k, i.e., $P_k = \frac{\langle |\{i \in \mathcal{V} : k_i = k\}| \rangle}{N}$. We may now also define the *Laplacian matrix* $\mathbf{L}$ of a simple network as [10]

$$L_{ij} = \begin{cases} k_i & \text{if } i = j, \\ -1 & \text{if } i \neq j \text{ and node } i \text{ is connected to node } j, \\ 0 & \text{otherwise.} \end{cases} \tag{3.3}$$

3.2.2. Average Path Length

The *average path length* $\mathcal{L}$ of a network with N nodes is defined as the mean value of the shortest path lengths between all possible pairs of nodes [10]. Thus, $\mathcal{L} = \frac{1}{N(N-1)} \sum_{i \neq j} \ell(i,j)$, where $\ell(i,j)$ is the length of the shortest path between nodes i and j.

3.2.3. Betweenness Centrality

The *betweenness centrality* bc_i of a node i is related to the fraction of shortest paths between all pairs of nodes that pass through that node [10]. For an N-node network, the betweenness centrality of each node may further be normalized by dividing by the number of node pairs $\left[\text{i.e., } \binom{N}{2}\right]$, resulting in values between 0 and 1. Thus, $bc_i = \frac{2}{N(N-1)} \sum_{j \neq k \neq i} \frac{\sigma^i_{j,k}}{\sigma_{j,k}}$, where $\sigma_{j,k}$ is the total number of shortest paths from node j to node k and $\sigma^i_{j,k}$ is the number of such shortest paths which pass through node i.

3.2.4. Clustering Coefficient

The *local clustering coefficient* $\mathcal{C}^L_i$ relates to the probability of the existence of an edge between two randomly selected neighbours of node i [10]. $\mathcal{C}^L_i$ is defined as the ratio between the number of links between nodes within the neighbourhood of node i and the number of links that could possibly exist between its neighbours. Thus, $\mathcal{C}^L_i = \frac{2}{k_i(k_i-1)} N^\Delta_i$, where N^Δ_i is the total number of closed triangles including node i (with degree k_i), which is bounded by the maximum possible value of $\frac{k_i(k_i-1)}{2}$. The *average local clustering coefficient* $\mathcal{C}^L$ of the network is then given by the mean of the local clustering coefficient of all nodes of the network, i.e., $\mathcal{C}^L = \frac{1}{N} \sum_{i=1}^{N} \mathcal{C}^L_i$ [10]. Likewise, the *global clustering coefficient* $\mathcal{C}^G$ of a network (often also called network *transitivity* [10, 25]) is related to the probability that two nodes with a common neighbour are themselves neighbours [10]. $\mathcal{C}^G$ is defined as the fraction of the total number of triplets in the network that are closed, i.e., $\mathcal{C}^G = \frac{\text{(number of closed triplets)}}{\text{(total number of triplets)}}$. In this case, a triplet means three vertices i, j and k with edges $(i,\, j)$ and $(j,\, k)$, while the edge $(i,\, k)$ may be present or not. To avoid terminological confusion, we emphasize that average local clustering coefficient $\mathcal{C}^L$ (as defined above) is often referred to as the global clustering coefficient (e.g., in Ref. [17]).

3.2.5. Assortativity Coefficient

The *assortativity coefficient* r of a network quantifies the overall preference of any of its nodes to connect with other nodes having a similar degree [26]. r is defined as the Pearson correlation coefficient between the degrees of all pairs of mutually connected nodes, i.e., $r = \frac{1}{\sigma^2_Q} \sum_{j,\,k} jk\,(E_{jk} - Q_j Q_k)$. Here, Q_k is the probability distribution of the *remaining degrees*, which relates to the number of edges leaving the node, excluding the one that connects the pair, and σ^2_Q is the associated variance. Given the probability distribution of degrees P_k, the probability distribution of the remaining degrees is given by $Q_k = \frac{(k+1)P_{k+1}}{\sum_{j \geq 1} jP_j}$. E_{jk}

represents the joint probability distribution of the remaining degrees of the two vertices. Positive values of r indicate a tendency of nodes with a similar degree to connect, while negative values of r indicate links between nodes of different degree.

3.3. Network Models

In the following, we discuss certain fundamental network models which have improved our understanding of the structural properties of manifold real-world complex networks and uncovered the fundamental principles governing their organization. The following network models can be categorized into the two groups of random and deterministic types. As the terminology suggests, the former group of network models comprise stochastic processes underlying their formation, while the latter constitute deterministic ones. The random network models we consider include the Erdős-Rényi model of random networks [27], Barabási-Albert model of random scale-free networks [18] and Watts-Strogatz model of small-world networks [17], while the deterministic network models comprise Barabási, Ravasz and Vicsek's model of deterministic scale-free network [28] and Dorogovtsev, Goltsev and Mendes' model of pseudofractal scale-free network [29]. In the following chapters, we investigate the stability and resilience of dynamical processes on these deterministic network models as well as their random counterparts described below.

3.3.1. Random Network Models

3.3.1.1. Erdős-Rényi Random Networks

The random network model by Erdős and Rényi [27] involves the construction of networks starting with a certain number of nodes N and thereafter connecting nodes randomly. Each edge out of the total number of $\binom{N}{2}$ possible edges is added with a fixed probability $p \in [0,\, 1]$, independently of every other edge. The expected number of edges and the average degree of an undirected Erdős-Rényi network are equal to $\langle E \rangle = \binom{N}{2} p$ and $\langle k \rangle = (N-1)\, p$ where $\binom{N}{2} = \frac{N(N-1)}{2}$ represents the total number of possible pairs of nodes in the network. The degree distribution in an Erdős-Rényi network $P_k = \binom{N-1}{k} p^k \, (1-p)^{N-1-k}$ is binomial, which is well-approximated by a Poisson distribution $P_k \approx \frac{(Np)^k e^{-Np}}{k!}$ for large N and $Np =$ constant. The binomial (or, approximately Poissonian) degree distribution of an Erdős-Rényi random network peaks around the average degree of the respective network and decays exponentially for values of k much smaller or larger than $\langle k \rangle$ (i.e., $k \gg \langle k \rangle$). This implies a relatively homogeneous degree distribution of nodes in such networks. The average path length and average local clustering coefficient in Erdős-Rényi random networks scale with the network size as $\mathcal{L} \sim \frac{\log N}{\log \langle k \rangle}$ and $\mathcal{C}^L \sim \frac{\langle k \rangle}{N}$, respectively [30, 31].

3.3.1.2. Barabási-Albert Model of Random Scale-free Networks

While Erdős-Rényi random networks are characterized by homogeneous degree distributions, many real-world complex networks have been reported to exhibit scale-free behaviour characterized by a probability P_k that a randomly selected node has exactly k links decaying as a power law, $P_k \sim k^{-\gamma}$, where $2 < \gamma < 3$ has been typically observed for the scaling exponent γ [18]. This leads to a heterogeneous degree distribution in such scale-free networks with mostly low degree nodes coexisting with a few very high degree nodes (also called *hubs*).

In the above context, the Barabási-Albert model [18] has been suggested for realizing random scale-free networks with growth and preferential attachment, where an incoming node is more likely to get randomly linked to an existing node with higher connectivity. While generating random scale-free networks using the Barabási-Albert model, the growing character of the network is incorporated by starting with a small number of connected nodes N_0 with uniform degree. Thereafter, at every time step a new node is introduced and linked to m nodes already present in the system (until the network comprises N nodes). Preferential attachment is incorporated by assuming that the probability Π_i that a new node will be connected to an existing node i depends on the degree k_i of node i, such that $\Pi_i = \frac{k_i}{\sum\limits_j k_j}$. This naturally creates the possibility of high degree nodes to continuously further increase their respective degrees, as new nodes added to the network prefer attachment with such hubs. The degree distribution in such a network indeed follows a power-law with $\gamma = 3$, while the average path length and average local clustering coefficient scale with network size as $\mathcal{L} \sim \frac{\log N}{\log \log N}$ and $\mathcal{C}^L \sim \frac{(\log N)^2}{N}$, respectively [31, 32]. Such random scale-free networks generated using the Barabási-Albert model generally exhibit shorter average path lengths as well as higher values of clustering coefficients than Erdős-Rényi random networks [31]. However, the Barabási-Albert model fails to capture the high levels of clustering exhibited by many real-world complex networks.

3.3.1.3. Watts-Strogatz Model of Small-world Networks

Many real-world complex networks exhibit the small-world property characterized by surprisingly short distances between nodes of such a network, even as its overall size increases substantially [10, 17]. Specifically, the average path length $\mathcal{L}$ scales as a logarithm of the number of nodes N, i.e., $\mathcal{L} \sim \log N$ for a small-world network. This is accompanied by a significant transitivity in such networks reflecting as high values of clustering coefficients of the respective topologies. However, neither the Erdős-Rényi model nor the Barabási-Albert model generate networks which collectively capture the aforementioned topological features. In this regard, the Watts-Strogatz model is used to create networks with small-world properties, thus exhibiting short characteristic path lengths between nodes and high clustering coefficients [17].

The Watts-Strogatz model produces networks by starting with a regular ring lattice of N nodes with (fixed) average degree $\langle k \rangle$ ($\langle k \rangle$ is even and preferably $\langle k \rangle \ll N$) such that each node is connected to its $\langle k \rangle$-nearest neighbours, with $\frac{\langle k \rangle}{2}$ on either side [10]. Then, for every node $i \in \{1, 2, \ldots, N\}$, its edge (i, j) connecting to node j ($i < j$) is selected and rewired with a probability $\beta \in [0, 1]$ by connecting the edge to some node v selected uniformly at random, while avoiding self-loops (i.e., $v \neq i$) and multiple edges (i.e., there should be no edge (i, v) already existing between the nodes i and v prior to rewiring).

For a ring lattice (i.e., when $\beta = 0$), the average path length scales linearly with system size such that $\mathcal{L} = \frac{N}{2\langle k \rangle}$, while the average local clustering coefficient is given by $\mathcal{C}^L = \frac{3(\langle k \rangle - 2)}{4(\langle k \rangle - 1)}$ which converges to a value of $\frac{3}{4}$ in the limit of large $\langle k \rangle$ [31]. On the other hand, in the limit of $\beta \to 1$, the model converges to a classical random graph for which $\mathcal{L} = \frac{\log N}{\log \langle k \rangle}$ and $\mathcal{C}^L = \frac{\langle k \rangle}{N}$ [31]. For $\beta \in (0, 1)$, the average path length rapidly drops with increasing β and quickly approaches its limiting value of $\frac{\log N}{\log \langle k \rangle}$. However, the average local clustering coefficient maintains a value quite close to that of the ring lattice as β is increased, and only declines for relatively high values of β. Thus, this intermediate regime for a broad range of β values where the average path length declines rapidly, while the average local clustering coefficient does not, generates networks with short characteristic path lengths and high clustering coefficients. In summary, the Watts-Strogatz model generates networks by randomly rewiring completely regular architectures (ring lattices), thus interpolating between absolutely regular and random networks with small-world properties appearing for intermediate rewiring. The degree distribution in a Watts-Strogatz network is relatively homogeneous and can be explicitly expressed as [31]

$$P_k = \sum_{n=0}^{f\left(k,\, \frac{\langle k \rangle}{2}\right)} \binom{n}{\frac{\langle k \rangle}{2}} (1-\beta)^n \, \beta^{\frac{\langle k \rangle}{2} - n} \frac{\left(\beta \frac{\langle k \rangle}{2}\right)^{k - \frac{\langle k \rangle}{2} - n}}{\left(k - \frac{\langle k \rangle}{2} - n\right)!} e^{-\beta \frac{\langle k \rangle}{2}},$$

where $f\left(k,\, \frac{\langle k \rangle}{2}\right) = \min\left(k - \frac{\langle k \rangle}{2},\, \frac{\langle k \rangle}{2}\right)$.

3.3.2. Deterministic Network Models

3.3.2.1. Deterministic Scale-free Network

The deterministic scale-free network was proposed by Barabási, Ravasz and Vicsek [28] as a simple model to generate scale-free topologies (with hierarchical assembly) in a deterministic fashion. It was later analytically studied by Iguchi and Yamada [33] in greater detail. We illustrate the topology developed over 2 generations of the deterministic scale-free network in Fig. 3.1(a). Such networks characterized by their fractal growth are categorized into the general class of *hierarchical networks* [34]. The construction of the network follows an iterative

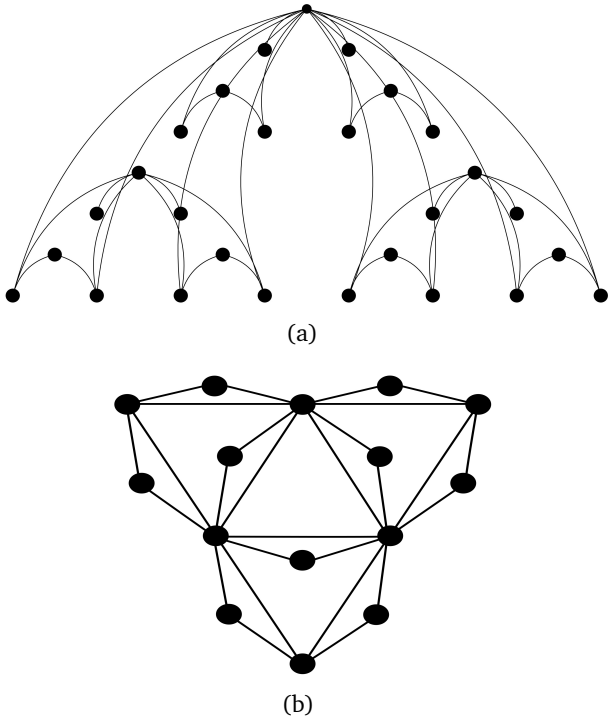

(a) (b)

Figure 3.1.: Topology of the (a) deterministic and (b) pseudofractal scale-free networks developed over two generations.

rule which starts with a single vertex labelled as the *root* node of the network. Subsequently, 2 nodes labelled as *bottom* nodes are added and connected to the root, thus completing the 1^{st} step of the construction process. Then, two identical copies of the resulting graph are created and each of the bottom nodes of these two units are connected to the root in the 2^{nd} step. Thus, the root gains 4 more edges and the resulting network now contains 9 nodes. In the 3^{rd} step, two copies of the resulting graph are created, and the 8 bottom nodes of each of these 2 units are connected to the root. Generalizing the aforementioned steps to the n^{th} iteration would involve adding two units of $3^n - 1$ nodes created in the $(n-1)^{\text{th}}$ step and then connecting the 2^n bottom nodes of each unit to the root node. We refer to each step of the algorithm as a *generation*.

The degree distribution of the network can be exactly solved for and follows $P_k \sim k^{-\frac{\log 3}{\log 2}}$ [28]. Also, the average path length of such a network developed over g generations can be analytically obtained to be $\mathcal{L} = \frac{8g3^{g-2}}{3^g-1}$, which in the limit of $N \to \infty$ is approximated by $\frac{8}{9\log 3}\log N$ [35]. Thus, the average path length scales logarithmically with the number of nodes for large deterministic scale-free networks. The model does not involve creation of triangles of nodes, thereby resulting in no clustering, i.e., $\mathcal{C}^L = 0$.

3.3.2.2. Pseudofractal Scale-free Network

The pseudofractal scale-free network was introduced by Dorogovtsev, Goltsev and Mendes [29]. Its topology developed over 2 generations is illustrated in Fig. 3.1(b). The scheme of growth of the pseudofractal scale-free web starts with a single edge connecting two nodes which comprises step -1. For each step thereafter, a new node is added for every edge which is then connected to the two nodes linked by the respective edge. Thus, at the end of step 0 the network comprises a triangle of edges connecting a triple of vertices. Similarly, the topology consists of 6 edges connecting 9 vertices at the end of step 1, and so on.

The network comprises a total of $N = \frac{3}{2}\left(3^g + 1\right)$ nodes and $E = 3^{g+1}$ edges after g steps or generations, implying $\langle k \rangle = \frac{2E}{N} = \frac{4}{(1+3^{-g})}$ [29]. The degree distribution of the pseudofractal scale-free network can be exactly solved for and follows $P_k \sim k^{-\left(1+\frac{\log 3}{\log 2}\right)}$ [29]. The average path length of the network developed over g generations when analytically solved for yields $\mathcal{L} = \frac{(4g+11)3^{2g}+10\times 3^g+3}{3(3^g+1)(3^{g+1}+1)}$, which in the limit of $N \to \infty$ approaches $\mathcal{L} = \frac{4}{9\log 3}\log N$ [29]. The average local clustering coefficient of the network developed over g generations is given by $\mathcal{C}^L = \frac{4}{5}\frac{6^g+\frac{3}{2}}{2^g(3^g+1)}$, which in the limit of $N \to \infty$ converges to a value of $\frac{4}{5}$ [29].

Chapter 4.

Stability and Resilience Concepts

In this chapter, we recapitulate the established fundamentals of *stability* and *resilience* of dynamical systems, which shall serve as a foundation for the conceptual and methodological developments to follow in this dissertation. The theoretical foundations outlined in this chapter are closely related to those of the associated publications P1, P2, P3, P4 and P5 and some of these details follow the corresponding sections in the respective publications.

4.1. Stability Concepts

Among the various notions of stability of a system, those of fundamental importance in studies of nonlinear dynamics include the *Lyapunov stability* of a system with respect to its equilibria, the *orbital stability* of the output trajectory of a system, and the *structural stability* of a system itself [1]. The *Lyapunov stability* of a system with respect to an equilibrium is related to the behaviour of the system output towards the respective equilibrium, i.e., whether it wanders nearby (stability in the sense of Lyapunov), or if it gradually approaches the equilibrium (*asymptotic stability*) [1]. *Orbital stability* is related to the resistance of a system's trajectory under small perturbations [1]. The *structural stability* of a system is related to its resistance to small perturbations (not affecting the dynamical state of a fixed system, instead) affecting the overall structure of the system itself [1].

The concept of an invariant set of a dynamical system was introduced in Sec. 2.8. An invariant set S must be *stable* in order to represent an observable asymptotic state of a dynamical system [21]. Next, we revisit the formal definition of the stability of invariant sets of a dynamical system.

4.1.1. Stability of Invariant Sets

An invariant set S of a dynamical system (described by Eq. (2.2)) is called stable if [21]:

(A) given any sufficiently small neighbourhood $U \supset S$, there exists a neighbourhood $V \supset S$ such that $\mathbf{\Phi}_t\left(\mathbf{x}\left(t_0\right)\right) \in U$, $\forall\, \mathbf{x}\left(t_0\right) \in V$ and $t \geq t_0$.

(B) there exists a neighbourhood $V_0 \supset S$ such that $\mathbf{\Phi}_t\left(\mathbf{x}\left(t_0\right)\right) \to S$, $\forall\, \mathbf{x}\left(t_0\right) \in V_0$ and $t \geq t_0$.

The properties (A) and (B) stated above comprise the formal definitions of stability in the sense of Lyapunov (*Lyapunov stability*) and *asymptotic stability*, described later in Sections 4.1.2 and 4.1.3, respectively.

In the following, we revisit the definitions of Lyapunov, asymptotic, orbital and structural stabilities in the specific case of a dynamical system described by Eq. (2.2).

4.1.2. Lyapunov Stability

We have already provided a formal definition of stability in the sense of Lyapunov (Lyapunov stability) and asymptotic stability in Sec. 4.1.1. Here, we intend to provide a more geometrical description of these stability concepts.

Let $\mathbf{x}^*$ represent an equilibrium of the system in Eq. (2.2). Then, the system is referred to as *stable in the sense of Lyapunov* with respect to $\mathbf{x}^*$, if for every $\epsilon > 0$ and time $t_0 \geq 0$ there exists a $\delta = \delta(\epsilon) > 0$ such that $\|\mathbf{x}(t_0) - \mathbf{x}^*\| < \delta \Rightarrow \|\mathbf{x}(t) - \mathbf{x}^*\| < \epsilon$ for all $t \geq t_0$ [1]. Figure 4.1(a) provides a geometric illustration of the concept of Lyapunov stability.

4.1.3. Asymptotic Stability

Given that the equilibrium $\mathbf{x}^*$ of the system in Eq. (2.2) is stable in the sense of Lyapunov, it is referred to as *asymptotically stable* if there exists a $\delta > 0$ such that $\|\mathbf{x}(t_0) - \mathbf{x}^*\| < \delta \Rightarrow \|\mathbf{x}(t) - \mathbf{x}^*\| \to 0$ as $t \to \infty$ [1]. A geometric illustration of the concept of asymptotic stability is provided in Fig. 4.1(b).

4.1.3.1. Exponential Stability

Further, given that the equilibrium $\mathbf{x}^*$ is asymptotically stable, it is referred to as *exponentially stable* if $\|\mathbf{x}(t_0) - \mathbf{x}^*\| < \delta \Rightarrow \|\mathbf{x}(t) - \mathbf{x}^*\| \leq \alpha \|\mathbf{x}(t) - \mathbf{x}^*\| e^{-\beta t}$ for constants $\alpha,\ \beta > 0$ and for all $t \geq t_0$ [1]. The concept of exponential stability is illustrated in Fig. 4.1(c).

Thus, Lyapunov, asymptotic and exponential stabilities deal with the intrinsic dynamical behaviour of the system around its equilibria. However, the concepts of orbital and structural stabilities which we describe below, capture the response of the system to perturbations affecting the dynamical state of the system and alterations to the overall dynamical structure of the system, respectively.

4.1.4. Orbital Stability

The *orbital stability* of a system output is concerned with the behaviour of a closed trajectory (orbit) of the system under the action of small external perturbations [1]. Given that the system in Eq. (2.2) has a p-periodic solution $\mathbf{\Phi}_t^p(\mathbf{x})$ associated with the closed orbit Γ in the state space, i.e., $\Gamma = \{\mathbf{x}' \mid \mathbf{x}' = \mathbf{\Phi}_t^p(\mathbf{x}(t_0)),\ \forall\, 0 \leq t < p \,\text{and}\, \mathbf{x}(t_0) \in \Gamma\}$. Then, the trajectory $\mathbf{\Phi}_t^p(\mathbf{x})$ is said to be

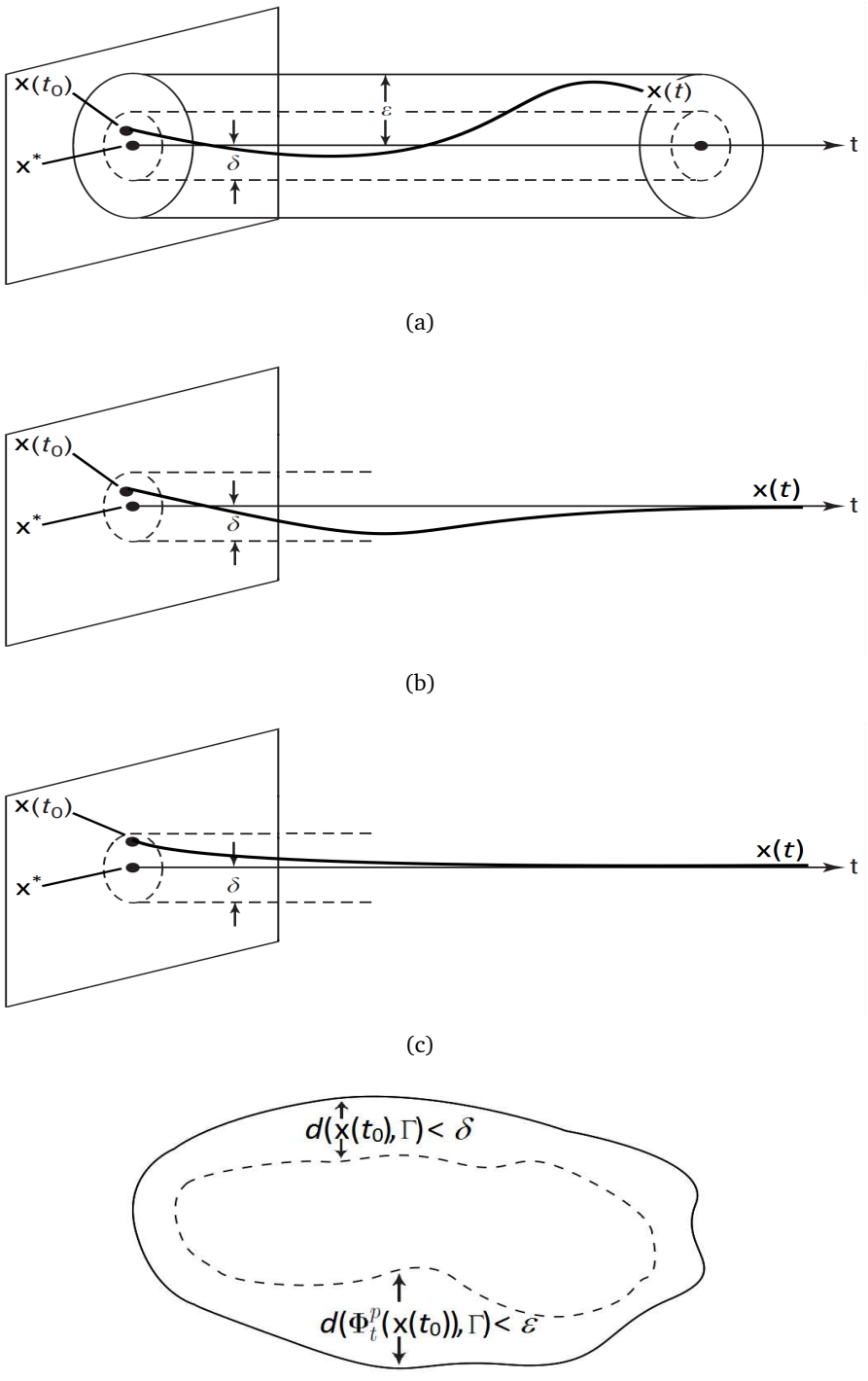

Figure 4.1.: Schematic illustrating the concepts of (a) Lyapunov stability (b) asymptotic stability (c) exponential stability and (d) orbital stability of a dynamical system (modelled via Eq. (2.2)).

orbitally stable if for any $\epsilon > 0$, there exists a $\delta = \delta(\epsilon) > 0$ such that the trajectory starting from the initial condition $\mathbf{x}(t_0)$ within the δ-neighbourhood of $\mathbf{\Phi}_t^p(\mathbf{x})$, also remains within the ϵ-neighbourhood of $\mathbf{\Phi}_t^p(\mathbf{x})$ for all $t \geq t_0$. Thus, given any $\epsilon > 0$, if there exists a $\delta = \delta(\epsilon) > 0$ such that for any $\mathbf{x}(t_0)$, the distance $d(\mathbf{x}(t_0), \Gamma) = \inf_{\mathbf{x}' \in \Gamma} \|\mathbf{x}(t_0) - \mathbf{x}'\| < \delta$ implies orbital stability of $\mathbf{\Phi}_t^p(\mathbf{x})$, given that $d(\mathbf{\Phi}_t^p(\mathbf{x}(t_0)), \Gamma) < \epsilon$ for all $t \geq t_0$. Figure 4.1(d) schematically illustrates the concept of orbital stability.

Asymptotic orbital stability may also be defined analogously by conjugating the concepts of asymptotic (Sec. 4.1.3) and orbital stabilities, for the description of the stability of limit cycles (i.e., closed orbits which attract nearby trajectories) [21] often exhibited by dissipative dynamical systems.

4.1.5. Structural Stability

A pair of dynamical systems is referred to as *topologically orbitally equivalent* if there exists a homeomorphism which transforms the family of trajectories of one system into that of the other, while preserving the direction of motion. Loosely defined, if one of the systems is considered to be a perturbed version of the other, then the latter is said to be *structurally stable*. We refer the reader to Ref. [1] for more precise details on the concept of *structural stability*.

We shall primarily be concerned with the Lyapunov/asymptotic stability of dynamical systems considered in this dissertation. In the following, we shall introduce the traditional methods of *linear stability analysis*, *Lyapunov functions* and the more recently introduced measure of *basin stability* in this regard for analysing the stability of invariant sets of a dynamical system.

4.1.6. Linear Stability Analysis

Consider a dynamical system of the type described by Eq. (2.3) with an equilibrium at $\mathbf{x}^*$. Initiating the system from $\mathbf{x}^*$ implies that it will forever remain there, until acted upon by external perturbations. The equilibrium is classified as asymptotically stable (Sec. 4.1.3) if any deviations of the system from its equilibrium state eventually die out. However, for infinitesimal perturbations, the behaviour of the system in the *local* neighbourhood of the equilibrium state can be assessed via linear stability analysis [24]. In this regard, we now state the *first method of Lyapunov* comprising the assessment of the linear stability of the equilibrium at $\mathbf{x}^*$ [1, 24, 36]:

Theorem. Let $\mathbf{J} \equiv \frac{\partial \mathbf{F}}{\partial \mathbf{x}}|_{\mathbf{x}=\mathbf{x}^*}$ represent the Jacobian of a continuous-time dynamical system described by Eq. (2.3), evaluated at the equilibrium $\mathbf{x}^*$. Then, $\mathbf{x}^*$ is classified as asymptotically stable if all the eigenvalues of $\mathbf{J}$ are negative. Similarly, for a discrete-time dynamical system described by Eq. (2.4), its equilibrium $\mathbf{x}^*$ is classified as asymptotically stable if all the eigenvalues of $\mathbf{J}$ are strictly smaller than 1.

4.1.7. Lyapunov Stability Criterion

The first method of Lyapunov is useful while investigating the (local) stability of equilibria of dynamical systems against infinitesimal perturbations. However, it does not guarantee the stability of equilibria in the face of non-infinitesimal (large) perturbations. In this context, the *second method of Lyapunov*, also referred to as the *Lyapunov stability criterion* provides for the assessment of the (Lyapunov) stability (Sec. 4.1.2) of an equilibrium against non-infinitesimal perturbations [1, 36]. In this regard, we now state the second method of Lyapunov [1, 36]:

Theorem. Consider a continuous-time dynamical system described by Eq. (2.3) having an equilibrium at $\mathbf{x}^* = 0$ (without loss of generality). The system is stable in the sense of Lyapunov (Sec. 4.1.2) with respect to the equilibrium $\mathbf{x}^*$, given that there exists a scalar-valued function $\mathbb{V}(\mathbf{x}) : \mathbb{R}^d \rightarrow \mathbb{R}$ defined on $\mathbf{x} \in V$ such that

(A) $\mathbb{V}(\mathbf{x}^*) = 0$,

(B) $\mathbb{V}(\mathbf{x}) > 0, \forall\, \mathbf{x} \in V$ and $\mathbf{x} \neq \mathbf{x}^*$,

(C) $\dot{\mathbb{V}}(\mathbf{x}) = \sum\limits_{i=1}^{d} \frac{\partial \mathbb{V}(\mathbf{x})}{\partial x_i} F_i(\mathbf{x}) = (\nabla \mathbb{V}) \cdot \mathbf{F} \leq 0, \forall\, \mathbf{x} \in V$ and $\mathbf{x} \neq \mathbf{x}^*$.

$\mathbb{V}(\mathbf{x})$ is called a *Lyapunov function*. Further, note that given the (negative semi-definite) condition (C) is replaced by the following (negative definite) condition:

(D) $\dot{\mathbb{V}}(\mathbf{x}) < 0, \forall\, \mathbf{x} \in V$ and $\mathbf{x} \neq \mathbf{x}^*$,

the system is then asymptotically stable with respect to the equilibrium $\mathbf{x}^* = 0$.

Similarly, for a discrete-time dynamical system described by Eq. (2.4), its equilibrium $\mathbf{x}^* = 0$ (again, without loss of generality) is asymptotically stable (Sec. 4.1.3) given that there exists a scalar-valued function $\mathbb{V}(\mathbf{x}) : \mathbb{R}^d \rightarrow \mathbb{R}$ defined on $\mathbf{x} \in V$ such that

(A) $\mathbb{V}(\mathbf{x}^*) = 0$,

(B) $\mathbb{V}(\mathbf{x}) > 0, \forall\, \mathbf{x} \in V$ and $\mathbf{x} \neq \mathbf{x}^*$,

(C) $\Delta\mathbb{V}(\mathbf{x}) = \mathbb{V}(\mathbf{x}(t)) - \mathbb{V}(\mathbf{x}(t-1)) < 0, \forall\, \mathbf{x} \in V$ and $\mathbf{x} \neq \mathbf{x}^*$,

(D) $\mathbb{V}(\mathbf{x}) \rightarrow \infty$, as $\|\mathbf{x} - \mathbf{x}^*\| \rightarrow \infty$.

The Lyapunov stability criterion was a ground breaking discovery concerning the analysis of non-local stability. However, given that there is no systematic process for designing Lyapunov functions for any arbitrary (dissipative) dynamical system, it poses a major drawback to the scope of this approach. In fact, as in the words of Prof. Steven H. Strogatz - "divine inspiration is usually required" to come up with such functions [37]. Thereafter, in the following, we shall

address this problem of the assessment and quantification of multistability from a point of view where we do not encounter such impediments as mentioned above. In this regard, we shall soon define and contemplate on the more recently introduced measure of *basin stability* for analysing the stability of invariant sets of a dynamical system against non-infinitesimal perturbations. However, we shall now briefly recapitulate the concept of attractors in a dissipative dynamical system and their corresponding *basins of attraction*, as these entities play a vital role in understanding the long-term behaviour of the associated systems as well as their stability and resilience.

4.1.8. Attractors and their Basins of Attraction

An *attractor* is roughly defined as a set of points which attracts nearby trajectories, i.e., to converge onto it. We define an attractor as a closed set $\mathcal{A}$ ($\mathcal{A} \subseteq \mathbf{X}$) characterized by the following properties [37]:

(A) $\mathcal{A}$ is forward invariant under $\mathbf{\Phi}_t$: if $\mathbf{x}(t_0) \in \mathcal{A}$ then $\mathbf{\Phi}_t(\mathbf{x}(t_0)) \in \mathcal{A}$, $\forall\, t \geq t_0$.

(B) $\mathcal{A}$ attracts an open set of initial conditions: there exists an open set U such that for all $\mathbf{x}(t_0) \in U$, $\mathbf{x}(t)$ enters $\mathcal{A}$ as $t \to \infty$. In other words, $\mathcal{A}$ attracts trajectories starting sufficiently close to it (inside U). The largest possible U for a particular attractor $\mathcal{A}$ is called its *basin of attraction* and denoted by $\mathcal{B}(\mathcal{A})$.

(C) $\mathcal{A}$ is minimal: there is no proper (non-empty) subset of $\mathcal{A}$ satisfying the properties (A) and (B) above.

Stable equilibrium points, limit cycles, quasi-periodic and chaotic attractors constitute notable examples of attractors prevalently observed in dynamical systems [37].

4.1.9. Multistability in Dynamical Systems

Nonlinear dissipative dynamical systems exhibit a great variety of different long-term behaviours. While many such systems possess only one attractor (and are referred to as *monostable* systems), systems exhibiting a multitude of coexisting attractors are also widely prevalent [4, 5]. This coexistence of several possible final stable states (attractors and their respective basins of attraction) for a given set of system parameters comprises the phenomenon of *multistability* [4, 5].

The ubiquity of dynamical systems exhibiting multistability can hardly be further exaggerated. The first account of multistability was in the context of visual perception [38]. However, the preliminary experimental evidence of the possibility of coexistence of attractors is credited to Arecchi and his co-workers [39, 40]. Besides its prevalence in nature, multistability has been thereafter widely

observed in different arenas of science (such as physics, chemistry, biology, economy, etc.) and engineering (cf. [4, 5] and references therein). The human brain [41], ecosystems [42], ice sheets [43], optical ring cavities [44], time-delay systems [EP1], synthetic genetic networks [45], chemical oscillators [46], etc. constitute notable examples among a large body of multistable systems [5]. Additionally, different classes of systems which exhibit multistability such as weakly dissipative, coupled, delayed feedback, parametrically excited, stochastic, etc. have been identified (cf. [4, 5] and references therein).

The long-term dynamics corresponding to one of the different attractors a multistable system converges to, is crucially governed by its initial condition [5]. As discussed earlier, this set of initial conditions giving rise to trajectories converging to the same attractor comprises its basin of attraction (Sec. 4.1.8). Therefore, there exists an intricate relationship between the possibility of observing one of the coexisting asymptotic states and its respective basin of attraction. Likewise, given a dynamical system operating in one of its multiple stable states, the stability of operation in the respective state in the face of non-infinitesimal random perturbations is closely associated with the structure of the basin of attraction of the respective state. In fact, the presence of noise or any external perturbation in many practical dynamical systems is capable of switching the system to (the basin of attraction of) an alternative stable state [4, 5]. In this context, the issue of control of multistability studied by Pisarchik and many others (cf. [5] and references therein) is particularly relevant for achieving the desired system performance. Naturally, the abundance of multistable dynamical systems in the real-world calls for an appropriate quantification of the respective stability (and control) of the multiple stable states/attractors of such systems. In this regard, we next describe the concept of *basin stability* which utilizes the volumes of the basins of attraction in quantifying the stability of the respective attractors in the face of random perturbations [9].

4.1.10. Basin Stability

Consider a dynamical system of the type described by Eq. (2.2):

$$\mathbf{x}(t) = \mathbf{\Phi}_t(\mathbf{x}(t_0)), \tag{2.2}$$

exhibiting M stable attractors $\mathcal{A}_i$ $(i = 1, 2, \ldots, M)$ in its state space $\mathbf{X}$. For the definitions to follow, we consider attractors as compact minimal invariant sets $\mathcal{A}_i \subseteq \mathbf{X}$ such that their respective basins of attraction $\mathcal{B}(\mathcal{A}_i)$ $(i = 1, 2, \ldots, M)$ have positive Lebesgue measure [47].

As noted earlier, the non-local stability of the various attractors of a system can be related to the structure of their respective basins of attraction. In this regard, Wiley et al. [8] have suggested utilizing the volume of the basin of attraction as a measure of the likelihood of the system (when started from a random initial condition) to *arrive* at the corresponding attractor. Menck et al. [9]

have suggested a novel extension of the aforementioned concept by drawing a relationship between the volume of the basin of attraction and the likelihood of *returning* to the corresponding attractor, following non-infinitesimal perturbations. In this regard, Menck et al. have proposed the measure of *basin stability* (BS) [9] as an answer to the question of *how stable* an attractor of a dynamical system is, in the face of non-infinitesimal perturbations.

For any attractor $\mathcal{A}_i$ $(i = 1, 2, \ldots, M)$, we now provide the formal definition of BS. In doing so, we consider that the system resides on the attractor $\mathcal{A}_i$, when it is affected by a random perturbation at time t_0 which pushes the system to a state $\mathbf{x}(t_0)$. We assume that the perturbed state $\mathbf{x}(t_0)$ is drawn from a probability distribution $\rho(\mathbf{x})$ with measure μ on $\mathbf{X}$, such that $\rho(\mathbf{x})\, d\mathbf{x}$ represents the likelihood that the system is perturbed to a state between $\mathbf{x}$ and $\mathbf{x} + d\mathbf{x}$. A representative example of such a measure that is also frequently resorted to during the course of this dissertation is one where ρ is considered to be a uniform distribution over a bounded region $\mathcal{Q}$ of the state space $\mathbf{X}$. This bounded region $\mathcal{Q}$ is referred to as the *reference subset*, in accordance with the terminology used by Menck et al. [9].

Formally, the BS of any given attractor $\mathcal{A}_i$ $(i = 1, 2, \ldots, M)$ of a multistable dynamical system (described by Eq. (2.2)) is defined as [9, 13]

$$S_B(\mathcal{A}_i) := \mu(\mathcal{B}(\mathcal{A}_i)) = \int \chi_{\mathcal{B}(\mathcal{A}_i)}(\mathbf{x})\ \rho(\mathbf{x})\ d\mathbf{x}, \tag{4.1}$$

where $\chi_{\mathcal{B}(\mathcal{A}_i)}(\mathbf{x}) = 1$ if the state $\mathbf{x}$ belongs to the basin of attraction $\mathcal{B}(\mathcal{A}_i)$ of the attractor $\mathcal{A}_i$ and $\chi_{\mathcal{B}(\mathcal{A}_i)}(\mathbf{x}) = 0$ otherwise. Again, $\rho(\mathbf{x})$ is the density of states in state space that the system may be pushed to via large perturbations, with $\int_{\mathbf{x}} \rho(\mathbf{x})\ d\mathbf{x} = 1$, where the integral is taken over the entire state space. In order to avoid terminological confusion, we emphasize that ρ is not the invariant density of the attractors. Thus, $S_B(\mathcal{A}_i) \in [0, 1]$ $(\forall\, i = 1, 2, \ldots, M)$ such that $S_B(\mathcal{A}) = 1$ for a *globally stable* attractor $\mathcal{A}$.

4.1.10.1. Numerical Estimation of Basin Stability

In general, volume integrals such as those involved in the calculation of BS (Eq. (4.1)) pose problems for high-dimensional systems. We thus estimate BS numerically using a Monte Carlo (rejection sampling) method [48, 49]. Below, we present the algorithm for estimating BS of any attractor $\mathcal{A}_i$ $(i = 1, 2, \ldots, M)$ of the system in Eq. (2.2):

(i) Draw a sample of I_C initial conditions distributed according to ρ (Sec. 4.1.10).

(ii) For each initial condition, start the system from the same and evolve it in time until it is clear whether and which attractor the system converges to.

(iii) Count the number F_C of initial conditions that arrive at the attractor $\mathcal{A}_i$.

(iv) Estimate the BS of attractor $\mathcal{A}_i$ as

$$\hat{S}_B\left(\mathcal{A}_i\right) = \frac{F_C}{I_C}. \tag{4.2}$$

Since, the above estimation of BS comprises I_C independent repeated Bernoulli trials with probability of success $S_B\left(\mathcal{A}_i\right)$, the estimate $\hat{S}_B\left(\mathcal{A}_i\right)$ entails a standard error of $\sqrt{\frac{S_B(\mathcal{A}_i)(1-S_B(\mathcal{A}_i))}{N}}$ due to sampling, which is independent of the overall dimensionality d of the system [9]. Note that for even $I_C = 500$ initial conditions, the standard error is less than 0.023 implying that the scope of BS is not prone to the curse of dimensionality.

As mentioned earlier, linear stability analysis (Sec. 4.1.6) is too local in state space to investigate the stability of a dynamical system against large perturbations or shocks. At the same time, there is no systematic way to design Lyapunov functions (Sec. 4.1.7), with further impediments when encountering high-dimensional systems. On the other hand, BS quantified in a non-local and nonlinear fashion, irrespective of the dimensionality of a system, is not subject to the aforementioned constraints associated with linear stability analysis and Lyapunov functions.

4.2. Resilience Concepts

The concept of *resilience* [15] was introduced into the ecological literature by Crawford S. Holling in 1973 to capture the capacity of natural systems to persist against disturbances, perturbations, or changes in ecosystem variables, while responding by quickly recovering from them.

There are at least two different definitions of resilience of a system, depending on the assumption of the presence of one or multiple stable states in the system. We briefly review these two definitions of resilience, prior to utilization of the concepts later in Chapters 6 and 7.

4.2.1. Engineering Resilience

The first definition due to Pimm [50] termed *engineering resilience* [16] by Holling, focussing on stability near an equilibrium state, is measured using the speed of return to its equilibrium, following a perturbation. It is also measured as the inverse of return time [51].

For example, consider the 1-dimensional system $\dot{x} = -\lambda x$ resting at its equilibrium $x^* = 0$, when a perturbation drives the system to a perturbed state δx. For $\lambda > 0$, the equilibrium is exponentially stable (Sec. 4.1.3.1) implying the return of the system $\left(\text{as } x\left(t\right) = \delta x\, e^{-\lambda t}\right)$ to the equilibrium. In this case, the engineering resilience of the system is determined by its rate of return λ to the equilibrium

x^*, such that the higher the value of λ, the higher is the engineering resilience of the system (with respect to its equilibrium at x^*).

4.2.2. Ecological Resilience

The second definition due to Holling [15] termed *ecological resilience* [16] is the capacity of a system to absorb disturbance and reorganize while undergoing change so as to still retain essentially the same function, structure, identity and feedbacks [14]. It emphasizes upon conditions far from any steady state, where instabilities can flip a system into another regime, i.e., to another stability domain [16]. In this case, the resilience of a system is measured by its capacity to remain in the same basin of attraction in the face of perturbations.

The two definitions of resilience reflect the different aspects of stability being emphasized. Engineering resilience implicitly assumes global stability, i.e., the existence of only one equilibrium state, or, if other operating states exist, they should be avoided by applying safe guards [52]. On the other hand, ecological resilience presumes the existence of multiple stable states and the tolerance of the system to disturbances that facilitate transitions among the stable states.

Walker et al. [14] identifies 'latitude' (L), 'resistance' (R) and 'precariousness' (Pr) as the three crucial aspects of ecological resilience. Below, we turn to the definitions of L, R and Pr proposed by Walker et al. [14]:

(A) *Latitude* L describes "the maximum amount the system can be changed before losing its ability to recover; basically the width of the basin of attraction" [14].

(B) *Resistance* R refers to "the ease or difficulty of changing the system; related to the topology of the basin - deep basins of attraction indicate that greater forces or perturbations are required to change the current state of the system away from the attractor" [14]. Pimm defined resistance as "the degree to which a variable is changed following a perturbation", and resistant systems as ones which "change less under a given disturbance" [50].

(C) *Precariousness* Pr addresses "the current trajectory of the system, and how close it currently is to a limit or threshold which, if breached, makes recovery difficult or impossible" [14].

In addition, the resilience of a multi-scale system is determined by the cross-scale interactions between the states and dynamics of its subsystems at different scales [14]. As a result, a fourth aspect of ecological resilience, namely, *panarchy* is utilized to capture this description. However, only the utilization of L, R and Pr (i.e., excluding panarchy) will be sufficient for the developments to follow in this dissertation.

The exemplary stability landscape (comprising the basins of attraction of all stable states of a system and the boundaries separating them) in Fig. 4.2 serves as

a heuristic device for illustrating the original conceptualizations of L, R and Pr as proposed by Walker et al. [14] for the basins of attraction of a dynamical system consisting of two state variables. We refer the reader to the review by Beisner et al. [53] for further understanding of the metaphor of stability landscapes as used in ecology.

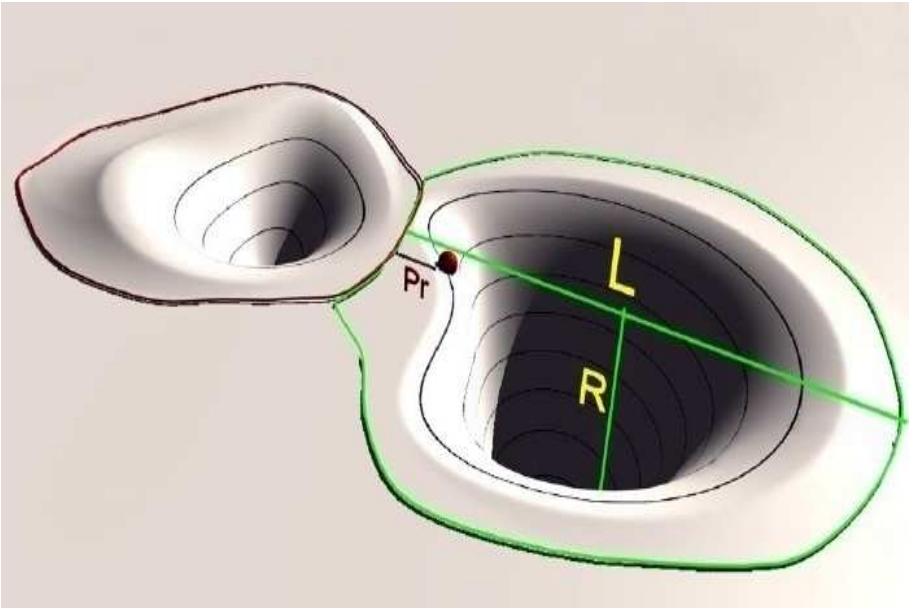

Figure 4.2.: Stability landscape of a bistable dynamical system consisting of two state variables (forming the two axes of the stability landscape while resistance, i.e., the depth of the basin of attraction constituting the vertical axis) showing the current state of the system (red dot) and three aspects of resilience: $L =$ Latitude, $R =$ Resistance, and $Pr =$ Precariousness as defined by Walker et al. [14] (adapted from Leuteritz et al. [54]). A deep basin of attraction (R) or, more precisely, a steeper slope at a point indicates that larger forces or perturbations are required to change the state of the system around that point. The bottoms of each of the two basins (either of which the system equilibrates to) are heuristic representations of the attractors of the bistable system while the red and green lines mark the basin boundaries. The smaller (larger) spacing between successive black contour lines in the neighbourhood of a particular point implies a steeper (shallower) slope of R or equivalently, greater (lesser) management efforts required to move the system around that point.

A central theme of this dissertation is the development of stability and resilience measures for quantifying the robustness of *synchronized* dynamics on complex oscillator networks. In this regard, we now briefly discuss the emergent phenomenon of *synchronization* [11], and thereafter review the framework of *master stability function* [12] for investigating the *synchronizability* of a complex network.

4.3. Synchronization of Complex Dynamical Networks

The word *synchronization*, derived from a conjugation of the Greek terms - $\sigma\acute{\upsilon}\nu$ (*syn*) meaning "same or common" and $\chi\rho\acute{o}\nu o\zeta$ (*chronos*) meaning "in time", literally translates to "occurring in the same time" [11]. Thereafter, synchronization implying the coordination of the different components of a system for their operation in unison, refers to a wide variety of phenomena in nature and society [11].

Christiaan Huygens, a 17^{th} century Dutch researcher has been credited with the first observation and description of the phenomenon of synchronization [11]. While laying sick in bed, Huygens observed the motion of two pendulum clocks suspended from hooks embedded in the same wooden beam and that their oscillations coincided perfectly such that the pendulums always moved in opposite directions. Further, he noted that following a disturbance, the pendulums adjusted their movements so as to re-establish their synchronized oscillation. He even attributed the conformity in the rhythms of the two clocks to their interaction via the hardly perceptible motion of the wooden beam. Contemporary scientific terminology would refer to this scenario as *anti-phase synchronization* between the clocks via their *coupling* through the wooden beam. Since its identification by Huygens, synchronization phenomena have been observed and reported in a large variety of systems, contexts and disciplines [11]. Interestingly however, in the due course of time, it has been explicated that seemingly different but synchronization-based phenomena actually have universality in their characteristic features.

Pikovsky, Rosenblum and Kurths [11] have more formally described synchronization as an "adjustment of rhythms of oscillating objects due to their weak interaction". We can further describe such "oscillating objects" as systems that are driven into oscillation by an energy source and are stable in their oscillations to small perturbations. Such systems which oscillate even in isolation, until their source of energy runs out are referred to as *self-sustained oscillators*. In the presence of several such oscillating objects, there exists the possibility of interactions among them. Such interactions are referred to as *couplings* among the oscillators, and the *coupling strength* describes how strong the interactions are.

Generally, a group of oscillators is said to be synchronized when each oscillators' frequency has locked onto the same value as all the others [11, 55, 56]. *Chaotic systems*, characterized by sensitive dependence upon initial conditions are expected to defy synchronization as the (infinitesimally different) trajectories from even two such identical systems (exhibiting *deterministic chaos*) would diverge quickly, although they share the same attractor [57]. Interestingly however, when weakly coupled together and initiated from heterogeneous initial conditions, certain chaotic systems have also been shown to exhibit *phase synchronization* [58]. In fact, in addition to locking of phases, coupled identical chaotic oscillators have been found to exhibit *complete synchronization*, wherein systems follow the same

trajectory in time [57].

Besides investigating the influence of the intrinsic dynamical properties of (isolated) oscillators on their ability to synchronize, researchers have also studied the relation between the *nature of coupling* between oscillators and their tendency for synchronization [11, 59]. Many systems of practical interest comprise large populations of coupled oscillators, such that their interactions can be appropriately represented as a complex network. The conjugation of nonlinear dynamics with network theory has provided particularly novel insights into relationships between network topology and dynamical processes (such as synchronization) taking place on complex networks of dynamical systems [11, 60–62]. A central focus of this dissertation is the investigation of stability of synchronized dynamics against perturbations of complex dynamical networks. In a related context, we now review the phenomenal work of Pecora and Carroll [12] proposing the framework of *master stability function* for deducing the local stability of the completely synchronized state in complex oscillator networks.

4.3.1. Master Stability Function Framework

In the following, we briefly review the framework of *master stability function* (MSF) [12] and the traditional quantifier of *synchronizability* of a complex network. Consider a network of N identical oscillators where the isolated dynamics of the i-th oscillator is described by

$$\dot{\mathbf{x}}^i = \mathbf{F}\left(\mathbf{x}^i\right);\, \mathbf{x}^i \in \mathbb{R}^d,\, i = 1,\, 2,\, \ldots,\, N, \tag{4.3}$$

and coupling is established via an output function $\mathbf{H} : \mathbb{R}^d \to \mathbb{R}^d$ (identical for all i). The topology of interactions is captured by the adjacency matrix $\mathbf{A}$, where $A_{ij} = 1$ if nodes i and $j\,(\neq i)$ are connected while $A_{ij} = 0$ otherwise (Sec. 3.1). The dynamical equations of the networked system read

$$\begin{aligned}\dot{\mathbf{x}}^i &= \mathbf{F}\left(\mathbf{x}^i\right) + \epsilon \sum_{j=1}^{N} A_{ij}\left[\mathbf{H}\left(\mathbf{x}^j\right) - \mathbf{H}\left(\mathbf{x}^i\right)\right] \\ &= \mathbf{F}\left(\mathbf{x}^i\right) - \epsilon \sum_{j=1}^{N} L_{ij}\mathbf{H}\left(\mathbf{x}^j\right)\end{aligned} \tag{4.4}$$

where ϵ represents the overall coupling strength and $\mathbf{L}$ is the graph Laplacian (Sec. 3.2.1) such that $L_{ij} = -A_{ij}$ if $i \neq j$ and $L_{ii} = k_i = \sum_{j=1}^{N} A_{ij}$ is the degree of node i. Since the Laplacian matrix $\mathbf{L}$ is symmetric, its eigenvalue spectrum $(\lambda_1,\, \lambda_2,\, \ldots,\, \lambda_N)$ is real and ordered as $0 = \lambda_1 < \lambda_2 \leq \ldots \leq \lambda_N$, assuming the network is connected [10]. Further, L has zero row sum by definition, guaranteeing the existence of a completely synchronized state, $\mathbf{x}^1\,(t) = \mathbf{x}^2\,(t) = \ldots = \mathbf{x}^N\,(t) = \mathbf{s}\,(t)$ as a solution of Eq. (4.4). Starting from heterogeneous initial

conditions, the oscillators (asymptotically) approach (and thus evolve on) the synchronization manifold $\mathbf{s}(t)$ corresponding to the solution of the uncoupled dynamics of the individual oscillators in Eq. (4.3) ($\dot{\mathbf{s}} = \mathbf{F}(\mathbf{s})$). The local stability of the completely synchronized state following an infinitesimal perturbation ξ can be determined by analysing the *master stability equation* [12]

$$\dot{\xi} = [D\mathbf{F}(\mathbf{s}) - \alpha D\mathbf{H}(\mathbf{s})]\,\xi, \tag{4.5}$$

where $\alpha \in \mathbb{R}$ is a parameter, $D\mathbf{F}$ and $D\mathbf{H}$ are the Jacobian matrices of $\mathbf{F}$ and $\mathbf{H}$ computed along the trajectory on $\mathbf{s}$, respectively. The largest Lyapunov exponent of Eq. (4.5) computed as a function of the parameter α and denoted by $\Lambda_{max}(\alpha)$ is referred to as the *master stability function* [12]. The synchronized state of the networked system in Eq. (4.4) is locally stable if $\Lambda_{max}(\epsilon\lambda_i) < 0$ for $\forall\ i = 2, \ldots, N$.

For a number of previously studied cases with different oscillator dynamics $\mathbf{F}$ and their respective coupling functions $\mathbf{H}$, the MSF $\Lambda_{max}(\alpha)$ has been found to be negative only in a single finite convex interval, $\alpha_1 < \alpha < \alpha_2$ [61]. This case of bounded MSFs requires $\epsilon\lambda_i \in (\alpha_1, \alpha_2)$ for $\forall\ i = 2, \ldots, N$ as a necessary condition for the local stability of the synchronized state of the network. More explicitly, this condition can be stated as

$$\alpha_1 < \epsilon\lambda_2 \leq \epsilon\lambda_3 \leq \ldots \leq \epsilon\lambda_N < \alpha_2. \tag{4.6}$$

For certain values of ϵ, this condition can be fulfilled when the *eigenratio* R satisfies

$$R \equiv \frac{\lambda_N}{\lambda_2} < \frac{\alpha_2}{\alpha_1}. \tag{4.7}$$

Note, that the right hand side of Eq. (4.7) depends on the dynamics of the individual oscillators $\mathbf{F}$ as well as their coupling configuration $\mathbf{H}$, whereas its left hand side comprising the eigenratio R depends solely on the structure of the network. Evidently, in such cases of bounded MSFs, the smaller the eigenratio R, the easier it is to satisfy the condition in Eq. (4.7). Thus, irrespective of $\mathbf{F}$ and $\mathbf{H}$, this condition has been extensively used to characterize the *synchronizability* of a network such that the lower the value of the eigenratio R, the more synchronizable the network and vice versa [61, 63–79].

4.3.2. Synchronizability and Basin Stability

The development of the concept of MSF has invited a host of studies investigating possible relationships between network topology and synchronizability [61]. In this regard, Hong et al. [80] found that networks with more random topologies favour synchronizability. However, real-world complex systems such as neural networks and power grids [17] where synchronization is particularly relevant,

have been found to exhibit small-world properties (Sec. 3.3.1.3), characterized by more regularity in their topological structure. These observations posed a long-standing puzzle concerning the robustness of synchronization on complex networks. Note that the theoretical insights emanating from the applications of MSF only relate to the stability of synchronization against small perturbations. However, real-world complex networks are prone to large perturbations. Subsequently, the concept of BS (Sec. 4.1.10), tailored towards investigating stability in the face of large perturbations, proved particularly useful in resolving the aforementioned long-standing puzzle.

Interestingly, Menck et al. [9] have shown that BS exhibits improvements with topological regularity, while being optimized particularly in the small-world regime. They have prompted at the possibility of a contest between linear stability favouring topological randomness, and BS promoting topological regularity, during the topological evolution of real-world synchronizing networks. They have thus conjectured that this couple of counteracting factors have subsequently resulted in a topological trade-off, thereby bestowing small-world properties to real-world synchronizing networks. However, we shall later revisit this claim in Chapter 9 and illustrate that it can be challenged.

Part II.

Methodological Developments and Applications

Chapter 5.

Multiple-node Basin Stability in Complex Dynamical Networks

5.1. Summary

As mentioned earlier, dynamical entities interacting with each other on complex networks often exhibit multistability. The stability of a desired steady regime (e.g., a synchronized state) to large perturbations is critical in the operation of many real-world networked dynamical systems such as ecosystems, power grids, the human brain, etc. This necessitates the development of appropriate quantifiers of stability of multiple stable states of such systems. In Chapter 4, we described the measure of basin stability (BS, Sec. 4.1.10) for quantifying the stability of the different coexisting attractors of a multistable complex dynamical system. In this chapter, we develop on the concept of BS in proposing here the framework of *multiple-node basin stability* (MNBS) for gauging the global stability and robustness of networked dynamical systems in response to non-infinitesimal perturbations simultaneously affecting multiple nodes of a system. The framework of MNBS provides an estimate of the critical number of nodes that, when simultaneously perturbed, significantly reduce the capacity of the system to return to the desired stable state. Further, this methodology can be applied to estimate the minimum number of nodes of the network to be controlled or safeguarded from external perturbations to ensure proper operation of the system. MNBS can also be utilized for probing the influence of spatially localized perturbations or targeted attacks to specific parts of a network. We demonstrate the potential of MNBS in assessing the stability of the synchronized state in a deterministic scale-free network of Rössler oscillators and a conceptual model of the power grid of the United Kingdom with second-order Kuramoto-type nodal dynamics. This chapter is based on the associated publication P1 and the following sections will closely follow the respective publication.

5.2. Introduction

Many complex systems involve large collections of dynamical units interacting with each other on complex networks [60, 81]. Coupled map lattices constitute

the simplest classes of such systems displaying multistability on account of the formation of clusters [82]. Other important examples include coupled weakly dissipative systems, logistic maps, Hénon maps, genetic elements, or mutually coupled semiconductor lasers (cf. [4] and references therein). Such coupled dynamical systems exhibit a great variety of emergent phenomena with synchronization (Sec. 4.3) being the most intensively reported and practically relevant one. In fact, the ubiquity of synchronization in networked dynamical systems can hardly be further exaggerated, and it plays a central role across various disciplines such as biology, ecology, climatology, sociology, engineering, etc. [11, 61]. The coexistence of synchronized and desynchronized dynamics in such systems is a typical case of bistability. In this regard, the presence of the fully synchronized state (for homogeneous initial conditions) and the chimera state (for particular heterogeneous initial conditions) in networks of oscillators with non-local coupling has gathered a lot of recent attention [83, 84]. It is essential to appropriately assess and quantify multistability, particularly, the robustness of the synchronized state to arbitrary perturbations of such coupled dynamical systems. In this direction, the framework of master stability function (MSF) (Sec. 4.3.1) as an extension of the linear stability concept to assess the stability of the completely synchronized state in coupled networks was a considerable development, but still locally restrictive to small perturbations. The application of basin stability (BS, Sec. 4.1.10) to assessing the stability of synchronized dynamics and its extension to the concept of single-node basin stability (SNBS) in quantifying the contributions of individual nodes to the overall stability of the synchronized state has been a major advancement and complements linear stability analysis substantially [9, 13].

SNBS of a node under investigation corresponds to the probability of the system (operating in the desired stable state) to return to its stable state after that particular node has been hit by a non-infinitesimal perturbation [13]. We reserve a formal definition of SNBS to Sec. 5.3.2. However, in many practical situations, disturbances affect a group of nodes of the network, significantly hampering its return to the desired operational state. Some of the most relevant examples are the collapse of ecological networks due to spatial perturbations [85], cascading failures in a power transmission grid on account of the breakdown of a few nodes [86], or epileptic seizures triggered by random perturbations of neural networks [87]. Subsequently, it is essential to develop a framework for assessing the robustness of networked dynamical systems to withstand perturbations simultaneously hitting several nodes of the system. In addition, such a framework should provide a critical number of nodes that when simultaneously perturbed significantly reduce the probability of the system to continue operating in the desired regime. Further, such a methodology could also solve the associated problem of estimating the minimum number of nodes of the network that need to be safeguarded from external perturbations to ensure proper functionality of the system. As a crucial first step in this direction, we extend here the concept of

SNBS to the framework of *multiple-node basin stability* (MNBS). We provide a formal definition of MNBS in Sec. 5.3.3.

Previous studies on the robustness of complex networks have mainly focused on static (topological) properties of networks and their ability to withstand failures and perturbations on account of the removal of nodes and/or links [86]. In this context, the framework of percolation theory has generated important insights that are useful for the analysis and prediction of resilience of complex networks by deriving a critical threshold for the fraction of nodes that need to be removed for the breakdown of the giant component of a complex network [88, 89]. Recently, Gao et al. [90] considered intrinsic nodal dynamics in developing an analytical framework of a universal resilience function to accurately unveil the resilience of networked dynamical systems. However, their approach considers node, weight and link losses as possible perturbations to the system and not actual non-infinitesimal disturbances to the dynamical state of individual or several nodes of the system, as addressed by SNBS and MNBS, respectively. Also, almost all stability studies assume no knowledge about the nature of perturbations to the system. The framework of MNBS developed here can be applied to probe the influence of spatially localized perturbations or targeted attacks to specific parts of a network, which can be more relevant in practice.

This chapter is further organized as follows: In Sec. 5.3, we outline the general methodology for calculating MNBS for a given networked dynamical system. In Sec. 5.4, we illustrate its application to a deterministic scale-free network of Rössler oscillators and a conceptual model of the power grid of the United Kingdom with second-order Kuramoto-type nodal dynamics. Finally, we present the conclusions of our work in Sec. 5.5.

5.3. Methods

5.3.1. Preliminaries

In the following, we outline the general methodology for estimating SNBS and MNBS values for any networked dynamical system. Consider a network of N oscillators (nodes) where the intrinsic dynamics of the i-th oscillator $\left(\text{represented by the } d\text{-dimensional state vector } \mathbf{x}_i(t) = \left(x_i^1,\, x_i^2,\, \ldots,\, x_i^d\right)^{\mathrm{T}}\right)$ is described by

$$\dot{\mathbf{x}}_i = \mathbf{F}_i\left(\mathbf{x}_i\right), \tag{5.1}$$

where $\mathbf{x}_i \in \mathbb{R}^d$; $\mathbf{F}_i : \mathbb{R}^d \rightarrow \mathbb{R}^d$, $\mathbf{F}_i = \left(F_i^1(\mathbf{x}), F_i^2(\mathbf{x}), \ldots, F_i^d(\mathbf{x})\right)^{\mathrm{T}}$ for $i = 1, 2, \ldots, N$. The dynamical equations of the networked system read

$$\dot{\mathbf{x}}_i = \mathbf{F}_i(\mathbf{x}_i) + \epsilon \sum_{j=1}^{N} A_{ij} \mathbf{H}_{ij}(\mathbf{x}_i, \mathbf{x}_j), \tag{5.2}$$

where ϵ is the overall coupling strength, $\mathbf{A}$ is the adjacency matrix which captures the interactions between the nodes such that $A_{ij} \neq 0$ if node j influences node i and $\mathbf{H}_{ij} : \mathbb{R}^d \times \mathbb{R}^d \rightarrow \mathbb{R}^d$ is an arbitrary coupling function from node j to node i. For the illustrations in this Chapter (Sec. 5.4), we consider identical nodal dynamics ($\mathbf{F}_i = \mathbf{F} \,\forall\, i$), symmetric adjacency matrices ($A_{ij} = A_{ji} = 1$ if nodes i and j are connected and $A_{ij} = A_{ji} = 0$ otherwise) and identical coupling functions ($\mathbf{H}_{ij} = \mathbf{H} \,\forall\, i, j$).

5.3.2. Single-node Basin Stability (SNBS)

Let us assume that the networked dynamical system of Eq. (5.2) has a stable synchronized state. Further, when initiating the system from such a synchronized state, perturbations to even a single node of the system can drive the entire network of oscillators to a desynchronized state. For example, consider the simplest case of two oscillators (each exhibiting one-dimensional nodal dynamics) represented by the state variables $\mathbf{x}_1(t)$ and $\mathbf{x}_2(t)$ such that the synchronized state is described by the fixed point, $\tilde{\mathbf{x}} = (\tilde{\mathbf{x}}_1, \tilde{\mathbf{x}}_2) = (\tilde{\mathbf{x}}_*, \tilde{\mathbf{x}}_*) = (2, 2)$ as illustrated

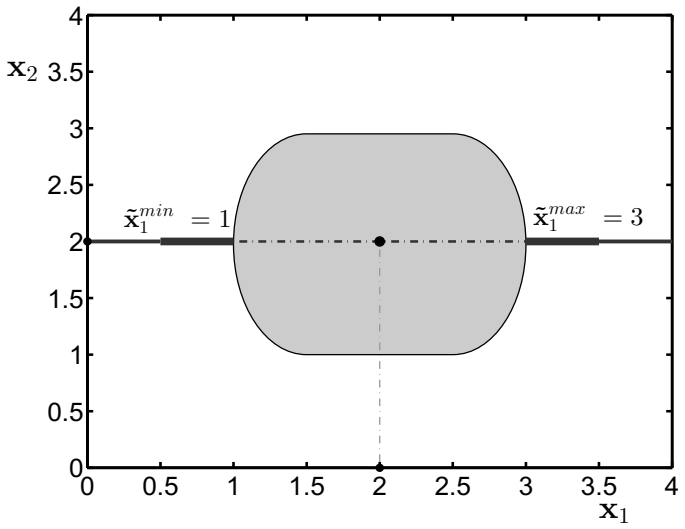

Figure 5.1.: Schematic illustrating the concept of single-node BS. The region inside the box comprises the entire state space of the two-oscillator network.

in Fig. 5.1. Please note that this illustration is purely conceptual. The gray region indicates the basin of attraction of the synchronized state. Let the subspace of the first oscillator be confined between $\mathbf{x}_1^{\min} = 0$ and $\mathbf{x}_1^{\max} = 4$. When initiating the system from the synchronized state, the dashed line (at $\mathbf{x}_2 = 2$) in Fig. 5.1 visualizes the set of perturbations to the first oscillator, after which the network converges back to the synchronized state. On the other hand, the solid lines in Fig. 5.1 indicate the set of perturbations to the first oscillator, which drive the network to the desynchronized state. When initiating the coupled system from the synchronized state, let $\tilde{\mathbf{x}}_1^{\min}$ and $\tilde{\mathbf{x}}_1^{\max}$ be the minimum and maximum admissible perturbed states, respectively, of the first oscillator, for which the coupled system will return to the synchronized state. The SNBS of the first oscillator is the fraction of the one-dimensional volume of the state space of the respective oscillator belonging to the basin of attraction of the synchronized state. In other words, it is the ratio between the length of the dashed line and the lengths of the solid and dashed lines combined, i.e., $\frac{\tilde{\mathbf{x}}_1^{\max} - \tilde{\mathbf{x}}_1^{\min}}{\mathbf{x}_1^{\max} - \mathbf{x}_1^{\min}} = \frac{3-1}{4-0} = \frac{1}{2}$.

Formally, the SNBS of the i-th oscillator is defined as the fraction of the d-dimensional volume of the state space of the oscillator belonging to the $(d \times N)$-dimensional basin of attraction of the synchronized state. In the example presented in Fig. 5.1, $d = 1$ and $N = 2$. Thus, the SNBS of any particular node of the network measures the probability of the system to remain in the basin of attraction of the synchronized state when random perturbations affect only that specific node.

Now, we present details on calculating the SNBS value of the i-th oscillator or node of a network (modelled using Eq. (5.2)). Perturbations to a (networked) dynamical system (and its nodes) are practically confined to a part of the state space that we refer to as the *reference subset*, in accordance with the terminology used by Menck et al. [9] and also explained in Sec. 4.1.10. In the computation of SNBS of a particular node of the network, perturbations to that specific node are realized by giving the respective oscillator initial conditions chosen randomly from the reference subset, while initiating the other oscillators from the synchronized state. For example, in the illustration given in Fig. 5.1, we arbitrarily consider that the dashed line and the thick solid lines (at $\mathbf{x}_2 = 2$) comprise the reference subset of the first oscillator. Put simply, these are the set of all possible initial conditions of the two-node system, which we shall use for calculating the SNBS of the first oscillator. Therefore, as a first step, select a reference subset q of the phase space of the i-th oscillator. Thus, for a network of identical oscillators, $\mathcal{Q} \equiv q^N$ comprises the reference subset of the complete $(d \times N)$-dimensional dynamical system. Below, we present the algorithm for calculating SNBS:

(i) Calculate the synchronization manifold $\tilde{\mathbf{x}}\,(t) = (\tilde{\mathbf{x}}_1,\, \tilde{\mathbf{x}}_2,\, \ldots,\, \tilde{\mathbf{x}}_N)^{\mathrm{T}}$.

(ii) When the attractor corresponding to the synchronized state is not a fixed point, choose $P\ (> 1)$ different points on the synchronization manifold. Otherwise, choose $P = 1$. In the former setting, the value of P as well as the

P different points on the synchronization manifold have to be chosen such that these points sufficiently trace all parts of the attractor corresponding to the synchronized state.

(iii) For a particular value of p ($p = 1, 2, \ldots, P$), perturb the i-th oscillator by uniformly drawing I_C random initial conditions from q, while each time initiating the system from the synchronized state using the p-th point on the synchronization manifold.

(iv) Count the number F_C of initial conditions that arrive at the synchronized state and estimate SNBS of the i-th oscillator ($S_B^1(i,\, p)$) for the p-th point on the synchronization manifold as

$$\hat{S}_B^1(i,\, p) = \frac{F_C}{I_C}. \tag{5.3}$$

(v) Finally, average over p to obtain the (mean) SNBS value of node i,

$$\langle S_B^1(i) \rangle = \frac{1}{P} \sum_{p=1}^{P} \hat{S}_B^1(i,\, p)\,. \tag{5.4}$$

The concept of SNBS is appropriate for extracting the contributions of individual nodes to the overall stability of the synchronized state. Further, it can be utilized to identify particularly vulnerable nodes of the system as well as more resilient ones.

By additionally averaging Eq. (5.4) over all nodes i, we may obtain a mean SNBS value for the network as a whole, denoted as $\langle S_B^1 \rangle$. Note that this property is distinctively different from the "global" BS S_B of Menck et al. [9] as it represents average information related to localized perturbations instead of that affecting the whole network at the same time. In this respect, this distinction is similar to that between the global clustering coefficient (average local property) and network transitivity (global property) in the structural characterization of complex networks [91, 92], discussed earlier in Sec. 3.2.4.

5.3.3. Multiple-node Basin Stability (MNBS)

Now we consider $m\,(\geq 1)$ nodes of the network being simultaneously perturbed such that the individual perturbations are independent of each other. In the following, we present details on calculating the MNBS, hereafter also referred to as *m-node* BS value of the network.

(i) For any particular value of m, generate an ensemble $\{E_j^m\}$ of m-*node sets*, each consisting of m nodes to be simultaneously perturbed. For an N-node network, there exists a possible maximum of $\binom{N}{m}$ of such m-node sets. At this point, MNBS can also be utilized for probing the influence of

spatially localized perturbations or targeted attacks to specific parts of a network by selecting a *specific* m-node set or a small ensemble thereof. For instance, given a spatially embedded network, one could perturb m nodes from a localized region. Here, for any particular value of m, we randomly choose M or $\binom{N}{m}$ (whichever is less) m-node sets, and we leave the explicit investigation of different perturbation configurations as a subject of future research.

(ii) Given a particular j-th m-node set E_j^m of the ensemble, for any particular value of p, collectively perturb the m nodes by uniformly drawing I_C random initial conditions from q^m, while each time initiating the system from the p-th point on the synchronization manifold (Sec. 5.3.2).

(iii) Count again the number F_C of initial conditions that arrive at the synchronized state and estimate the m-node BS $S_B^m\,(E_j,\,p)$ of the j-th m-node set of the ensemble for the p-th point on the synchronization manifold as

$$\hat{S}_B^m\,(E_j,\,p) = \frac{F_C}{I_C}. \tag{5.5}$$

(iv) Finally, average over p as well as over all the m-node sets of the ensemble to obtain the (mean) m-node BS value of the network as,

$$\langle S_B^m \rangle = \frac{1}{\min\left(M,\,\binom{N}{m}\right)} \sum_j \frac{1}{P} \sum_p \hat{S}_B^m\,(E_j,\,p)\,. \tag{5.6}$$

For $m = 1$, we obtain $\langle S_B^1 \rangle$ as described above as a special case.

The total number of subsets of nodes $\binom{N}{m}$ that can be simultaneously perturbed is generally very large, making it computationally extremely expensive to compute MNBS. Therefore, to obtain a computationally feasible estimate of MNBS, we consider a smaller number M $\left(M \ll \binom{N}{m}\right)$ of such m-node sets selected uniformly at random [1].

The framework of MNBS is highly relevant for assessing global stability and robustness of networked dynamical systems in response to non-infinitesimal perturbations simultaneously affecting multiple nodes. Importantly, it provides an estimate of the critical number of nodes (m_{crit}) that when simultaneously perturbed significantly reduces the ability of the system to return to the desired stable state. For the illustrations provided in the remainder of this Chapter (Sec. 5.4), we estimate m_{crit} by setting a threshold value of MNBS $(\langle S_B \rangle_{th})$,

[1] In our calculations, we have implicitly assumed a uniform distribution for the contributions of different m-node sets to the overall BS of a stable state. However, that may not be the case and therefore, it would be an interesting and computationaly challenging task to explore the nature of this distribution. Further, one can also check for the presence of universality in this distribution with respect to local dynamics and network topology.

such that m_{crit} is defined as the minimum value of m for which $\langle S_B^m \rangle \leq \langle S_B \rangle_{th}$. The value of $\langle S_B^m \rangle$ generally falls drastically with an increase in the sizes of the reference subsets of the individual nodes, and it can be potentially small for large reference subsets [2].

5.4. Examples

5.4.1. Deterministic Scale-free Network of Rössler Oscillators

We consider a network of N identical Rössler oscillators, where the autonomous evolution of each individual unit is given by [93]

$$\begin{aligned} \dot{x}^1 &= -x^2 - x^3, \\ \dot{x}^2 &= x^1 + ax^2, \\ \dot{x}^3 &= b + x^3\left(x^1 - c\right). \end{aligned} \tag{5.7}$$

We use the parameter values of $a = b = 0.2$ and $c = 7.0$ for which each uncoupled Rössler oscillator in Eq. (5.7) exhibits chaotic dynamics. We consider diffusive coupling in the x^2-variable between two coupled nodes such that the full dynamical equations of node i (in analogy with Eq. (5.2)) read

$$\begin{aligned} \dot{x}_i^1 &= -x_i^2 - x_i^3, \\ \dot{x}_i^2 &= x_i^1 + ax_i^2 + \epsilon \sum_{j=1}^{N} A_{ij}\left(x_j^2 - x_i^2\right), \\ \dot{x}_i^3 &= b + x_i^3\left(x_i^1 - c\right). \end{aligned} \tag{5.8}$$

We consider an undirected deterministic scale-free topology, introduced earlier in Sec. 3.3.2.1. For the simulations carried out in this section, we generate a deterministic scale-free network developed over 3 generations comprising $N = 81$ nodes.

Single-node Basin Stability

We are interested in the stability of the completely synchronized state, which corresponds to all oscillators following the same trajectory. In this context, we select a reference subset for each node as $q = [-15,\, 15] \times [-15,\, 15] \times [-5,\, 35]$; $\epsilon = 0.8$ is chosen from the stability interval predicted by the MSF (Sec. 4.3.1); $P = 10$ points on the attractor of the completely synchronized state and $I_C = 500$ trials for estimating the (mean) SNBS ($\langle S_B^1 \rangle$) values, using the procedure described in Sec. 5.3.2.

[2] In such situations, the choice of the value of the threshold is also small as we will illustrate using examples in Sec. 5.4.

We calculate and present the $\langle S_B^1 \rangle$ values of all the $N = 81$ nodes in Fig. 5.2(a). Interestingly, all the nodes have similar and relatively high $\langle S_B^1 \rangle$ values (as also evident from the histogram in Fig. 5.2(b)). Figures 5.2(c) and 5.2(d) show the relationship of the $\langle S_B^1 \rangle$ values with the topological features of degree (k, Sec. 3.2.1) and betweenness centrality (bc, Sec. 3.2.3) of the nodes, respectively. Apparently, the $\langle S_B^1 \rangle$ values within any particular generation do not show a strong trend with respect to the k or bc of the nodes. This is further validated by the cross-correlation values of -0.2687 and -0.2108 of $\langle S_B^1 \rangle$ with k and bc, respectively. We summarize our results in Fig. 5.3, which displays the network topology where the size of each node is proportional to the degree, and the colour corresponds to the $\langle S_B^1 \rangle$ value of the respective node.

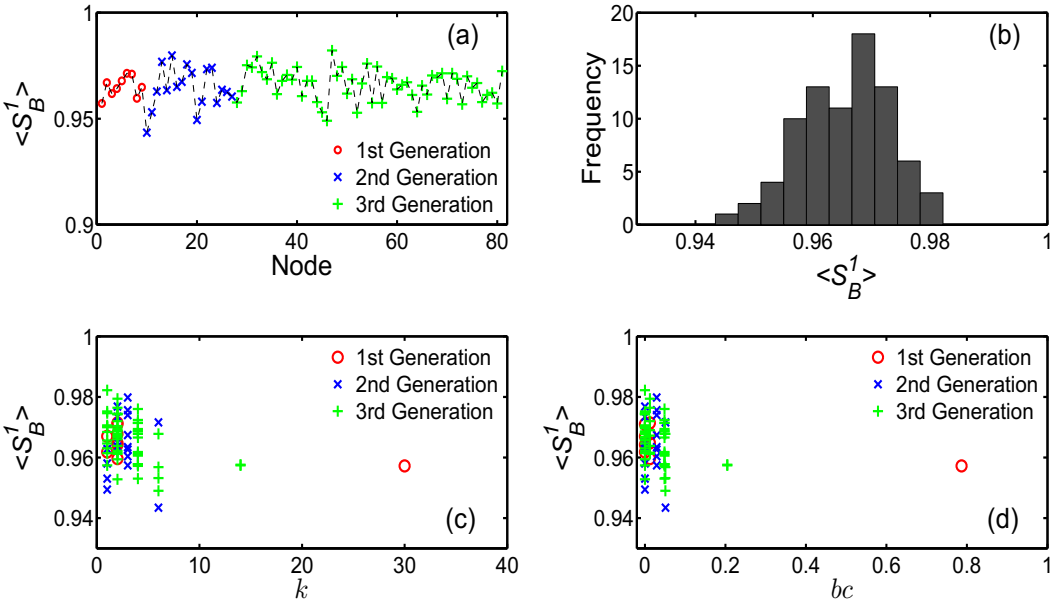

Figure 5.2.: (a) (Mean) SNBS $\langle S_B^1 \rangle$ of all the $N = 81$ nodes of the 3 generations of the undirected deterministic scale-free network of N identical Rössler oscillators. The first 9 nodes comprise the 1^{st} generation, the next 18 nodes the 2^{nd} generation and the final 54 nodes the 3^{rd} generation. (b) Histogram of $\langle S_B^1 \rangle$ of all the $N = 81$ nodes. (c, d) Relationship of $\langle S_B^1 \rangle$ with (c) degree (k) and (d) betweenness centrality (bc) of the nodes, respectively.

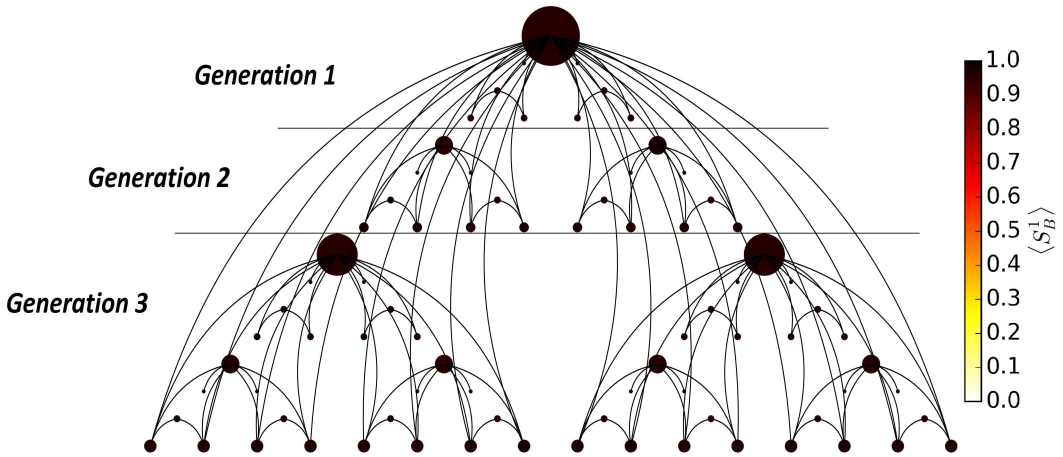

Figure 5.3.: Network topology of the undirected deterministic scale-free network of $N = 81$ identical Rössler oscillators. The size of each node is proportional to the degree and the colour indicates the $\langle S_B^1 \rangle$ value of the respective node. Note that in agreement with Fig. 5.2(b), the SNBS values are very similar for all nodes.

Multiple-node Basin Stability

Next, using the algorithm described in Sec. 5.3.3, we calculate the (mean) m-node BS ($\langle S_B^m \rangle$) values (for $M = 200$) and show the results in Fig. 5.4 for m varying from 1 to $N\,(= 81)$. Clearly, $\langle S_B^m \rangle$ declines significantly with increasing m. Interestingly, we observe that the variation of $\langle S_B^m \rangle$ values with increasing m can be suitably modelled by an exponentially decaying function as illustrated in Fig. 5.4. Future studies on the vulnerability of networked dynamical systems should focus on investigating and unraveling the mechanism underlying this observation.

In our example, we set $\langle S_B \rangle_{th} = 0.1$ and find (from the inset in Fig. 5.4) that $\langle S_B^m \rangle < \langle S_B \rangle_{th}$ for $m \geq 60$, implying $m_{crit} = 60$. Thus, simultaneously perturbing more than 60 nodes of the network (on average) significantly reduces the stability of the synchronized state below the critical threshold of $\langle S_B \rangle_{th} = 0.1$. We emphasize that this value refers to the average response of the network to randomly located perturbations. In the case of targeted attacks, a much lower number of affected nodes can be sufficient to drive the system out of the synchronized state. To further address this aspect, it would be worth considering the full distribution of individual MNBS values $\hat{S}_B^m(E_j, p)$ for all m-node subsets, and using the associated minimum (maximum) values for describing worst-case (best-case) situations. We leave a detailed exploration of this problem as a subject for future work.

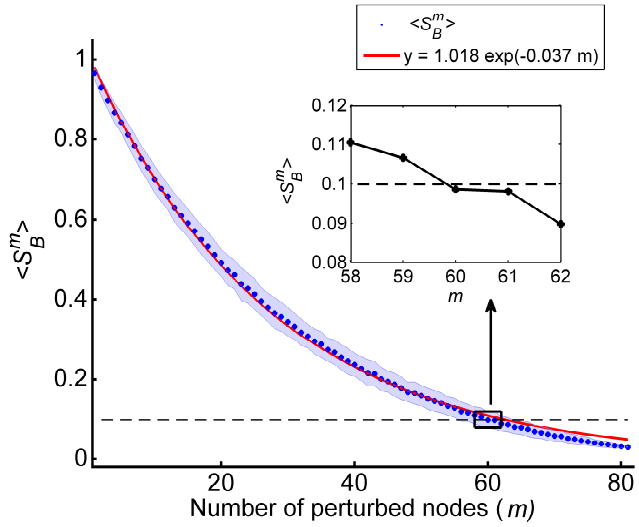

Figure 5.4.: (Mean) MNBS $\langle S_B^m \rangle$ (blue dots) for m varying from 1 to $N = 81$ in the undirected deterministic scale-free network of N identical Rössler oscillators. The shaded areas are representative of the standard deviations of the m-node BS values for the ensembles of *m-node sets* chosen for computing $\langle S_B^m \rangle$ for a particular value of m. The red line is an exponential fit of $\langle S_B^m \rangle$ ($\approx 1.018 \exp(-0.037m)$).

Our example clearly illustrates how m-node BS turns out to be a relevant concept for gauging the vulnerability of networked dynamical systems to global perturbations, and it emerges as a useful measure of the minimum fraction of nodes (on average) that when perturbed simultaneously, significantly reduces the stability of the synchronized state. In turn, we recommend controlling or safeguarding at least $N - m_{crit} = 81 - 60 = 21$ nodes of the network (on average) to ensure its functionality in the synchronized state in the face of large perturbations. Depending on the choice of the critical threshold $\langle S_B \rangle_{th}$, the value of m_{crit} and, hence, the number of nodes to be controlled will vary. Notably, as for the detailed investigation of "attack efficiencies" of different m-node subsets discussed above, the problem of "optimal control" for safeguarding the synchronized state would also require further investigation of the full distribution of individual MNBS values $\hat{S}_B^m(E_j, p)$.

5.4.2. Power Grid of the United Kingdom

As a more realistic example, we consider a conceptual model of the power transmission grid of the United Kingdom with second-order Kuramoto-type nodal dynamics [94–96]. The network consists of $N = 120$ nodes and 165 transmission lines (as illustrated in Fig. 5.5) which corresponds to a mean nodal degree of 2.75 [97].

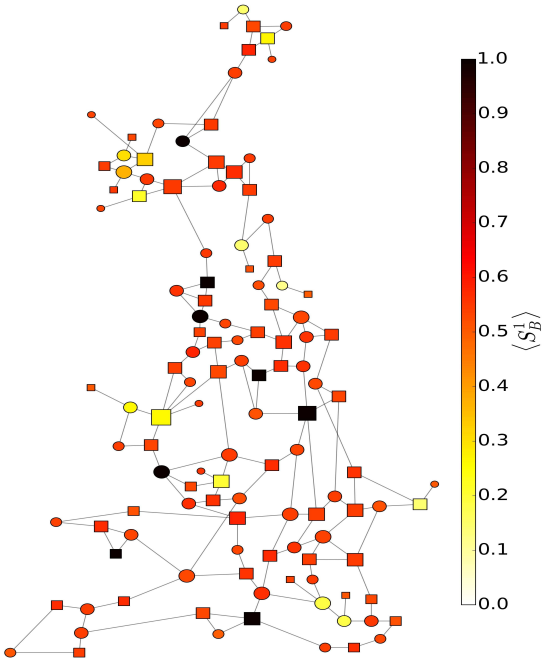

Figure 5.5.: Network topology of the power transmission grid of the United Kingdom (comprising $N = 120$ nodes) with second-order Kuramoto-type nodal dynamics. Circular nodes are net generators while square nodes are net consumers. The size of each node is proportional to the degree, and its colour corresponds to the $\langle S_B^1 \rangle$ value of the respective node.

In order to capture the relevant dynamical aspects and collective phenomena exhibited by a power grid, we consider a coarse-scale model comprising second-order Kuramoto-type oscillators coupled on the aforementioned network topology [94–96]. Such models consist of synchronous generators (representing power plants) and motors (representing consumers) characterized by the electrical power P_i that the machines generate ($P_i > 0$) and consume ($P_i < 0$), respectively. The dynamical state of each machine is represented by its mechanical phase $\phi_i(t) = \Omega t + \theta_i(t)$ and its phase velocity $\dot{\phi}_i(t)$, where $\Omega\,(= 2\pi \times 50$ Hz or $2\pi \times 60$ Hz) is the reference frequency of the grid. Considering the law of conservation of energy, the power generated or consumed by each unit $P_{source,\,i}$ must be equal to the sum of its power exchanged (given to or taken from) with the grid $P_{trans,\,i}$, its accumulated power $P_{acc,\,i}$, and its dissipated power $P_{diss,\,i}$. The power dissipated by each machine is given by $P_{diss,\,i} = \kappa_i \dot{\phi}_i^{\,2}$ where κ_i is the dissipation coefficient of the respective unit. The power accumulated by each rotating machine is given by $P_{acc,\,i} = \frac{dE_{kin,\,i}}{dt}$ where $E_{kin,\,i} = \frac{I_i \dot{\phi}_i^{\,2}}{2}$ is the kinetic energy and I_i is the moment of inertia of the respective unit. The power transmitted between two machines i and j is given by

$P_{trans,\,ij} = P_{max,\,ij}\,\sin\left(\phi_i - \phi_j\right)$, where $P_{max,\,ij}$ is the maximum capacity of the respective transmission line. The condition of conservation of energy at each node of the network yields

$$\begin{aligned} P_{source,\,i} &= P_{diss,\,i} + P_{acc,\,i} + P_{trans,\,i}, \\ &= P_{diss,\,i} + P_{acc,\,i} + \sum_{j=1}^{N} P_{trans,\,ij}, \\ &= \kappa_i \dot{\phi_i}^2 + I\ddot{\phi_i} + \sum_{j=1}^{N} P_{max,\,ij}\,\sin\left(\phi_i - \phi_j\right). \end{aligned} \tag{5.9}$$

For simplicity, we consider that all the machines have identical moments of inertia $I_1 = \ldots = I_N = I$ and dissipation coefficients $\kappa_1 = \ldots = \kappa_N = \kappa$ [13]. Further, substituting $\phi_i(t) = \Omega t + \theta_i(t)$ in Eq. (5.9) and assuming that the rate of phase changes is much slower than the reference frequency (i.e., $|\dot{\theta}| \ll \Omega$) leads to the following equation of motion:

$$\ddot{\theta}_i = -\alpha\dot{\theta}_i + P_i + \sum_{j=1}^{N} \epsilon_{ij} \sin\left(\theta_i - \theta_j\right), \tag{5.10}$$

where $\alpha = \frac{2\kappa}{I}$, $P_i = \frac{P_{source,\,i} - \kappa\Omega^2}{I\Omega}$ and $\epsilon_{ij} = \frac{P_{max,\,ij}}{I\Omega}$. We further assume the capacity of all transmission lines to be equal, i.e., $\epsilon_{ij} = \epsilon A_{ij}$ (where ϵ and $\mathbf{A}$ again denote the overall coupling strength and the adjacency matrix, respectively), such that the dynamical equations of the system (in analogy with Eq. (5.2)) read

$$\begin{aligned} \dot{\theta}_i &= \omega_i, \\ \dot{\omega}_i &= -\alpha\omega_i + P_i + \epsilon \sum_{j=1}^{N} A_{ij} \sin\left(\theta_j - \theta_i\right), \end{aligned} \tag{5.11}$$

where ω_i denotes the frequency of the i-th oscillator. Furthermore, we randomly choose $\frac{N}{2}$ net generators and $\frac{N}{2}$ net consumers with $P_i = +P_0$ and $P_i = -P_0$, respectively [13]. In the following, we use the parameter values $\alpha = 0.1$, $P_0 = 1.0$ and $\epsilon = 8.0$ for obtaining the results described below.

Single-node Basin Stability

We consider the stability of the synchronized state, which corresponds to all oscillators having constant phases $\tilde{\theta}^i$ and frequencies $\tilde{\omega}^i = 0$. We select a reference subset for each node as $q = [0,\, 2\pi] \times [-100,\, 100]$; $P = 1$ point on the attractor of the synchronized state and $I_C = 1000$ trials. The $\langle S_B^1 \rangle$ values of all the $N = 120$ nodes are shown in Fig. 5.6(a). Figure 5.6(b) displays a histogram of all $\langle S_B^1 \rangle$ values, where the nodes split into three classes displaying poor $(\langle S_B^1 \rangle \leq 0.4)$, fair $(0.4 < \langle S_B^1 \rangle < 0.75)$ and high $(\langle S_B^1 \rangle \geq 0.75)$ values of (mean)

SNBS. Figures 5.6(c) and 5.6(d) again illustrate the distribution of $\langle S_B^1 \rangle$ in comparison with k and bc, respectively. The cross-correlation values of $\langle S_B^1 \rangle$ with k and bc are 0.061 and 0.281, respectively, ruling out the existence of a systematic dependence between $\langle S_B^1 \rangle$ and the two considered topological node characteristics. Figure 5.5 displays the network topology together with the individual $\langle S_B^1 \rangle$ values in full analogy with Fig. 5.3 for the Rössler network. Finally, note that the nodes which show up with the lowest $\langle S_B^1 \rangle$ values comprise the 'dead ends' of the network, in agreement with Menck et al. [13].

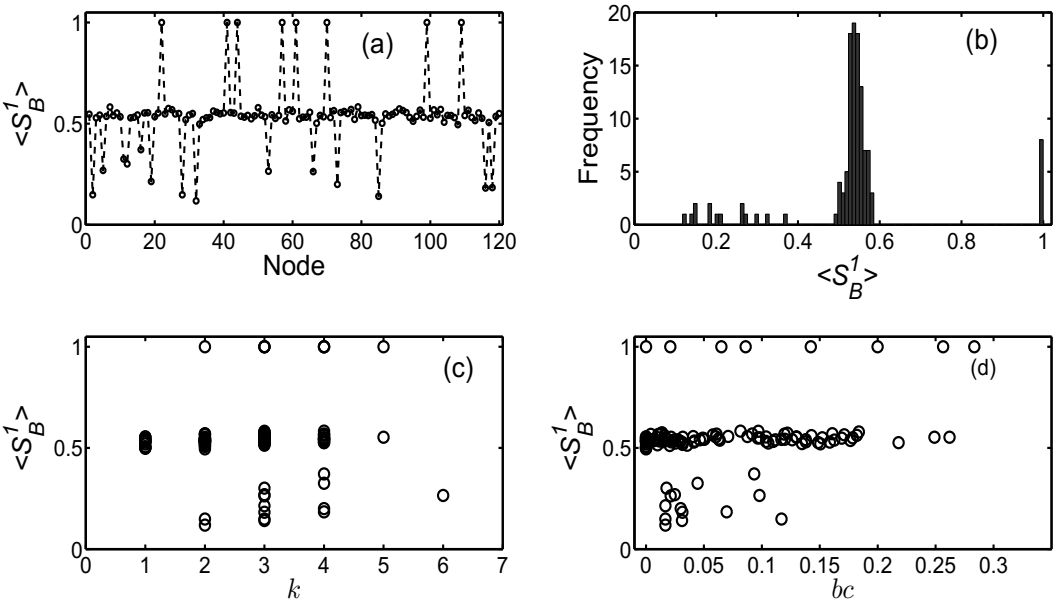

Figure 5.6.: As in Fig. 5.2 for the $N = 120$ nodes of the power grid of the United Kingdom with second-order Kuramoto-type nodal dynamics.

Multiple-node Basin Stability

Finally, we study the variation of the (mean) m-node BS $\langle S_B^m \rangle$ for m again varying from 1 to $N\,(= 120)$ and $M = 1000$ or $\binom{N}{m}$ (whichever is less) randomly chosen m-node sets (Fig. 5.7). Clearly, $\langle S_B^m \rangle$ declines rapidly with increasing m until $m \approx 12$, beyond which it decreases gradually until $m \approx 80$, thereafter saturating at a value ≈ 0.0005. For $\langle S_B \rangle_{th} = 0.001$, we find (from the inset in Fig. 5.7) that $\langle S_B^m \rangle < \langle S_B \rangle_{th}$ for $m \geq 70$, i.e., $m_{crit} = 70$. Thus, safeguarding at least 50 nodes of the network (on average) ensures the functionality of the power grid in the synchronized state in the considered setting. Notably, we again observe that the decay of $\langle S_B^m \rangle$ values can be fitted by an exponential function of m as illustrated

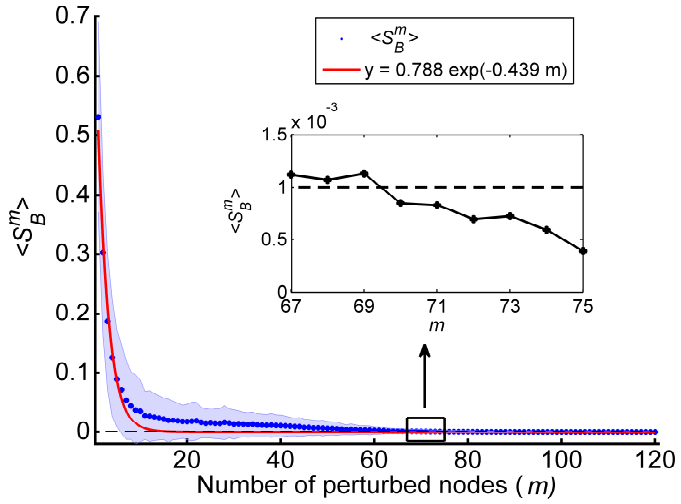

Figure 5.7.: (Mean) MNBS $\langle S_B^m \rangle$ (blue dots) for m varying from 1 to $N = 120$ for the power grid of the United Kingdom with second-order Kuramoto-type nodal dynamics. The shaded background is representative of the standard deviation of the m-node BS values for the ensemble of m-*node sets* chosen for computing $\langle S_B^m \rangle$ for a particular value of m. The red line shows an exponential fit of $\langle S_B^m \rangle$.

in Fig. 5.7, suggesting that this feature is not exclusive to the hierarchical network organization of our first example (Sec. 5.4.1).

5.5. Conclusion

The ubiquity of multistability in complex networks of dynamical systems calls for the development of suitable quantifiers of the respective stability of the multiple stable states of such systems. This has recently led to the development of basin stability (BS) and its extension to the concept of single-node basin stability (SNBS). The SNBS of a particular node of a network corresponds to the probability of the system to return to the desired stable state in the face of large perturbations hitting the respective node. However, in general, networked dynamical systems can also be subject to perturbations simultaneously affecting several nodes of the system.

In this regard, we proposed the framework of *multiple-node basin stability* (MNBS) for gauging the global stability and robustness of networked dynamical systems in response to non-infinitesimal perturbations simultaneously hitting multiple nodes of the system. Although the established framework of the master stability function (MSF) for assessing the stability of the synchronized state was a major advancement, it has still been locally confined to small perturbations. Moreover, the MSF-based approach is mostly restricted to studying the stability

of synchronization in coupled identical (or nearly identical) systems [12, 98]. However, the framework of SNBS and MNBS is applicable to non-identical systems as well as scenarios with non-identical functions coupling them.

Importantly, MNBS provides an estimate of the minimum fraction of nodes (on average), which when perturbed simultaneously significantly hampers the ability of the system to return to the desired stable state. Furthermore, MNBS can also be used to identify the exact set of nodes or oscillators of the network that are most susceptible to perturbations and constitute the dynamically least robust sub-components of the network. As examples, we have studied the stability of the synchronized state in a deterministic scale-free network of Rössler oscillators and a conceptual model of the United Kingdom power grid with second-order Kuramoto-type nodal dynamics. In both the above illustrations, we observed an exponential decay of MNBS with the number of perturbed nodes. Subsequently, we foresaw the framework of MNBS as a paradigm for assessing stability and resilience in complex networks of dynamical systems from various fields of application.

Chapter 6.

Integral Stability: An Ecological Resilience-based Quantifier of Multistability

6.1. Summary

In the previous chapters, we described various stability concepts and developed new concepts of stability based upon that of basin stability in quantifying the global stability of the respective attractors of a multistable complex dynamical system. Motivated by the concept of ecological resilience, we now propose a novel and pragmatic measure called *integral stability* (IS) which integrates different aspects commonly addressed separately by existing local and global stability concepts. We demonstrate the potential of IS by using exemplary multistable dynamical systems such as the damped driven pendulum, a model of Amazonian rainforest (as a known tipping element of the climate system) and the Daisyworld model. A crucial feature of IS lies in its potential of arresting a gradual loss of the stability of a system when approaching a tipping point, thus providing a potential early-warning signal sufficiently prior to a qualitative change of the system's dynamics. This chapter is based on the associated publication P2 and the following sections will closely follow the respective publication.

6.2. Introduction

Linear stability analysis (Sec. 4.1.6), based on the local assessment of the sign and magnitude of the Lyapunov exponents in the attractor's neighbourhood, in conjugation with the recently proposed global measure of basin stability (BS, Sec. 4.1.10), quantified using the volume of the basin of attraction, constitute state of the art methods of gauging stability in dynamical systems theory. In this chapter, we identify various aspects characterizing the stability of a multistable dynamical system and demonstrate that linear stability and BS are unable to capture all of them. Subsequently, we propose the novel and pragmatic measure of *integral stability* (IS) for holistically inferring stability, overcoming the main insufficiencies of the existing metrics.

The foundation of IS rests upon the concept of *ecological resilience*, previously recapitulated in Sec. 4.2.2. As mentioned earlier, Walker et al. [14] identifies 'latitude' (L), 'resistance' (R) and 'precariousness' (Pr) as the three crucial aspects of ecological resilience. Below, we redefine L, R and Pr in the context of dynamical systems, for usage throughout this text as a basis for the formal definition of IS:

- *Latitude* L: Here, we consider the volume of the basin of attraction as a quantitative measure of the latitude of a stable state.

- *Resistance* R: Qualitatively, we identify the resistance of a system with its capacity of overcoming changes, following a perturbation. More precisely, each point in the state space of a deterministic stationary multistable dynamical system is associated with a unique trajectory approaching a particular attractor. A perturbation drives the system to a different point in the state space, associated with a different trajectory. Building upon our qualitative definition of resistance, and combining it with engineering resilience (Sec. 4.2.1), we define resistance at a particular point in the state space as the instantaneous rate at which the system converges to the unperturbed trajectory following a perturbation. Subsequently, we associate the resistance at a particular point in the state space with the local Lyapunov exponents evaluated at the respective point in state space [24]. For any point, the negative of the local Lyapunov exponents measure the rate of convergence of nearby trajectories to the trajectory starting at the state space point in question. Further, the growth of separation in the direction corresponding to the largest among the local Lyapunov exponents overwhelms the growth of separation along other directions. Subsequently, we quantify the resistance at any point in state space as the negative of the largest local Lyapunov exponent, evaluated at the respective point. The detailed procedure for calculating the local Lyapunov exponents is described in Sec. 6.3.3.

- *Precariousness* Pr: We here consider the precariousness of a stable state as the minimum perturbation required to drive the system residing on the attractor corresponding to the stable state, outside its basin of attraction. This definition of the precariousness of a stable state corresponds to the definition of *stability threshold* proposed by Klinshov et al. [99].

We emphasize that the redefinitions of L, R and Pr constitute the crucial aspects characterizing the stability of attractors of a multistable dynamical system.

Linear stability analysis provides a (locally restrictive) measure of resistance in the immediate neighbourhood of the attractor and does not account for resistance at the global level. On the other hand, BS is an exclusively latitude-based measure which does not consider resistance as well as the position of the attractor within the basin, i.e., precariousness (illustrated with the example of an Amazonian

vegetation model in Sec. 6.4.2). For example, for a system with the same basin size (corresponding to a particular stable state) for two different parameter values, BS is the same irrespective of the dynamics (leading to possibly different resistances). Similarly, consider a system with the same basin size for two different parameter values. In one case, the attractor is at the centre of the basin, thus making it equally vulnerable to perturbations in all directions implying relatively high precariousness. In the other case, assume that the attractor is very close to the basin boundary, thus making it highly vulnerable to perturbations in the direction of closest proximity to the basin boundary implying relatively low precariousness. Clearly, BS is unable to identify this change in the vulnerability of the system to perturbations for the two different parameter values. Thus, the existing methods of linear stability and BS do not individually and collectively capture all three crucial aspects of multistability, motivating the need for a new generally applicable measure integrating the features of L, R and Pr.

BS has been identified as a potential tool for assessing multistable climate tipping elements as demonstrated by its application to an Amazonian vegetation model [9]. Although BS captures the qualitative change in the system's dynamics in terms of a sudden decline in its value when approaching the tipping point, it does not provide a convincing early-warning signal prior to the change. On the other hand, IS exhibits a gradual loss in its value when approaching the tipping point, thus providing a potential early-warning signal prior to such critical transitions. This feature of IS (demonstrated with examples in the subsequent sections) turns out to be one of the key advantages of the measure.

This chapter is further organized as follows: In Sec. 6.3, we outline the general methodology for calculating IS values for a given dynamical system. In Sec. 6.4, we illustrate applications of IS to paradigmatic multistable dynamical systems such as the damped driven pendulum, a model of Amazonian rainforest and the Daisyworld model. Finally, we present the conclusions of our work in Sec. 6.5.

6.3. Methods

6.3.1. Preliminaries

In the following, we outline the general methodology for calculating IS values for a given dynamical system. Consider an N-dimensional (continuous- or discrete-time) dynamical system represented by the state vector $\mathbf{x}(t) = (x_1, x_2, \ldots, x_N)^{\mathrm{T}}$ exhibiting M stable attractors $\mathcal{A}_i$ $(i = 1, 2, \ldots, M)$. The precariousness $Pr(\mathcal{A}_i)$ of the i-th attractor is the minimum perturbation required to drive the system presently residing on the attractor $\mathcal{A}_i$, outside its basin of attraction $\mathcal{B}(\mathcal{A}_i)$. Thus,

$$Pr(\mathcal{A}_i) = \inf\{\mathrm{dist}(a, b) \,|\, a \in \mathcal{A}_i, b \in \delta\mathcal{B}(\mathcal{A}_i)\},\ i = 1, 2, \ldots, M, \tag{6.1}$$

where dist$(\cdot, \cdot)$ is the Euclidean distance and $\delta\mathcal{B}(\mathcal{A}_i)$ is the border of the basin of attraction of the attractor $\mathcal{A}_i$ [99].

Let $\Lambda(\mathbf{x}) = \{\Lambda_1, \Lambda_2, \ldots, \Lambda_N\}$ be the set of N local Lyapunov exponents evaluated at the state $\mathbf{x}$ (see Sec. 6.3.3). The resistance $R(\mathbf{x})$ at the state $\mathbf{x}$ is the negative of the largest local Lyapunov exponent of the trajectory starting at $\mathbf{x}$. Thus,

$$R(\mathbf{x}) = -\text{max}\{\Lambda_1, \Lambda_2, \ldots, \Lambda_N\}. \tag{6.2}$$

6.3.2. Integral Stability (IS)

We now define a measure of *integral stability* $S_I(\mathcal{A}_i)$ of the i-th attractor as,

$$S_I(\mathcal{A}_i) = \frac{Pr(\mathcal{A}_i) \int\limits_{\mathbf{x}\in\mathcal{B}(\mathcal{A}_i)} R(\mathbf{x})\, d\mathbf{x}}{\sum\limits_{j=1}^{M} \left[Pr(\mathcal{A}_j) \int\limits_{\mathbf{x}\in\mathcal{B}(\mathcal{A}_j)} R(\mathbf{x})\, d\mathbf{x} \right]}. \tag{6.3}$$

The integral over the basin of attraction of the i-th attractor with $d\mathbf{x} = \prod\limits_{k=1}^{N} dx_k$ as the differential volume element keeps track of the latitude.

By defining IS in the particular form of Eq. (6.3), we assume that the ingredients of L, R and Pr carry equal weights in quantifying the stability of any particular attractor. Subsequently, we multiply the ingredients together and integrate them over the entire basin of the attractor under investigation. Moreover, normalizing the product facilitates the quantitative comparison of the respective stability of an attractor (between 0 and 1) when modulating a particular parameter of the system. The exact value of the product of L, R and Pr is no longer important but only the value of IS of the attractor under question compared to that of the other attractors. Finally, normalization ensures that IS is a dimensionless ratio, which nullifies the effect of units of measurement to some extent.

6.3.3. Local Lyapunov Exponents

In the following, we present details on calculating the local Lyapunov exponents as a prerequisite for computing the measure of IS in Eq. (6.3). Recall that the resistance at a particular point in state space was defined as the instantaneous rate at which the system converges to the unperturbed trajectory (starting from the state space point in question) following a perturbation. Further, the rate of convergence of nearby trajectories (on account of perturbations) to the trajectory starting at the state space point in question is associated with the negative of the

local Lyapunov exponents evaluated at the respective point. Below, we outline the procedure for computing the local Lyapunov exponents at a given point in state space of a continuous-time dynamical system. However, the procedure remains essentially the same for a discrete-time dynamical system.

Consider an N-dimensional flow represented by the state vector $\mathbf{x}(t) = (x_1,\, x_2,\, \ldots,\, x_N)^{\mathrm{T}}$ and described by the following equations of motion:

$$\dot{\mathbf{x}} = \mathbf{F}\left(\mathbf{x}\right);\, \mathbf{x} \in \mathbb{R}^N;\, \mathbf{F} :\, \mathbb{R}^N \,\rightarrow\, \mathbb{R}^N,\, \mathbf{F} = \left(F_1\left(\mathbf{x}\right),\, F_2\left(\mathbf{x}\right),\, \ldots,\, F_N\left(\mathbf{x}\right)\right)^{\mathrm{T}}. \quad (6.4)$$

Consider a trajectory starting at $\mathbf{x}$, with an infinitesimal perturbation $\delta\mathbf{x}$. The perturbation is then transported by the flow $\mathbf{F}$ along the (perturbed) trajectory starting at $\mathbf{x} + \delta\mathbf{x}$. We study the deformation of the infinitesimal neighbourhood using the flow linearised around $\mathbf{x}$, following from the variational equations obtained by Taylor expansion of Eq. (6.4) to first order,

$$\begin{aligned} &\dot{\mathbf{x}} + \dot{\delta\mathbf{x}} = \mathbf{F}\left(\mathbf{x} + \delta\mathbf{x}\right) \approx \mathbf{F}\left(\mathbf{x}\right) + D_x\mathbf{F}\left(\mathbf{x}\right) = \mathbf{F}\left(\mathbf{x}\right) + \mathbf{A}\left(\mathbf{x}\right)\, \delta\mathbf{x}, \\ &\implies \dot{\delta\mathbf{x}} = \mathbf{A}\left(\mathbf{x}\right)\, \delta\mathbf{x}, \end{aligned} \quad (6.5)$$

where $\mathbf{A}\left(\mathbf{x}\right)$ is the stability matrix $\left(\text{such that } A_{ij}\left(\mathbf{x}\right) = \frac{\partial F_i}{\partial x_j}\left(\mathbf{x}\right)\right)$, describing the instantaneous rate of shearing of the neighbourhood of $\mathbf{x}$ by the flow. Since resistance measures the instantaneous rate at which the perturbation grows (or decays), we calculate the growth of the perturbation for an infinitesimal change in time dt,

$$\delta\mathbf{x}(dt) = \delta\mathbf{x} + \mathbf{A}\left(\mathbf{x}\right)\, \delta\mathbf{x}\, dt = \left(\nVdash_{N\times N} + \mathbf{A}\left(\mathbf{x}\right)\, dt\right)\, \delta\mathbf{x} = \mathbf{J}_{dt}\left(\mathbf{x}\right)\, \delta\mathbf{x}, \quad (6.6)$$

where $\mathbf{J}_{dt} = \nVdash_{N\times N} + \mathbf{A}\left(\mathbf{x}\right)\, dt$ is the instantaneous Jacobian matrix. It describes the deformation of an infinitesimal neighbourhood in time dt of the trajectory starting at $\mathbf{x}$. For a map, the instantaneous Jacobian matrix simply consists of the partial derivatives of the map with respect to the state variables, evaluated at the respective point in state space.

The square roots of the eigenvalues of the right (left) Cauchy-Green strain tensor $\mathbf{J}_{dt}^{\mathrm{T}}\,\mathbf{J}_{dt}$ $\left(\mathbf{J}_{dt}\,\mathbf{J}_{dt}^{\mathrm{T}}\right)$, called the 'principal stretches' and denoted by $\sigma_j\left(\mathbf{x}\right)$, $j = 1,\, 2,\, \ldots,\, N$, measure the instantaneous stretching of the neighbourhood of the trajectory at $\mathbf{x}$. The local Lyapunov exponents measuring the rate of stretching are given by [100],

$$\Lambda_j\left(\mathbf{x}\right) = \frac{1}{dt}\, \ln\left(\sigma_j\left(\mathbf{x}\right)\right),\, j = 1,\, 2,\, \ldots,\, N. \quad (6.7)$$

6.4. Examples

In the following, we demonstrate the potential of the proposed measure of IS in quantifying the stability of the attractors of exemplary multistable dynamical

systems.

6.4.1. Damped Driven Pendulum

We consider the stability of a classical damped pendulum driven by a constant angular acceleration. The dynamical equations of the system read [9]

$$\begin{aligned} \dot{\phi} &= \omega, \\ \dot{\omega} &= -\alpha\,\omega + T - K\,\sin\phi, \end{aligned} \tag{6.8}$$

where ϕ is the angular position, ω is the angular velocity, $\alpha > 0$ is the dissipation coefficient, T is the constant angular acceleration and $K = \frac{g}{l}$, with g and l being the gravitational acceleration and the length of the pendulum, respectively. For $0 \leq T < K$, the pendulum has two equilibrium points, $x_i = (\phi_i,\, \omega_i)$ for $i = 1,\, 2$,

$$\begin{aligned} \phi_{1,\,2} &= \arcsin\left(\frac{T}{K}\right), \\ \omega_{1,\,2} &= 0, \end{aligned} \tag{6.9}$$

where ϕ_1 is the solution of the arcsin inside $\left[0,\, \frac{\pi}{2}\right]$ and $\phi_2 = \pi - \phi_1$.

For $0 < T < K$ with fixed K and α, x_1 is a stable equilibrium and x_2 is an unstable saddle. In addition, for $T_{\text{mult}} < T < K$, the pendulum can also converge to a limit cycle, thus exhibiting multistability. On varying T with $\alpha = 0.1$ and $K = 1$, we observe the limit cycle becoming stable at $T_{\text{mult}} \approx 0.13$.

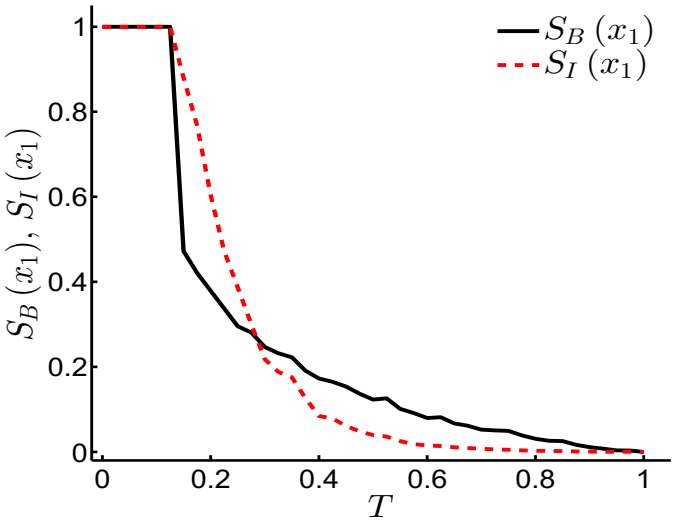

Figure 6.1.: IS $S_I\,(x_1)$ and BS $S_B\,(x_1)$ of the equilibrium point x_1 vs. T, at $\alpha = 0.1$ and $K = 1$.

As already stated in Menck et al. [9], linear stability (related to the maximum Lyapunov exponent of the stable equilibrium x_1) is not a reliable proxy for detecting the pendulum's transition between x_1 and the limit cycle under large perturbations (Supplementary Fig. S3 of Menck et al. [9]). On the contrary, the measure of IS proposed in Eq. (6.3) clearly detects the transition (and closely follows the measure of BS) as evident from Fig. 6.1.

6.4.2. Amazonian Vegetation Model

In a second example, we explore the stability of a simple paradigmatic model of an important potential climate tipping element, the Amazonian rainforest [6, 9, 101]. The dynamical equations of the model read [9]

$$\frac{dC}{dt} = F(C) = \begin{cases} r\,(1-C)\,C - x\,C & \text{if } C > C_{crit}, \\ -y\,C & \text{if } C < C_{crit}, \end{cases} \tag{6.10}$$

where C is the relative forest cover that grows at a rate r if $C > C_{crit}$ and dies with a rate x (y) if $C > C_{crit}$ $(C < C_{crit})$, assuming $r > x$ $(y) > 0$. C_{crit} is the critical forest cover threshold, which is assumed to increase linearly with aridity A, i.e., $C_{crit} = C_1\,A + C_2$, where C_1 and C_2 are arbitrary constants. The aridity is an indicator of the degree of dryness of the climate at a given location. In the following, we set $C_1 = 1$ and $C_2 = 0$ for convenience, which implies that $C_{crit} = A$. Thus, the critical forest cover threshold is set equal to the aridity. This model has two equilibria, the forest state $C_F = 1 - \frac{x}{r}$ and the savanna state $C_S = 0$. The equilibrium C_F (C_S) exists and is stable if $C_F > C_{crit}$ $(C_{crit} > 0)$.

Menck et al. [9] argue that owing to the local nature of linear stability and small-perturbation convergence rate, these measures fail to identify the decrease (increase) in the global stability of the forest (savanna) state C_F (C_S) on account of the shrinkage (expansion) of its basin of attraction on increasing the aridity A, which is however successfully quantified by BS (Fig. 6.2). Likewise, IS proposed in Eq. (6.3) clearly detects the change in the stability of the forest (savanna) state C_F (C_S) as evident from Fig. 6.2(a) (Fig. 6.2(b)).

As pointed out in Sec. 6.2, BS is unable to identify the change in the stability of an equilibrium state of a system on varying its position with respect to the basin boundary. For example, the forest state at $C_F = 1 - \frac{x}{r}$ comes closer to the basin boundary at C_{crit} on increasing x, which increases the vulnerability of the forest state to perturbations in the direction of the basin boundary at C_{crit}. The inset in Fig. 6.3(a) clearly illustrates the decreasing value of the precariousness $Pr(C_F)$ of the forest state upon increasing x, which finally goes to 0 at the point of critical transition. However, it is easy to identify from the inset that the constant value of BS $S_B(C_F)$, does not capture this decrease in the precariousness of C_F prior to the transition. This is aptly captured by the proposed measure as evident from the decreasing value of IS of the forest state with rising x in Fig. 6.3(a). In the

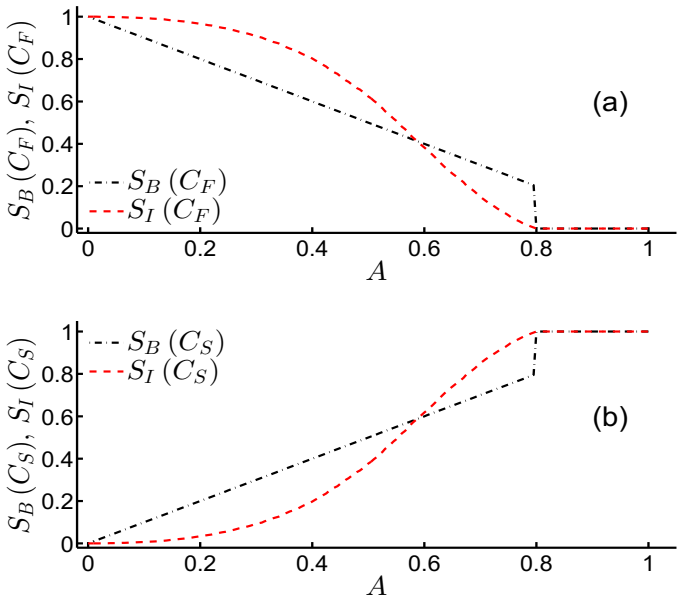

Figure 6.2.: IS S_I and BS S_B of (a) the forest state $C_F = 1 - \frac{x}{r}$ vs. aridity A and (b) the savanna state $C_S = 0$ vs. A, at $C_{crit} = A$, $x = 0.2$, $r = 1.0$ and $y = 1.0$.

latter case, the fixed value of y implies that the local Lyapunov exponent of the savanna state $C_S = 0$ is constant and equal to $y\,(= 0.1)$ even as x is varied. The above example clearly magnifies the advantage of IS in comparison with linear stability and BS by demonstrating its ability to capture the gradual loss in the stability of an equilibrium state on account of reduced precariousness.

Further, as mentioned in Sec. 6.2, BS does not consider the local dynamics in quantifying the stability of an attractor. For example, it does not quantify the change in the stability of the savanna state $C_S = 0$ upon varying the value of y as this varies the resistance in the neighbourhood of the savanna state. Such changes in the resistance affect the rate of convergence to the equilibrium (identified as *engineering resilience* (Sec. 4.2.1) of the equilibrium state) on being perturbed. Consider the situation when $C_{crit} = A = 0.6$, $r = 1.0$ and $y = x$ such that the local Lyapunov exponent of the savanna state is equal to $-y = -x$, implying an increase in the resistance (in this case, increase in the rate of convergence) in the neighbourhood of C_S with increasing x. Subsequently, at any value of x, the situation when $y = x$ leads to larger stability of the savanna state (for $x > 0.1$) as compared to the scenario when the value of y is held constant at 0.1, as clearly evident from Fig. 6.3(b). Thus, the ability of IS to consider the local dynamics around an attractor, thus taking the aspect of resistance into account, further escalates its potential as a quantifier of multistability.

Thus far, we have highlighted the capacity of IS in effectively capturing the three crucial aspects of L, R and Pr. Now, we want to further highlight one of

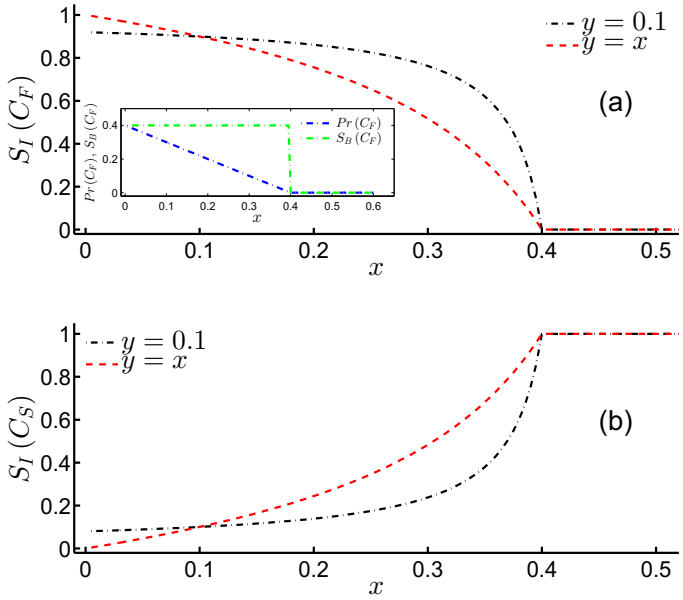

Figure 6.3.: IS S_I of (a) the forest state C_F vs. x for $y = 0.1$ (black) and $y = x$ (red) and (b) the savanna state C_S vs. x for $y = 0.1$ (black) and $y = x$ (red), at $C_{crit} = A = 0.6$ and $r = 1.0$. The inset in (a) illustrates the decreasing value of the precariousness Pr (blue) and the constant value of BS S_B (green) of the forest state with increasing x.

the most important benefits of IS which lies in its ability of arresting a gradual loss of the stability of a system (as opposed to an abrupt one captured by BS) when approaching a tipping point. For example, in the Amazonian rainforest, the forest state ceases to exist for $A > 0.8$ as evident from Fig. 6.2 where the entire state space is occupied by the savanna state. This transition is indicated by the BS of the forest state abruptly dropping to 0 with no convincing early-warning signal. On the contrary, IS demonstrates a gradual and continuous decline in the stability of the forest state. Moreover, it provides a precursor/early-warning signal by capturing a reduced value of the stability of the forest state much prior to the value of $A = 0.8$. This feature of IS is also demonstrated in the following for the case of the Daisyworld model (Fig. 6.4).

6.4.3. Daisyworld

The Daisyworld model relates to interactions between the climate and the biosphere of a hypothetical world orbiting around a star that becomes brighter with time [102, 103]. The biosphere inhabiting the planet comprises only white and black daisies differing characteristically in their albedo (i.e., the proportion of the incident light or energy they reflect back). The surface covered with white daisies

has a higher albedo and reflects a larger proportion of the incoming radiation from the star as compared to that reflected by the bare ground or the surface covered with black daisies. Effectively, the fractional coverages of the planetary area by white and black daisies, denoted by x_w and x_b, respectively, determine the overall planetary albedo which subsequently modulates the surface temperature of the planet. Let p be the fraction of the fertile ground in the Daisyworld such that $x_g \equiv p - x_w - x_b$ constitutes the proportion of uninhabited fertile ground. In the following, we set $p = 1$ for convenience. The dynamical equations comprising the original Daisyworld model [102], describing the growth of the daisies read

$$\begin{aligned} \dot{x}_w &= x_w \left[x_g \, \beta \left(T_w\right) - \gamma\right], \\ \dot{x}_b &= x_b \left[x_g \, \beta \left(T_b\right) - \gamma\right], \end{aligned} \tag{6.11}$$

where γ is a constant death rate. The birth rate of the white (black) daises denoted by $\beta\left(T_w\right)$ $\left(\beta\left(T_b\right)\right)$ depends on the local temperature T_w $\left(T_b\right)$ experienced by the respective daisy type as,

$$\beta\left(T\right) = \begin{cases} 1 - k \, \left(T - T_{\text{opt}}\right)^2 & \text{if } |T - T_{\text{opt}}| < k^{-\frac{1}{2}}, \\ 0 & \text{otherwise,} \end{cases} \tag{6.12}$$

where k expresses the sensitivity of the birth rate to the local temperature and T_{opt} is the optimal temperature for daisy growth. Denoting the albedo of white and black daisies and that of bare ground by a_w, a_b and a_g, respectively, we obtain the mean planetary albedo as,

$$A = a_w \, x_w + a_b \, x_b + a_g \, x_g; \; a_b < a_g < a_w. \tag{6.13}$$

The local temperatures, T_w and T_b depend on the effective planetary temperature T as,

$$\begin{aligned} T_w^4 &= q \left(A - a_w\right) + T^4, \\ T_b^4 &= q \left(A - a_b\right) + T^4, \end{aligned} \tag{6.14}$$

where the parameter q is introduced as the heat transfer coefficient. Finally, the mean planetary albedo (A), the average energy incident on the surface of the planet radiating from the star (S_0) and the luminosity (L) determine the effective planetary temperature (T) via the global energy balance equation,

$$\sigma \, T^4 = S_0 \, L \left(1 - A\right), \tag{6.15}$$

where σ is the Stefan-Boltzmann constant. For the fixed parameter values of $\sigma = 5.67 \times 10^{-8} \, W \, m^{-2} \, K^{-4}$, $S_0 = 917 \, W \, m^{-2}$, $\gamma = 0.3 \, s^{-1}$, $T_{\text{opt}} = 295.5 \, K$, $k = 3.265 \times 10^{-3} \, K^{-2} \, s^{-1}$, $a_w = 0.75$, $a_b = 0.25$, $a_g = 0.5$, $q = 2.06 \times 10^9 \, K^4$, and $L \in (1.22, \, 1.38)$, the Daisyworld model of Eq. (6.11) exhibits multistability by

admitting four equilibrium points:

(i) a stable abiotic solution implying complete in-existence of daisies, $x_1 \equiv (x_w^*,\, x_b^*) = (0,\, 0)$;

(ii) two saddles with white daisy-only solutions, $x_2 \equiv (x_w^*,\, x_b^*) = (x_{w2}^*,\, 0)$ and $x_3 \equiv (x_w^*,\, x_b^*) = (x_{w3}^*,\, 0)$, where $x_{w3}^* > x_{w2}^* > 0$;

(iii) a stable biotic solution implying co-existence of daisies, $x_4 \equiv (x_w^*,\, x_b^*) = (x_{w4}^*,\, x_{b4}^*)$, where $x_{w4}^*,\, x_{b4}^* > 0$.

The measures of IS $S_I(x_1)$ $(S_I(x_4))$ and BS $S_B(x_1)$ $(S_B(x_4))$ of the abiotic solution x_1 (biotic solution x_4) are depicted in Fig. 6.4. Note that the system switches the state having greater stability at some intermediate value of $L \in (1.22,\, 1.38)$. This transition is clearly detected by both measures. The biotic solution x_4 with coexisting daisy populations ceases to exist when the luminosity exceeds a value of 1.38, where the white daisy-only solution x_3 becomes stable. As a result, $S_B(x_4)$ abruptly plummets to 0 when $L > 1.38$, indicating a discontinuous loss in the stability of this solution. However, the IS measure $S_I(x_4)$ $(S_I(x_1))$ detects the gradual loss (gain) in the stability of the biotic (abiotic) solution depicted by a very smooth transition to ≈ 0 (1), much prior to the abrupt transition suggested by BS. We have identified this feature of IS earlier in the case of the Amazonian rainforest model (Fig. 6.2) as well. Thus, the capacity of IS in pronouncing a gradual loss/gain in the stability of an equilibrium state (as well as much prior to that captured by BS) can be a potential precursor/early-warning signal to such transitions in dynamical systems.

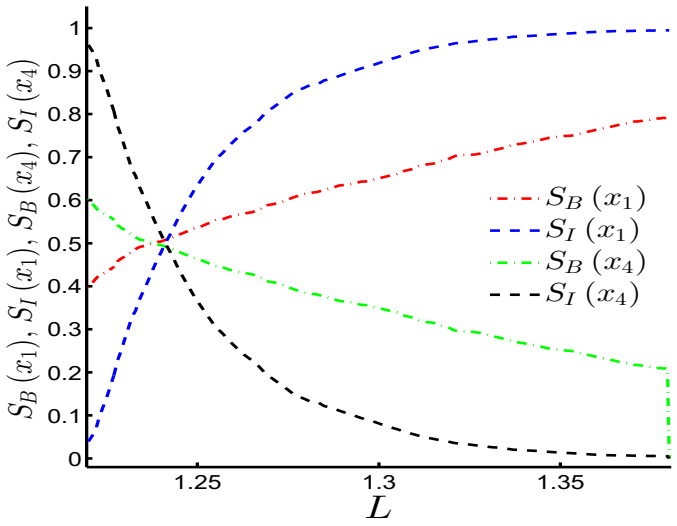

Figure 6.4.: IS $S_I(x_1)$ (blue) $[S_I(x_4)$ (black)] and BS $S_B(x_1)$ (red) $[S_B(x_4)$ (green)] of the abiotic solution x_1 [biotic solution x_4] vs. Luminosity (L).

6.4.4. High-dimensional Dynamics

Thus far, we have applied IS to several exemplary but low-dimensional systems in order to demonstrate its potential as an effective quantifier of multistability. In this section, we illustrate that the scope of this measure is not associated with the dimensionality of the system. For this purpose, we demonstrate its application to a multistable high-dimensional dynamical system.

We consider a chain of N one-variable bistable cubic Nagumo systems [104] where the evolution of each isolated unit is given by

$$\dot{x} = x(x-\eta)(1-x), \text{ with } 0 < \eta < 1. \tag{6.16}$$

We assume a nearest-neighbour coupling between the systems with a coupling strength denoted by α (> 0) such that the dynamical equations read

$$\dot{x}_i = x_i(x_i-\eta)(1-x_i) + \alpha\left(x_{i+1} + x_{i-1} - 2x_i\right), \; i = 1, 2, \ldots, N. \tag{6.17}$$

The coupled system of Equations (6.17) with (at least) two stable equilibria at

$$\begin{aligned} X_1^* &: x_i^* = 0, \; \forall\, i = 1, 2, \ldots, N, \\ X_2^* &: x_i^* = 1, \; \forall\, i = 1, 2, \ldots, N, \end{aligned} \tag{6.18}$$

has been investigated in greater detail by Mackay et al. [104]. We refer the reader to this original study for further details on the dynamics of the model.

Here, we analyse the model in Eq. (6.17) for a sufficiently large number

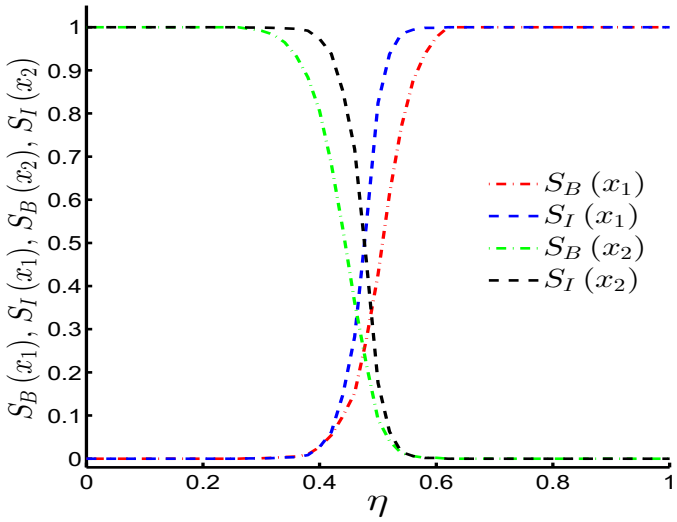

Figure 6.5.: IS $S_I\,(X_1^*)$ (blue) [$S_I\,(X_2^*)$ (black)] and BS $S_B\,(X_1^*)$ (red) [$S_B\,(X_2^*)$ (green)] of the equilibrium point X_1^* [X_2^*] vs. η, at $\alpha = 0.5$.

of $N = 50$ units for it to qualify as a high-dimensional system. We utilize IS to quantify the stability of the bistable stationary states (Eq. (6.18)) of the network. The measures of IS $S_I(X_1^*)$ $(S_I(X_2^*))$ and BS $S_B(X_1^*)$ $(S_B(X_2^*))$ of the equilibrium point X_1^* (X_2^*) vs. η at a value of $\alpha = 0.5$ are depicted in Fig. 6.5. Just like the Daisyworld model addressed in Sec. 6.4.3, the system in Eq. (6.17) switches the state having greater stability at some intermediate value of $\eta \in (0, 1)$. This transition is clearly detected by both measures. As clearly evident from Fig. 6.5, the measure of IS closely follows the measure of BS. Thus, we conclude that IS is equally well applicable to a high-dimensional system (just like BS) and that it is not prone to the curse of being dimensionally restrictive.

6.5. Conclusion

The developments in this chapter were motivated by the pervasiveness of multistability in dynamical systems and the associated need for suitable quantifiers of the stability of multiple attractors of such systems. We redefined the three crucial aspects of ecological resilience (L, R and Pr) for generic dissipative dynamical systems and utilized it as a foundation for characterizing multistability. Subsequently, identifying the inability of the state of the art measures of multistability in collectively capturing L, R and Pr, we proposed the novel measure of *integral stability* (IS) in Eq. (6.3).

IS has demonstrated its capacity of capturing a gradual loss of the stability of a system when approaching a transition point as opposed to BS, which exhibits a rather abrupt transition in the same setting. Thus, IS provides a potential early-warning signal prior to such qualitative changes in the dynamics of a complex system, making it a prospective tool for assessing such situations arising in many dynamical systems from various fields of application.

In the examples presented above, IS has been primarily applied to low-dimensional systems. We foresee that future efforts could be directed towards probing multistability in high-dimensional systems as well. As an initial exercise in this direction, we applied IS to a multistable high-dimensional system (Sec. 6.4.4) where we demonstrated that IS appropriately quantifies the associated multistability. Thus, the scope of IS is not associated with the dimensionality of the complex system under assessment.

Also, we suggested that the aspects of L, R and Pr be combined in a way such that they carry equal weights in quantifying IS (Eq. (6.3)) of any particular attractor. However, one may also choose to separately inspect L, R and Pr in assessing the stability of an attractor [105]. At the same time, instead of combining the ingredients of L, R and Pr as in Eq. (6.3), one may also consider IS as a function of other combinations of L, R and Pr, i.e., $S_I(\mathcal{A}_i) = f(\{L(\mathcal{A}_j), R(\mathcal{A}_j), Pr(\mathcal{A}_j)\}_{j=1,2,...,M})$. Also, we suggested the Euclidean metric for calculating Pr (Eq. (6.1)). However, as per the situation at hand, one may also resort to a different metric for the above purpose.

Chapter 7.

Recovery Time after Localized Perturbations in Complex Dynamical Networks

7.1. Summary

As continuously emphasized in the previous chapters, maintaining the synchronous motion of dynamical systems interacting on complex networks is often critical to their functionality. However, real-world networked dynamical systems operating synchronously are prone to random perturbations driving the system to arbitrary states within the corresponding basin of attraction, thereby leading to epochs of desynchronized dynamics with a priori unknown durations. Thus, it is highly relevant to have an estimate of the duration of such transient phases before the system returns to synchrony, following a random perturbation to the dynamical state of any particular node of the network. We address this issue here by proposing the framework of *single-node recovery time* (SNRT) which provides an estimate of the relative time scales underlying the transient dynamics of the nodes of a network during its restoration to synchrony. We utilize this in differentiating the particularly *slow* nodes of the network from the relatively *fast* nodes, thus identifying the critical nodes which when perturbed lead to significantly enlarged recovery time of the system before resuming synchronized operation. Further, we reveal explicit relationships between the SNRT values of a network, and its *global relaxation time* when starting all the nodes from random initial conditions. Earlier work on relaxation time generally focused on investigating its dependence on macroscopic topological properties of the respective network. However, we employ the proposed concept for deducing microscopic relationships between topological features of nodes and their respective SNRT values. The framework of SNRT is further extended to a measure of engineering resilience (Sec. 4.2.1) of the different nodes of a networked dynamical system. We demonstrate the potential of SNRT in networks of Rössler oscillators on paradigmatic topologies and the model of the power grid of the United Kingdom with second-order Kuramoto-type nodal dynamics (introduced in Sec. 5.4.2) illustrating the conceivable practical applicability of the proposed concept. This

chapter is based on the associated publication P3 and the following sections will closely follow the respective publication.

7.2. Introduction

The abundance of dynamical systems involving large collections of individual entities interacting with each other on complex networks can hardly be further exaggerated [10, 31, 60, 69, 81, 106]. Such networked dynamical systems often exhibit a multitude of stable states, whereby sustained operation of the system in the desired state is of central importance. The desired operational state (DOS) in such systems is commonly associated with the synchronized motion of the dynamical components coupled on their networked architecture [11, 13]. *Permissible* and *impermissible* random perturbations (according to the terminology used by Menck et al. [9]) often disrupt the functionality of coupled dynamical systems operating in the synchronized state, driving them away either to an arbitrary state still inside the basin of attraction of the synchronized state, or to an altogether different dynamical regime. The former situation arising on account of permissible perturbations, leads to arbitrary durations of desynchronized dynamics before the system regains synchronous motion. On the other hand, impermissible perturbations permanently forbid the return of the system to the synchronized state, unless again affected by an appropriate external perturbation.

The stability of the synchronized state against the aforementioned perturbations is critical in the operation of many real-world networked dynamical systems. Subsequently, the influence of topological features on network synchronizability and the stability of the synchronized state has been well-investigated [11, 61]. In this context, significant developments constitute the master stability function (MSF, Sec. 4.3.1), basin stability (BS, Sec. 4.1.10) and its extensions to single-node BS (SNBS, Sec. 5.3.2), multiple-node BS (Sec. 5.3.3), and survivability [107]. On the contrary, the issue of *recovery time* (RT) of complex dynamical networks following a random perturbation, which is a measure of how quickly the network relaxes back to the DOS (e.g., a synchronized state) after being perturbed from the same, has received considerably less attention and is currently under active investigation [108–119]. However, this is an important problem concerning dynamical robustness of complex networks, i.e., the ability of a network to restore its dynamical activity to the DOS when its components are subject to random perturbations. For example, the loss of synchrony in engineered systems such as power grids can lead to large-scale power blackouts [13]. In biological systems such as the human brain, it can impede cognitive functions such as information transfer [120] and memory [121]. Thus, quickly restoring synchrony following desynchronizing perturbations is crucial in such coupled dynamical systems. Consequently, it is highly desirable to have an estimate of the RT of the system to the desired stable regime, following a perturbation to a particular node of the network (otherwise operating in the DOS). This creates the

possibility of identifying (and safeguarding) specific nodes which when perturbed lead to a particularly large RT of the system. In this regard, we propose here the framework of *single-node recovery time* (SNRT) addressing the aforementioned issue. We reserve a formal definition of SNRT to Sec. 7.3.3.

SNRT of a node under investigation relates to the time taken by the system operating in the DOS (e.g., a synchronized state) to return to the same, following a random perturbation to the dynamical state of the respective node. The framework of SNRT provides information on the different relative time scales underlying the transient dynamics of the respective nodes of the network during its restoration to the DOS. This can be utilized in revealing the particularly *slow* nodes of the network in contrast to the relatively *fast* ones, leading to the identification of the vulnerable nodes which when perturbed significantly elevate the RT of the whole system. Further, this can provide an insight into the *global relaxation time* (GRT) of the network to the DOS, when starting all its nodes from arbitrary initial conditions. We provide a formal definition of GRT in Sec. 7.3.4. The GRT is referred to as the *global synchronization time* when the synchronized state is the DOS of the network.

Previously, the dependence of synchronization time on various macroscopic topological properties of the corresponding networks has been investigated. For example, Grabow et al. [116] have shown that, largely insensitive to the type of oscillators (phase, multi-dimensional, neural), their intrinsic dynamics (periodic, chaotic) and their coupling schemes (phase-difference, diffusive, pulse-like), networks with a fixed average path length consistently synchronize slowest in the small-world regime. This is a rather unexpected phenomenon given that small-world topology has been suggested to facilitate network synchronization at weaker coupling strengths (than for analogous, appropriately normalized globally coupled systems) [17, 63, 64] as well as being more robust to random perturbations [9]. Also, the MSF approach (Sec. 4.3.1) has been extended by Grabow et al. [117] to provide analytical predictions for the asymptotic synchronization times, which is, however, locally restrictive to small perturbations. Further, the dependence of synchronization time on various macroscopic topological features such as the average path length, global clustering coefficient, etc. has been systematically studied [117]. In this context, the framework of SNRT introduced in this chapter is capable of providing a microscopic view on the response to arbitrary perturbations of individual nodes as well as exploring relationships between various topological features of the nodes and their respective SNRT values.

Finally, we advance on the framework of SNRT for quantifying the resilience (Sec. 4.2) of networked dynamical systems. As described earlier in Sec. 4.2, resilience of a given dynamical system has been defined in at least two different ways, namely, *engineering resilience* (Sec. 4.2.1) and *ecological resilience* (Sec. 4.2.2). Engineering resilience (according to Pimm [50]) of a dynamical system characterizes its resistance to disturbance and speed of return to its equi-

librium, following a perturbation [16, 52]. It implicitly assumes global stability, i.e., the existence of only one equilibrium state, or, if other operating states exist, they should be avoided by applying safeguards [16, 52]. On the other hand, ecological resilience [14] presumes the existence of multiple stable states and the tolerance of the system to disturbances that facilitate transitions among the stable states [16, 52]. In this case, resilience of the system is measured by its capacity to remain in the same basin of attraction in the face of random perturbations [16, 52].

Ecological resilience of the multiple stable states of a system relates to the volume and geometry of their respective basins of attraction. In this context, we reconsidered the concept of ecological resilience and its three crucial aspects of *latitude* (L), *resistance* (R) and *precariousness* (Pr) in Chapter 6. We redefined L, R and Pr in a rigorous dynamical systems' context, utilized it as a foundation for characterizing multistability and proposing the quantifier of *integral stability* [P2]. Besides its extension to quantifying multistability, the framework of ecological resilience has generated widespread interest (cf. [122] and references therein). On the other hand, the facet of engineering resilience, perhaps on account of its restrictive scope to globally stable systems has received considerably less attention. However, it is equally crucial to know how long does a system operating in its desired stable state take to retain functionality in the respective dynamical state, following a random perturbation. As mentioned earlier, networked dynamical systems often exhibit multiple stable states, such as the coexistence of synchronized and desynchronized dynamical regimes, which is a notable example of bistable behaviour. Thus, we extend here the traditional scope of engineering resilience to quantifying the resilience of the DOS (e.g., the synchronized state) in such multistable coupled dynamical systems. More precisely, we relate the engineering resilience of each node of a networked dynamical system to the SNRT (with respect to its DOS) of the corresponding node such that a node with a lower value of SNRT is considered more resilient and vice versa. Thus, the proposed architecture of engineering resilience (SNRT) complements the existing framework of ecological resilience (SNBS) in characterizing the overall resilience of networked dynamical systems.

This chapter is further organized as follows: In Sec. 7.3, we outline the general methodology for calculating SNRT values for a given networked dynamical system. In Sec. 7.4, we illustrate applications of SNRT to networks of Rössler oscillators and the model of the power grid of the United Kingdom with second-order Kuramoto-type nodal dynamics (introduced in Sec. 5.4.2). Finally, we present the conclusions of our work in Sec. 7.5.

7.3. Methods

7.3.1. Preliminaries

In the following, we outline the general methodology for estimating SNRT values for any networked dynamical system. We again consider a network of N oscillators (nodes) where the intrinsic dynamics of the i-th oscillator is described by Eq. (5.1), such that the dynamical equations of the networked system (in analogy with that of Eq. (5.2)) read

$$\dot{\mathbf{x}}_i = \mathbf{F}_i\left(\mathbf{x}_i\right) + \epsilon \sum_{j=1}^{N} A_{ij}\mathbf{H}_{ij}\left(\mathbf{x}_i,\, \mathbf{x}_j\right), \tag{5.2}$$

where again ϵ is the overall coupling strength, $\mathbf{A}$ is the adjacency matrix which captures the interactions between the nodes such that $A_{ij} \neq 0$ if node j influences node i and $\mathbf{H}_{ij} : \mathbb{R}^d \times \mathbb{R}^d \to \mathbb{R}^d$ is an arbitrary coupling function from node j to node i. For the illustrations in this chapter (Sec. 7.4), we consider identical nodal dynamics ($\mathbf{F}_i = \mathbf{F}\,\forall\, i$), symmetric adjacency matrices ($A_{ij} = A_{ji} = 1$ if nodes i and j are connected and $A_{ij} = A_{ji} = 0$ otherwise) and identical coupling functions ($\mathbf{H}_{ij} = \mathbf{H}\,\forall\, i,\, j$).

We assume the desired operational state (DOS) is an attractor of the system that we denote by $\mathcal{A}$ with the corresponding basin of attraction $\mathcal{B}\left(\mathcal{A}\right)$. We usually denote a trajectory on $\mathcal{A}$ by $\tilde{\mathbf{x}}(t)$.

7.3.2. Regularized Reaching Time

For a trajectory initiated from $\mathbf{x}(0) = \left(\mathbf{x}_1(0),\, \mathbf{x}_2(0),\, \ldots,\, \mathbf{x}_N(0)\right)^{\mathrm{T}} \in \mathcal{B}\left(\mathcal{A}\right)$, the attractor is usually reached asymptotically. This implies that the associated reaching time is not finite, thus posing a problem in its measurement. A way to address this problem is regularization of the time variable [119]. We now discuss the framework of *regularized reaching time* proposed by Kittel et al. [119] and then resort to the same in dealing with the above issue.

The distance of a state at time t on a trajectory initiated from $\mathbf{x}(0)$, to the desired attractor is given by,

$$d\left(\mathbf{x}\left(t,\, \mathbf{x}(0)\right), \mathcal{A}\right) = \inf\left\{\left\|\mathbf{x}\left(t,\, \mathbf{x}(0)\right) - \mathbf{x}'\right\| : \mathbf{x}' \in \mathcal{A}\right\},$$

where $\mathbf{x}\left(t,\, \mathbf{x}(0)\right)$ represents the state of the system after a time t has elapsed. The last-entry time for the corresponding trajectory to enter a δ-neighbourhood around the desired attractor $\mathcal{A}$ is given by

$$t_L\left(\mathbf{x}(0),\, \delta\right) = \inf\left\{T : d\left(\mathbf{x}\left(t,\, \mathbf{x}(0)\right), \mathcal{A}\right) < \delta,\, \forall\, t \geq T\right\},$$

where $\delta \to 0$ leads to the aforementioned divergence.

Kittel et al. [119] argued that even though the actual reaching times diverge for the respective trajectories, their differences actually converge. Subsequently, they proposed the *regularized reaching time* $T_{RR}\left(\mathbf{x}(0)\right)$ for any trajectory (starting from $\mathbf{x}(0)$) as the difference between the last-entry times along the respective trajectory and a reference trajectory (starting from $\mathbf{x}_{ref}$), for a given $\delta > 0$. This can be interpreted as the additional time the trajectory starting from $\mathbf{x}(0)$ needs to arrive in the vicinity of the desired attractor, after the reference trajectory starting from $\mathbf{x}_{ref}$ has reached it. Thus,

$$T_{RR}\left(\mathbf{x}(0)\right) = \lim_{\delta \to 0} \left(t_L\left(\mathbf{x}(0),\, \delta\right) - t_L\left(\mathbf{x}_{ref},\, \delta\right)\right). \tag{7.1}$$

A positive or negative value of $T_{RR}\left(\mathbf{x}(0)\right)$ indicates that the considered trajectory arrives by this value *later* or *earlier* than the reference trajectory, respectively. This allows the distinction between *slower* and *faster* trajectories of the system during their return to the desired attractor (cf. Kittel et al. [119] for further details on T_{RR}).

7.3.3. Single-node Recovery Time (SNRT)

In the following, we outline the general methodology for calculating SNRT values for all nodes of any networked dynamical system. We assume that the networked dynamical system of Eq. (5.2) is in its DOS $\tilde{\mathbf{x}}(t)$. Now, consider a permissible random perturbation $\Delta\mathbf{x}_i$ to the dynamical state of the i-th oscillator of the network. The system (otherwise functioning in its DOS) is pushed to a perturbed state $\mathbf{x}_{\Delta i} = (\tilde{\mathbf{x}}_1,\, \tilde{\mathbf{x}}_2,\, \ldots,\, \tilde{\mathbf{x}}_i + \Delta\mathbf{x}_i,\, \ldots,\, \tilde{\mathbf{x}}_N)^{\mathrm{T}}$. The perturbed state (on account of the perturbation being permissible) remains in the basin of attraction $\mathcal{B}\left(\mathcal{A}\right)$ of the DOS (because we chose $\Delta\mathbf{x}_i$ to be permissible), thus ensuring the system's return to the same. We then define the SNRT of the i-th oscillator as,

$$\left\langle T_R^1\left(i\right)\right\rangle = \frac{\displaystyle\int_{P_i(\mathcal{B}(\mathcal{A}))} \rho_i\left(\mathbf{x}_{\Delta i}\right)\, T_{RR}\left(\mathbf{x}_{\Delta i}\right)\, d\Delta\mathbf{x}_i}{\displaystyle\int_{P_i(\mathcal{B}(\mathcal{A}))} \rho_i\left(\mathbf{x}_{\Delta i}\right)\, d\Delta\mathbf{x}_i}, \tag{7.2}$$

where P_i is the projector into the subspace of the i^{th} oscillator, i.e., $P_i(\mathbf{x}) = \mathbf{x}_i$. $\rho_i\left(\mathbf{x}_{\Delta i}\right)$ is the density of permissible perturbed states in state space that the i-th oscillator may be pushed to even via large perturbations with $\int \rho_i\left(\mathbf{x}_{\Delta i}\right)\, d\Delta\mathbf{x}_i = 1$, where this integral is performed over the subspace of the i-th oscillator. The integrals in the numerator and denominator of Eq. (7.2) are performed over the basin of attraction of the DOS (i.e., $\mathbf{x}_{\Delta i} \in \mathcal{B}\left(\mathcal{A}\right)$). Thus, the SNRT of the i-th oscillator $\left\langle T_R^1\left(i\right)\right\rangle$ corresponds to the mean regularized reaching time of the

system to the DOS, after a random permissible perturbation hits the respective oscillator.

Equation (7.1) demands the choice of a reference initial condition $\mathbf{x}_{ref} \in \mathcal{B}(\mathcal{A})$ that needs to be kept fixed for all single-node perturbations to allow comparability between SNRT values of the different nodes of the network. However, different choices of $\mathbf{x}_{ref}$ (as long as we do not choose it on $\mathcal{A}$) simply lead to a shift of all $\langle T_R^1(i)\rangle$ values by a constant only [119]. Although not posing a serious problem, this methodology of choosing $\mathbf{x}_{ref}$ leaves an element of arbitrariness. As we seek to utilize the $\langle T_R^1\rangle$ values in estimating the duration by which a particular node of the network returns *faster* or *slower* than another, this naturally leads to the condition demanding the lowest $\langle T_R^1(i)\rangle$ value to be 0,

$$\min_i \left(\langle T_R^1(i)\rangle\right) = \langle T_R^1\rangle_{min} = 0. \tag{7.3}$$

Using this equation, we can fix $\mathbf{x}_{ref}$ implicitly instead of explicitly specifying it. We denote the node (or one representative if there might be more) with $\langle T_R^1(i)\rangle = 0$ by i_{ref}. The resulting values of $\langle T_R^1\rangle$ now represent differences in time by which nodes of the network return *slower* than the reference node i_{ref}. As opposed to arbitrarily choosing $\mathbf{x}_{ref}$, thereby resulting in negative T_{RR} values (which is counter-intuitive when measuring time), the above choice of $\mathbf{x}_{ref}$ ensures non-negativity of $\langle T_R^1(i)\rangle$ values, besides eliminating the arbitrariness associated with the choice of $\mathbf{x}_{ref}$. Further details on the choice of the reference trajectory are provided in Sec. 7.3.3.1.

We now present an algorithm for estimating the SNRT of the i-th oscillator/node of a network (modelled using Eq. (5.2)):

(i) Identify the DOS of the network. This state often corresponds to the synchronized dynamics of the oscillators coupled on the network.

(ii) When the attractor corresponding to the DOS $\mathcal{A}$ is not a fixed point, choose $P\ (>1)$ different points on the attractor. Otherwise, choose $P = 1$.

(iii) For a particular value of p ($p = 1, 2, \ldots, P$), initiate the system from the DOS corresponding to the p-th point on $\mathcal{A}$. Then, perturb the i-th oscillator by drawing I_C randomly distributed (according to $\rho_i(\mathbf{x}_{\Delta i})$) initial conditions $\mathbf{x}_{\Delta i}^p(j = 1, 2, \ldots, I_C)$ from inside the basin of attraction of the DOS. For the results described in this chapter, we assume a uniform distribution of $\rho_i(\mathbf{x}_{\Delta i})$.

(iv) For a fixed value of $\delta > 0$, calculate the last-entry time $t_L\left(\mathbf{x}_{\Delta i}^p(j), \delta\right)$ of the system for the j-th initial condition.

(v) Estimate the SNRT of the i-th oscillator $(T_R^1(i,\,p))$ for the p-th point on the attractor as,

$$\hat{T}_R^1(i,\,p) = \frac{\sum_{j=1}^{I_C} t_L\left(\mathbf{x}_{\Delta i}^p(j)\,,\,\delta\right)}{I_C}, \tag{7.4}$$

and then average over p to obtain,

$$\langle T_R^1(i)\rangle = \frac{1}{P}\sum_{p=1}^{P} \hat{T}_R^1(i,\,p)\,. \tag{7.5}$$

(vi) Finally, we identify the node i_{ref} with the minimum $\langle T_R^1\rangle$ value (as computed above for all nodes) $\langle T_R^1\rangle_{min}$ and subtract this value from the $\langle T_R^1(i)\rangle$ of the i-th oscillator computed above, thus yielding the SNRT value of the respective oscillator.

The parameters P, I_C and δ of the above algorithm have to be selected prior to its implementation. The actual values should be chosen according to the specifics of the system under investigation, as also illustrated with the different applications presented in this chapter (Sec. 7.4). It is conclusive however, that higher values of P and I_C yield better estimates of $\langle T_R^1(i)\rangle$.

As mentioned earlier, this concept of SNRT can be utilized in identifying the *slow* and *fast* nodes/sub-components of networked dynamical systems. Also, the proposed machinery can be used in revealing systematic relationships between SNRT values of different nodes and their respective topological features. Further, it can be extended to a measure of (engineering) resilience of the different nodes of a networked dynamical system (see Sec. 7.3.6) and thereby utilized in identifying the particularly vulnerable nodes of the network as well as the more resilient ones. Subsequently, this framework of SNRT can be potentially relevant in selecting specific nodes to be safeguarded from external perturbations.

7.3.3.1. On the choice of the reference trajectory

We elaborate here on the existence of a reference state such that the condition in Eq. (7.3) is fulfilled. For any arbitrary $\mathbf{x}_{ref}$ we have the corresponding T_{RR} function, and hence $\langle T_R^1(i)\rangle$ as well. Now, we can take a new $\mathbf{x}'_{ref} = \varphi(-t,\,\mathbf{x}_{ref})$ where $\varphi(-t,\,\cdot)$ is the time-evolution operator shifting a state for the time t backwards along the flow and $t = \langle T_R^1\rangle_{min}$. Using $\mathbf{x}'_{ref}$, we have a corresponding T'_{RR} function and $\langle T_R^{1\prime}(i)\rangle$. In particular, $\langle T_R^{1\prime}\rangle_{min} = 0$ holds by construction. So, taking $\mathbf{x}'_{ref}$ as the reference state fulfils Eq. (7.3).

We now define the *global relaxation time* of a network, which relates to the overall time scale of the dynamics of a network during its relaxation to the DOS.

7.3.4. Global Relaxation Time (GRT)

Starting all nodes of a networked dynamical system from random initial conditions inside the basin of attraction of the desired attractor involves a transient time before the system reaches the associated attractor. We refer to the duration of this transient regime as the *relaxation time* of the system for the respective initial state. We estimate the *global relaxation time* $\langle T_R \rangle$ of a network as follows:

(i) Draw I_C random initial conditions from inside the basin of attraction of the DOS. The j-th initial condition can be written as $\mathbf{x}(j) = \left(\mathbf{x}^1, \mathbf{x}^2, \ldots, \mathbf{x}^N\right)^{\mathrm{T}}$ where $j = 1, 2, \ldots, I_C$. Note, that the value of I_C chosen for computing the GRT can be different from the one chosen for calculating SNRT above (Sec. 7.3.3).

(ii) For the j-th initial condition, calculate the last-entry time $t_L(\mathbf{x}(j), \delta)$ of the system with the same value of δ as chosen for computing SNRT (Sec. 7.3.3).

(iii) Calculate the GRT of the network as,

$$\langle T_R \rangle = \frac{1}{I_C} \sum_{j=1}^{I_C} t_L(\mathbf{x}(j), \delta). \tag{7.6}$$

(iv) Finally, subtract the value of $\langle T_R^1 \rangle_{min}$ (obtained in Sec. 7.3.3) from the $\langle T_R \rangle$ computed above in obtaining the GRT of the network.

When the DOS of the network is a synchronized state, its GRT is referred to as the *global synchronization time* of the system.

The GRT of a network is useful for quantifying the expected transient time to reach the DOS, when starting the system from a random initial condition. In Sec. 7.4, we will illustrate the relationship between SNRT values and the GRT of a network for different systems.

In order to avoid terminological confusion, we explicitly distinguish between the usage of *recovery*, *reaching* and *relaxation* time. We use the term *recovery* with reference to the time taken by the system to recover from a perturbation and resume operation in the DOS. On the other hand, when initiating all the nodes of the system from arbitrary conditions, the term *relaxation* is used with reference to the time before the system relaxes to the DOS. It is the difference between the relaxation times of a trajectory starting from a particular initial condition and that of a reference trajectory, which is termed as the regularized *reaching* time for the respective initial condition.

It should be noted that the situation following a perturbation may also be viewed as the system starting from a particular initial condition (corresponding to the perturbed state) and subsequently, relaxing to the respective attractor. However, we want to specifically distinguish between relaxation following a perturbation as a process of *recovery*, and the traditional formalism of *relaxation*

of the system when starting the entire network from random initial conditions. Subsequently, we seek to utilize the above terminology in order to maintain this distinction during the course of this text.

7.3.5. Single-node Basin Stability (SNBS)

As previously described in Sec. 4.1.10, the BS of a particular attractor relates the volume of its basin of attraction to the likelihood of returning to the same attractor in the face of random perturbations. More precisely, the BS of a particular attractor is defined as the fraction of the volume of the state space belonging to the basin of attraction of the respective attractor (Sec. 4.1.10). In practice, BS of any particular attractor is estimated (as per the prescription in Sec. 4.1.10.1) using a numerical Monte Carlo procedure by drawing random initial states from a chosen subset of the entire state space, simulating the associated trajectories, and calculating the fraction of trajectories that approach the respective attractor. As mentioned earlier, the ecological resilience (Sec. 4.2.2) of a stable state is (among other properties) determined by the size and shape of its basin of attraction, and is therefore closely related to its BS.

BS has been further extended to the framework of single-node BS (SNBS), as elaborated upon in Sec. 5.3.2. SNBS $\langle S_B^1 \rangle$ of a node under investigation corresponds to the probability of the network (operating in the DOS) to return to the DOS, after that particular node has been hit by a non-infinitesimal perturbation. We refer to the procedure outlined in Sec. 5.3.2 for the general methodology used throughout this chapter for estimating SNBS values for any networked dynamical system.

7.3.6. Engineering Resilience

SNBS is a measure related to the ecological resilience of a node subjected to a random perturbation (when the entire network was functioning in the DOS prior to the disturbance). The time elapsed before the network returns to its DOS, following a permissible random perturbation to a particular node determines the engineering resilience of the respective node. We recommend incorporating the engineering resilience of a node (besides its ecological resilience as characterized by its SNBS value) quantified as being inversely related to its SNRT value, in measuring the overall resilience of the respective node. For example, it may be possible that two nodes of a networked dynamical system have very similar values of SNBS. However, the SNRT values of the respective nodes may differ significantly (as we shall illustrate using examples in Sec. 7.4). In such a situation, the proposed framework of SNRT should complement that of SNBS in appropriately assessing the resilience of the respective nodes of a network.

7.4. Examples

We shall now illustrate applications of SNRT to various networked dynamical systems. Here, we specifically apply the framework to networks of oscillators with continuous-time dynamics (Eq. (5.2)) exhibiting bistability on account of coexisting synchronized and desynchronized regimes, where the former is considered as the DOS of the system. However, the framework is generally applicable to (continuous- or discrete-time) networked dynamical systems with multiple coexisting states as well. It should be noted that the values of the measures for the different networks/examples studied in this chapter are not directly comparable. Also, the algorithmic parameters for each application have been chosen according to the specific system under investigation.

7.4.1. Deterministic Scale-free Network of Rössler Oscillators

In analogy with the example presented in Sec. 5.4.1, we first consider a network of N identical Rössler oscillators, with diffusive coupling in the x^2-variable between two coupled nodes such that the full dynamical equations of node i (in correspondence with Eq. (5.2)) read

$$\begin{aligned}
\dot{x}_i^1 &= -x_i^2 - x_i^3, \\
\dot{x}_i^2 &= x_i^1 + a x_i^2 + \epsilon \sum_{j=1}^{N} A_{ij} \left(x_j^2 - x_i^2 \right), \\
\dot{x}_i^3 &= b + x_i^3 \left(x_i^1 - c \right).
\end{aligned} \tag{5.8}$$

We use the parameter values of $a = b = 0.2$ and $c = 7.0$ for which the intrinsic dynamics of each uncoupled Rössler oscillator is chaotic.

As a specific network topology, we again use the undirected deterministic scale-free network (Sec. 3.3.2.1). For the simulations carried out in this section, we generate a deterministic scale-free network developed over 3 generations and hence, comprising $N = 81$ nodes (Fig. 7.1).

We consider the completely synchronized state as the DOS of the network, which corresponds to all oscillators following the same trajectory. Further, we choose $\epsilon = 0.8$ for which the completely synchronized state in Rössler oscillators diffusively coupled via the x^2-variable is stable (cf. [123] for further details on the calculation of the stability interval) and set $\delta = 10^{-4}$ for estimating the SNRT ($\langle T_R^1 \rangle$) values, using the procedure described in Sec. 7.3.3 [3].

[3] We suggest choosing a value of δ depending upon the system of interest. This choice should be made to ensure that the system comes sufficiently close to the desired attractor $\mathcal{A}$ as well as being computationally efficient. For example, we choose a value of $\delta = 10^{-4}$ for the deterministic scale-free network, whereas $\delta = 10^{-6}$ for the random scale-free network. This is because in the former case, the system generally takes a longer time to enter the δ-environment around $\mathcal{A}$. For a further discussion on the estimation of T_{RR}, we refer the reader to Ref. [119].

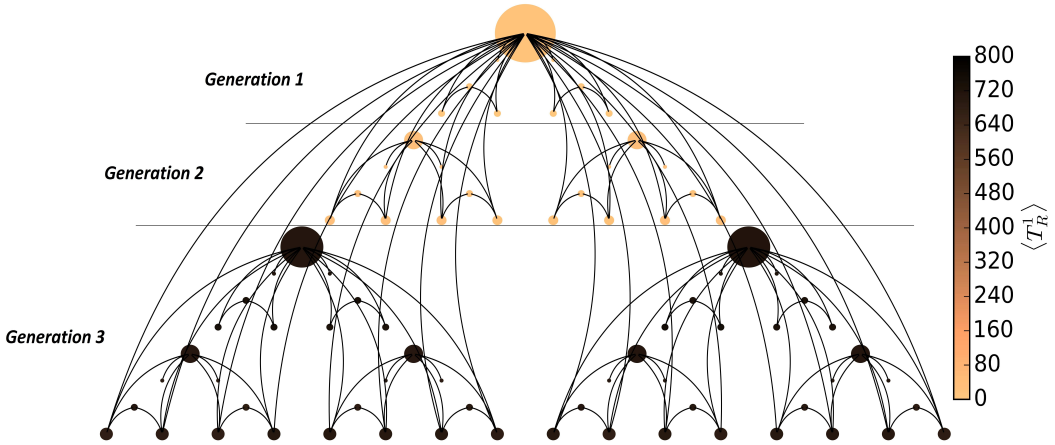

Figure 7.1.: Network topology of the undirected deterministic scale-free network of $N = 81$ identical Rössler oscillators. The size of each node is proportional to its degree and the colour indicates the $\langle T_R^1 \rangle$ value of the respective node.

We calculate and present the individual $\langle T_R^1 \rangle$ (on $\log_{10}$ scale) values of the nodes in Fig. 7.2(a). Interestingly, the 3 generations of nodes split into three classes in terms of their $\langle T_R^1 \rangle$ values such that the lower the generation in the hierarchy, the higher is the SNRT of the individual nodes comprising it (as evident from the histogram in Fig. 7.2(b)).

We next compare these findings with two key topological features of degree (k, Sec. 3.2.1) and betweenness centrality (bc, Sec. 3.2.3) of the nodes of the deterministic scale-free network. Figures 7.2(c) and 7.2(d) show the relationship of the $\log_{10}\left(\langle T_R^1 \rangle\right)$ values with the topological features of degree k and betweenness centrality bc of the nodes, respectively. The $\langle T_R^1 \rangle$ values do not exhibit any marked relationship with these two characteristics. This is further illustrated by the correlation coefficient of -0.040 (-0.085) between $\langle T_R^1 \rangle$ and k (bc). We summarize our results in Fig. 7.1, which displays the network topology where the size of each node is proportional to the degree and the colour corresponds to the $\langle T_R^1 \rangle$ value of the respective node.

The nodes in the 3^{rd} generation of the deterministic scale-free network comprise its *slow* nodes. It is expected that the overall time scale of synchronization of a network should be governed by the node with the highest SNRT, i.e., the *slowest* node of the system. The *slowest* node of the deterministic scale-free network has $\langle T_R^1 \rangle \approx 749.8$. We also computed the GRT $\langle T_R \rangle$ of the deterministic scale-free network using the methodology described in Sec. 7.3.4. We find $\langle T_R \rangle \approx 750.04$ being very close to the maximum $\langle T_R^1 \rangle$ value of the network. Thus, we conclude that the *slowest* nodes of the deterministic scale-free network indeed govern its overall time scale of synchronization. However, this result cannot be generalized

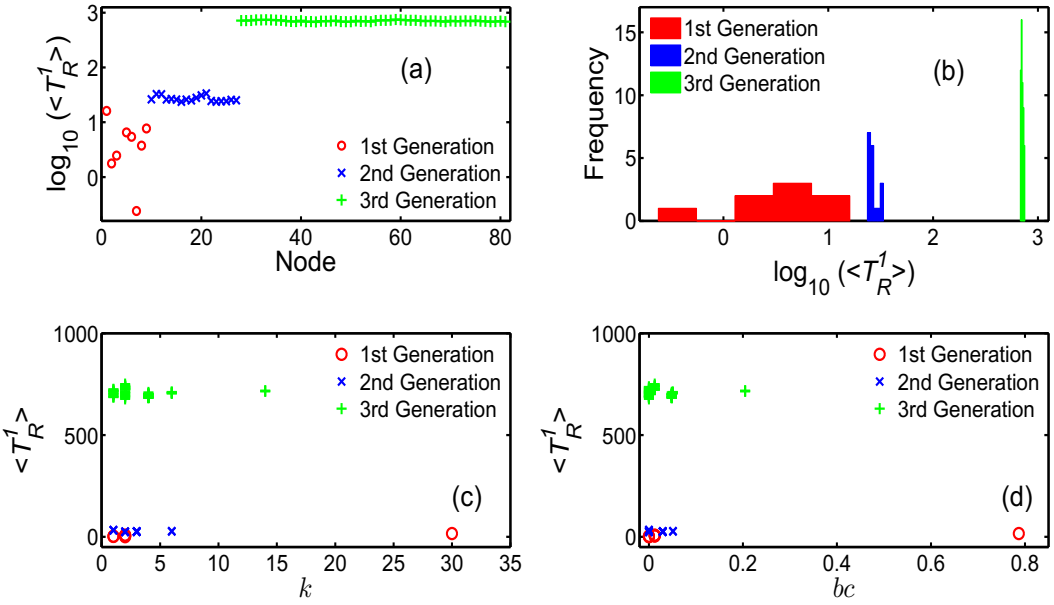

Figure 7.2.: (a) SNRT $\langle T_R^1 \rangle$ (on $\log_{10}$ scale) of the nodes of the 3 generations of the undirected deterministic scale-free network of N identical Rössler oscillators (Eq. (5.8)). The first 9 nodes comprise the 1^{st} generation, the next 18 nodes the 2^{nd} generation and the final 54 nodes the 3^{rd} generation. Node 4 having the minimum SNRT value $\langle T_R^1(4) \rangle = 0$ of the network (implying divergence of $\log_{10}\left(\langle T_R^1(4) \rangle\right)$) has not been shown in the plot. Note that the $\langle T_R^1 \rangle$ values of the 9 nodes comprising the 1^{st} generation are actually between 0 and 17. However, as the $\langle T_R^1 \rangle$ values are presented on a $\log_{10}$ scale, they appear to be much more dispersed than the $\log_{10}\left(\langle T_R^1 \rangle\right)$ values of the nodes in the other two generations. However, the $\langle T_R^1 \rangle$ values of the nodes in all the three generations actually have similar variations. (b) Histogram of $\log_{10}\left(\langle T_R^1 \rangle\right)$ of the nodes. (c, d) Relationship of $\langle T_R^1 \rangle$ with (c) degree (k) and (d) betweenness centrality (bc) of the nodes.

to any arbitrary topology, as we will demonstrate in the following.

7.4.2. Random Scale-free Networks of Rössler Oscillators

Next, we consider an ensemble of 100 random scale-free networks (generated using the classical Barabási-Albert (BA) model of growth and preferential attachment [18]) of $N = 81$ Rössler oscillators each, with the same parameter values as for the deterministic scale-free network. We refer the reader to Sec. 3.3.1.2 for further details on the BA network model. We set $N_0 = 3$ and $m = 2$ for generating the ensemble of random scale-free networks considered in this section. While the deterministic scale-free network of $N = 81$ Rössler oscillators studied

in Sec. 7.4.1 had 130 edges, equivalently, an edge density of $\frac{130}{\binom{81}{2}} \approx 0.04$, the random scale-free networks generated using the classical BA model have edge densities of 0.049, i.e., 158 edges in each realization. This means that the BA random scale-free networks have 22.5% more edges than the deterministic scale-free network considered earlier in Sec. 7.4.1. Therefore, the results obtained for both topologies are not directly comparable quantitatively.

The distribution of SNBS $\langle S_B^1 \rangle$ values of the $N = 81$ nodes of the considered ensemble is presented in Fig. 7.3(a). Surprisingly, all nodes have similar and very high $\langle S_B^1 \rangle$ values. Similar results were observed in our study in Sec. 5.4.1 on SNBS values in the deterministic scale-free network of Rössler oscillators. Figures 5.2 and 5.3 present the distribution of the $\langle S_B^1 \rangle$ values of the $N = 81$ nodes of the deterministic scale-free network, considered in Sec. 5.4.1/Sec. 7.4.1. Clearly, the $\langle S_B^1 \rangle$ values of all the nodes are very high (~ 0.95) as well as very similar. Likewise, Fig. 7.3(a) here illustrates the distribution of the $\langle S_B^1 \rangle$ values of all the nodes of the considered ensemble of BA random scale-free networks, which are again equally high (~ 0.95) and also quite similar for all nodes of

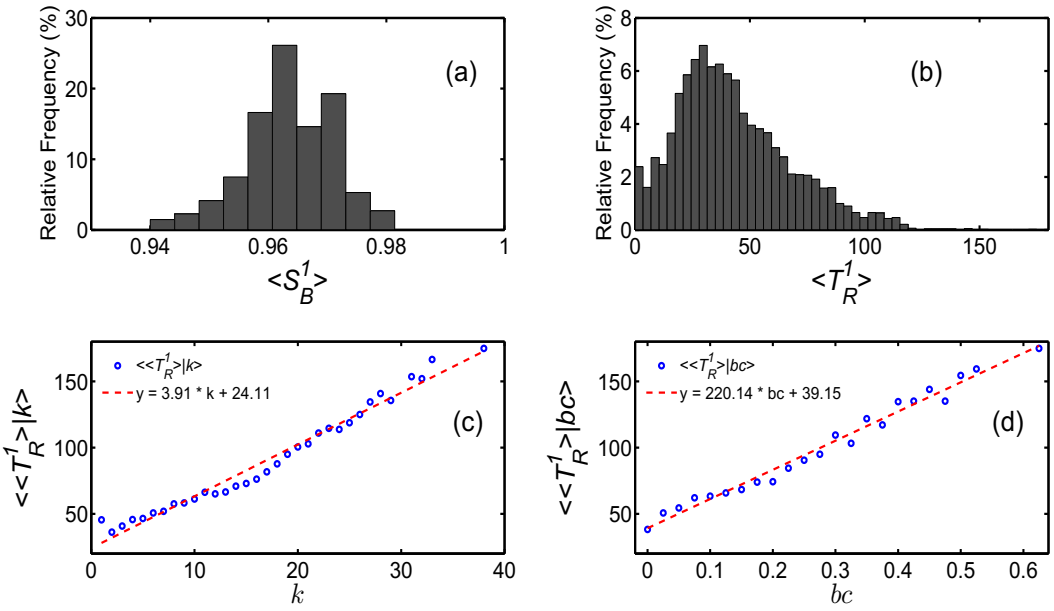

Figure 7.3.: (a) Histogram of SNBS $\langle S_B^1 \rangle$ of all nodes of the considered ensemble of random scale-free networks. The relative frequencies (%) correspond to the percentage of nodes with $\langle S_B^1 \rangle$ values lying within the respective bin of the histogram. (b) Same for the $\langle T_R^1 \rangle$ values. (c, d) Conditional means (blue circles) of $\langle T_R^1 \rangle$ with respect to (c) degree $\left(\langle \langle T_R^1 \rangle \mid k \rangle\right)$ and (d) betweenness centrality $\left(\langle \langle T_R^1 \rangle \mid bc \rangle\right)$ of the nodes. The red lines indicate linear fits to the conditional means.

the ensemble. These observations lead to two important conclusions. Firstly, the similar and rather high $\langle S_B^1 \rangle$ values indicate that the synchronized state in scale-free networks is generally very robust to perturbations affecting a single node of the system. Secondly, we observe that the presence or lack of a specific macroscopic (hierarchical) structure (as in the deterministic scale-free network but not in its random counterpart) in the respective scale-free network does not affect the distribution of its $\langle S_B^1 \rangle$ values markedly. In contrast to the latter finding, we have already observed an influence of the hierarchical structure on $\langle T_R^1 \rangle$ for the deterministic scale-free network (Fig. 7.2(a)). On this note, we shall further unfold dependences of $\langle T_R^1 \rangle$ values on different topological features of random scale-free networks.

The corresponding distribution of $\langle T_R^1 \rangle$ (for $\delta = 10^{-6}$) of all nodes of the considered ensemble of random scale-free networks is shown in Fig. 7.3(b) [3]. As in the case of the deterministic scale-free network, we next consider the mutual dependence between SNRT and the local topological characteristics of the network. For this purpose, we study the distribution of $\langle T_R^1 \rangle$ values of all nodes of the ensemble with respect to their degree and betweenness centrality. We collect all nodes of the ensemble having a particular degree k and calculate the mean over the $\langle T_R^1 \rangle$ values of all these nodes which corresponds to the conditional mean $\langle \langle T_R^1 \rangle \mid k \rangle$. Similarly, we bin the bc values of all nodes of the ensemble and calculate the conditional mean $\langle \langle T_R^1 \rangle \mid bc \rangle$ over the $\langle T_R^1 \rangle$ values of all nodes belonging to the respective bin. Interestingly, the conditional mean values exhibit a strong linear dependency with respect to k and bc as illustrated in Figures 7.3(c) and 7.3(d), respectively. This is further underlined by correlation coefficients of 0.987 (0.991) of the conditional means with k (bc). Thus, nodes with high k and bc, namely the hubs in the random scale-free network, can be classified as its *slow* nodes. Perturbations to a more central node of a scale-free network (operating in the synchronized state) can easily spread to other nodes of the network driving them further away from the synchronized state. As a result, a scale-free network operating in synchrony may take longer to resynchronize when its more central nodes are perturbed as opposed to less central ones. This observation is supported by the positive correlation between the conditional mean $\langle \langle T_R^1 \rangle \mid bc \rangle$ and bc. Further, given the strong linear relationship of the conditional mean SNRT with bc, a similar dependence for k is to be expected (and vice versa) since random scale-free networks generally exhibit a strong correlation between k and bc of their nodes [124]. However, the relationship of the conditional mean SNRT with k and bc being specifically linear is surprising and revealing the underlying reason requires further investigation. We emphasize that the observed relations are not specific to the relatively small network size. For example, an ensemble of 100 random BA scale-free networks, each comprising 243 Rössler oscillators constituting the nodal dynamics (with similar parameter values as above but for $\epsilon = 1.3$) yield similar results (presented in Appendix A).

We now calculate and present the GRT $\langle T_R \rangle$ of all members of the considered

ensemble of random scale-free networks (Fig. 7.4(a), black circles). Interestingly, we observe that unlike for the deterministic scale-free network, the overall time scale of synchronization in the different network realizations of its random counterpart differs markedly from the maximum SNRT (red crosses) of the respective realization. To further study this finding, for each network realization we compute the average of the $\langle T_R^1 \rangle$ values of all its $N = 81$ nodes and denote it by $\langle\langle T_R^1 \rangle\rangle$. Notably, the $\langle T_R \rangle$ value of every network realization appears closely related to $\langle\langle T_R^1 \rangle\rangle$ (blue crosses) as illustrated in Fig. 7.4(a). This is also corroborated by a correlation coefficient of 0.991 between $\langle T_R \rangle$ and $\langle\langle T_R^1 \rangle\rangle$.

Figure 7.4(b) shows the maximum betweenness centrality bc_{max} of all nodes of each network realization and its relationship with the GRT $\langle T_R \rangle$ of the respective realization. As mentioned earlier, perturbing the node with bc_{max} in a scale-free network (operating in the synchronized state) may lead to a particularly large relaxation time to the synchronized state. Thus, the higher the maximum betweenness centrality of a scale-free network, the higher is the GRT of the system, which is underlined by the positive correlation coefficient of 0.882 between $\langle T_R \rangle$

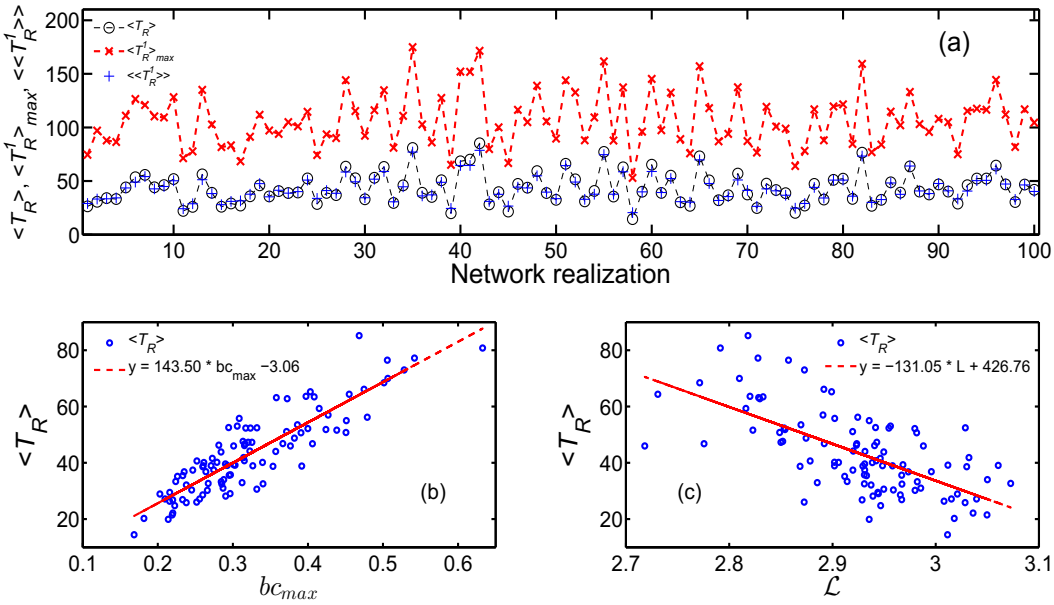

Figure 7.4.: (a) Global RT $\langle T_R \rangle$ (black circles), maximum SNRT $\langle T_R^1 \rangle_{max}$ (red crosses) and average SNRT $\langle\langle T_R^1 \rangle\rangle$ (blue crosses) of all network realizations from the considered ensemble of random scale-free networks. (b) Relationship between $\langle T_R \rangle$ (blue circles) and the maximum betweenness centrality (bc_{max}) of all nodes of the respective network realization. (c) As in (b) for $\langle T_R \rangle$ and average path length $(\mathcal{L})$ of the respective network realization. The red lines in (b, c) indicate linear fits.

and bc_{max} in Fig. 7.4(b).

The dependence of the GRT $\langle T_R \rangle$ of each network realization on its average path length ($\mathcal{L}$) (Sec. 3.2.2) is presented in Fig. 7.4(c). We observe that $\langle T_R \rangle$ exhibits a negative correlation coefficient of -0.658 with respect to $\mathcal{L}$, i.e., random scale-free networks with shorter characteristic path lengths synchronize slower. This result is compatible with the fact that random scale-free networks with longer characteristic path lengths have been previously shown to promote synchronizability [64]. The underlying heuristic picture is that a small $\mathcal{L}$ in such networks corresponds to a large amount of traffic passing through the few 'central' nodes connected to each other which facilitate communication between the much larger population of the other oscillators. This may lead to destructive interference of the different signals passing through such nodes. Subsequently, there may not be significant overall communication between the different oscillators of the network, thereby culminating in its reduced synchronizability [64].

7.4.3. Erdős-Rényi Random Networks of Rössler oscillators

Here, we consider an ensemble of 100 Erdős-Rényi random networks (Sec. 3.3.1.1) of $N = 81$ Rössler oscillators each, again with the same parameter values as for the deterministic scale-free network (Sec. 7.4.1) and the ensemble of random scale-free networks of Rössler oscillators (Sec. 7.4.2). We consider a

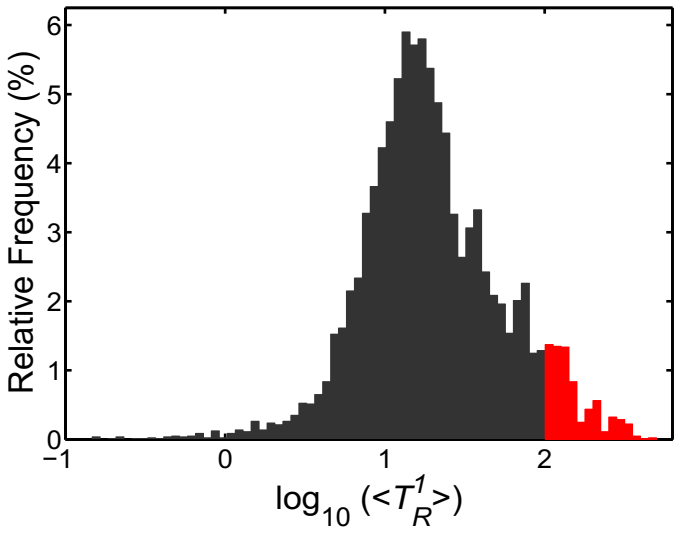

Figure 7.5.: Distribution of SNRT $\langle T_R^1 \rangle$ (on $\log_{10}$ scale) of all nodes of the considered ensemble of Erdős-Rényi random networks. The relative frequencies (%) correspond to the percentage of nodes with $\log_{10}\left(\langle T_R^1 \rangle\right)$ values lying within the respective bin. The *fast* nodes of the ensemble with $\langle T_R^1 \rangle \leq 100$ are shown in black while the *slow* nodes having $\langle T_R^1 \rangle > 100$ are marked in red.

probability $p = 0.04$ of a connection between any pair of vertices of a network, resulting in a total of 130 edges in each realization.

For $\delta = 10^{-6}$, we calculate and present the distribution of $\langle T_R^1 \rangle$ (on $\log_{10}$ scale) values of all nodes of the considered ensemble of Erdős-Rényi random networks in Fig. 7.5 [3]. It is evident from the distribution that most nodes have rather low values of $\langle T_R^1 \rangle$ (≤ 100), which comprise the *fast* nodes of the respective network. However, we also observe the existence of very few *slow* nodes which exhibit much higher $\langle T_R^1 \rangle$ (> 100) values. The $\langle T_R^1 \rangle$ values again do not exhibit any strong linear relationship with k (bc), as validated by the correlation coefficient of 0.743 (0.36).

7.4.4. Power grid of the United Kingdom

As a final more realistic example, we reconsider the conceptual model of the power transmission grid of the United Kingdom with second-order Kuramoto-type nodal dynamics (Sec. 5.4.2). As previously noted, the network consists

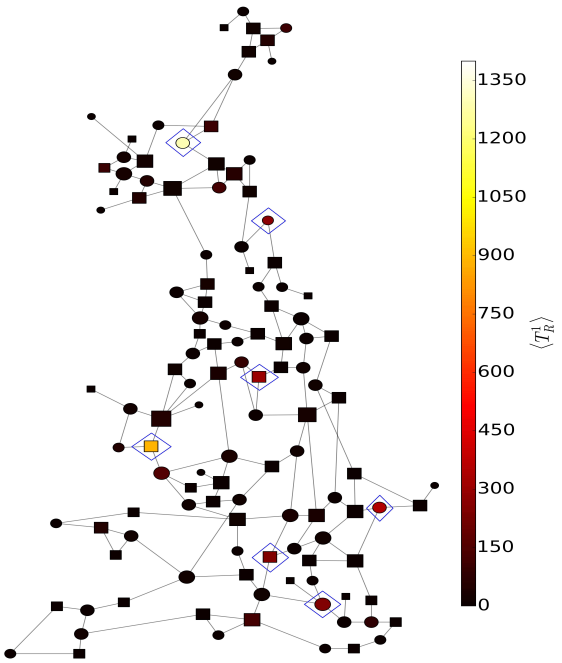

Figure 7.6.: Network topology of the power transmission grid of the United Kingdom (comprising $N = 120$ nodes) with second-order Kuramoto-type nodal dynamics. Circular nodes denote net generators while square nodes are net consumers. The size of each symbol is proportional to the degree, and its colour corresponds to the $\langle T_R^1 \rangle$ value of the respective node. The 7 nodes further encircled by blue diamonds comprise the *slow* nodes of the grid in our simplified model.

of $N = 120$ nodes and 165 transmission lines (as illustrated in Fig. 7.6) with topological properties much different from those of a scale-free network. The dynamical equations of the system (in analogy with Eq. (5.2)) read

$$\begin{aligned} \dot{\theta}_i &= \omega_i, \\ \dot{\omega}_i &= -\alpha\omega_i + P_i + \epsilon \sum_{j=1}^{N} A_{ij} \sin\left(\theta_j - \theta_i\right), \end{aligned} \tag{5.11}$$

where θ_i, ω_i, α and P_i denote the phase, frequency, electromechanical damping constant and net power input of the i-th oscillator, respectively. Furthermore, we randomly choose $\frac{N}{2}$ net generators and $\frac{N}{2}$ net consumers with $P_i = +P_0$ and $P_i = -P_0$, respectively [13]. We use the parameter values of $\alpha = 0.1$, $P_0 = 1.0$ and $\epsilon = 9.0$ for obtaining the results described below.

We again consider the synchronized state, which corresponds to all oscillators having constant phases $\tilde{\theta^i}$ and frequencies $\tilde{\omega^i} = 0$, as the DOS of the grid. We select $I_C = 1000$ trials for calculating the SNRT values of the network. The $\langle T_R^1 \rangle$ values (for $\delta = 10^{-4}$) of all the $N = 120$ nodes are shown in Fig. 7.7(a) and Fig. 7.7(b) displays a histogram of all $\langle T_R^1 \rangle$ values [3]. Interestingly, we observe from Figures 7.7(a) and 7.7(b) that 113 nodes have low values of SNRT ($\langle T_R^1 \rangle \leq 200$), which are shown in black in Fig. 7.7. However, we also observe 7 *slow* nodes that exhibit substantially higher values ($\langle T_R^1 \rangle > 200$), which are marked in red in Fig. 7.7. Therefore, (individually or collectively) perturbing any of these 7 nodes of the network will result in dysfunction of the grid and a significantly longer time until the system retaliates to the synchronized state. In turn, it is recommended to control or safeguard these 7 specific nodes of the network to avoid a long waiting time for the system to return to the synchronized state in the face of random perturbations. The choice of the boundary at $\langle T_R^1 \rangle = 200$ for distinguishing between the *fast* and *slow* nodes is motivated by the fact that we observe a first substantial gap in the histogram in Fig. 7.7(b) around the aforementioned value. We also find similar results from a cluster analysis of the $\langle T_R^1 \rangle$ values of the network. These 7 nodes are not found to exhibit any specific topological features leading to their relatively higher respective $\langle T_R^1 \rangle$ values. Further investigations analyzing these results may provide potentially important insights in this regard.

We emphasize that the Erdős-Rényi random networks of Rössler oscillators (explored in Sec. 7.4.3) were found to exhibit similar distributions of $\langle T_R^1 \rangle$ values as above. Figures 7.7(c) and 7.7(d) illustrate the values of $\langle T_R^1 \rangle$ in comparison with k and bc, respectively. The correlation coefficients of $\langle T_R^1 \rangle$ with k and bc are 0.102 and 0.061, respectively, ruling out the existence of a systematic dependence between $\langle T_R^1 \rangle$ and k or bc. Figure 7.6 displays the network topology together with the individual $\langle T_R^1 \rangle$ values in analogy with Fig. 7.1 for the deterministic scale-free network of Rössler oscillators.

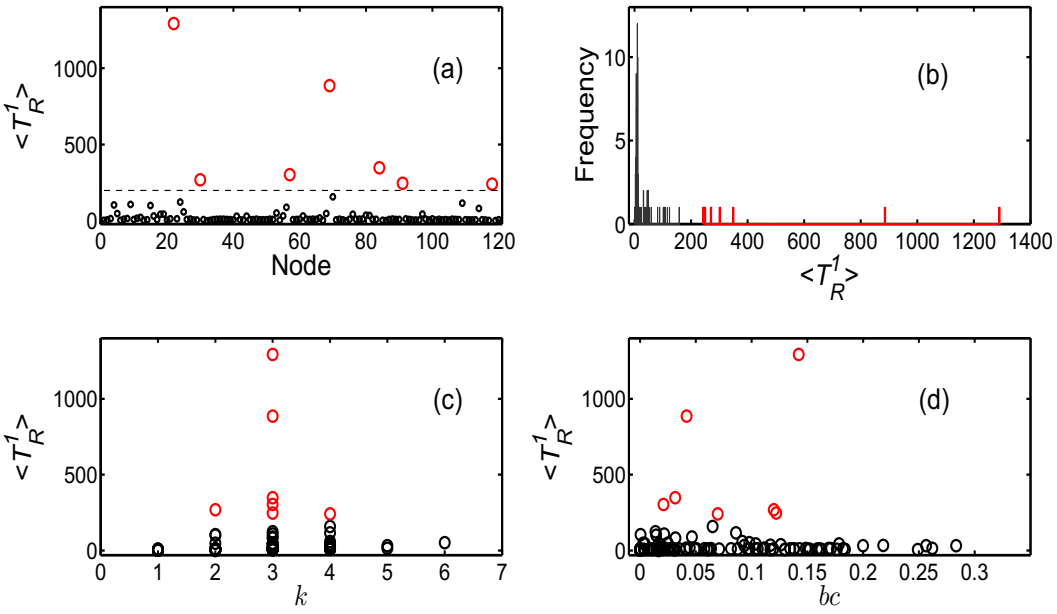

Figure 7.7.: (a) SNRT $\langle T_R^1 \rangle$ of all the $N = 120$ nodes of the power grid of the United Kingdom with second-order Kuramoto-type nodal dynamics. (b) Histogram of $\langle T_R^1 \rangle$ of all the $N = 120$ nodes. (c, d) Dependence of $\langle T_R^1 \rangle$ on (c) degree (k) and (d) betweenness centrality (bc) of the nodes. The *fast* nodes of the grid with $\langle T_R^1 \rangle \leq 200$ are shown in black while the *slow* nodes having $\langle T_R^1 \rangle > 200$ are marked in red.

7.5. Conclusion

Complex systems modelled as networks of interacting dynamical units are ubiquitous and often exhibit multiple stable states. Maintaining operation of such systems in the desired stable state (which often concurs with the synchronized state of the network) is vital to their functionality. Subsequently, this has generated a lot of attention in studying stability of the desired operational state (DOS) in such coupled dynamical systems. However, given that the DOS is stable in principle, it is equally important that the system relaxes back to the same as quickly as possible, following a random perturbation to a particular node of the network. We have addressed this issue here by proposing the framework of *single-node recovery time* (SNRT) which relates to the time taken by the system operating in the DOS to return to the same, following a non-infinitesimal perturbation to the dynamical state of the respective node. It is important to note that we did not address the problem of driving the perturbed system to the DOS. Instead, we aimed at unveiling the different relative time scales underlying the transient dynamics of individual nodes of the network during its relaxation to the DOS,

in order to identify specific nodes which when perturbed lead to significantly enlarged recovery time. We thus recommend taking precautionary measures of safeguarding primarily these nodes of the network from external perturbations.

Importantly, the proposed machinery can be utilized in revealing relationships between topological features of nodes and their respective SNRT values and in turn, the *global relaxation time* (GRT) of the overall network. Further, we have suggested the association of SNRT with the concept of engineering resilience in quantifying the resilience of such networked dynamical systems. Finally, we have applied the framework of SNRT to deterministic and random (scale-free and Erdős-Rényi) networks of Rössler oscillators and a conceptual model of the power grid of the United Kingdom with second-order Kuramoto-type nodal dynamics.

Chapter 8.

Rewiring Hierarchical Scale-free Networks: Influence on Synchronizability and Topology

8.1. Summary

Many real-world complex networks simultaneously exhibit topological features of *scale-free* behaviour and *hierarchical* organization. In this regard, deterministic scale-free (DSF, Sec. 3.3.2.1) and pseudofractal scale-free (PSF, Sec. 3.3.2.2) networks constitute notable models which simultaneously incorporate the aforementioned properties. The rules governing the formation of such networks are completely deterministic. However, real-world networks are presumably neither completely deterministic, nor perfectly hierarchical. Therefore, we suggest here initially perfectly hierarchical scale-free networks with subsequently randomly rewired edges as better representatives of practical networked systems. In particular, we preserve the scale-free degree distribution of the deterministic networks but successively relax the hierarchical structure while rewiring them. We utilize the framework of master stability function (Sec. 4.3.1) in investigating the synchronizability of dynamical systems coupled on such rewired networks. Interestingly, this reveals that the process of rewiring is capable of significantly enhancing as well as deteriorating the synchronizability of the resulting networks. We investigate the influence of rewiring edges on the topological properties of the rewired networks and, in turn, their relation to the synchronizability of the respective topologies. Finally, we compare the synchronizability of DSF and PSF networks with that of random scale-free networks (generated using the classical Barabási-Albert (BA) model of growth and preferential attachment (Sec. 3.3.1.2)). We find that the BA random scale-free networks promote synchronizability better than the rewired versions of their deterministic counterparts of DSF and PSF networks. This chapter is based on the associated publication P4 and the following sections will closely follow the respective publication.

8.2. Introduction

Complex systems involving large collections of dynamical elements interacting with each other on complex networks are abundant across several disciplines of sciences and engineering [10, 31, 69, 106]. This has generated a consolidated effort towards unveiling structural properties of manifold real-world networked systems and uncovering fundamental principles governing their organization [60]. A significant milestone amid such explorations was the exposition of the *small-world* behaviour of diverse real networks, characterized by a small average path length between nodes and a high clustering coefficient (Sec. 3.3.1.3). Further, the interplay between topological properties of complex networked systems and the collective dynamics exhibited by them has been simultaneously investigated, particularly with reference to the phenomenon of synchronization (Sec. 4.3).

As mentioned earlier, synchronization is among the most relevant emergent behaviours in complex networks of dynamical systems and is often critical to their functionality [11, 13, 61]. As a result, there has been a persistent drive towards unravelling the influence of topological features of networks on their ability to synchronize, often with the objective of designing topologies for better synchronizability [65, 67, 68, 70–76]. In this regard, small-world networks (Sec. 3.3.1.3) have been particularly known to facilitate synchronization of dynamical systems coupled on them [63, 125–128]. Besides the small-world property, real-world networks often exhibit two other remarkable generic features, namely, *scale-free* behaviour (Sec. 3.3.1.2) and *hierarchical* structure [19, 129].

As described earlier in Sec. 3.3.1.2, scale-free behaviour is characterized by the probability P_k that a randomly selected node has exactly k links decaying as a power law ($P_k \sim k^{-\gamma}$) and appears in good approximation in diverse real networked systems such as the internet [130], the world wide web [18], networks of metabolic reactions [131], protein interaction networks [132], the web of Hollywood actors linked by movies [133], social networks such as the web of human sexual contacts [134], etc. In this context, the Barabási-Albert (BA) model (Sec. 3.3.1.2) has been suggested for realizing random scale-free networks with growth and preferential attachment, where an incoming node is more likely to get randomly linked to an existing node with higher connectivity.

Also, manifold real-world systems such as metabolic networks in the cell [129], ecological niches in food webs [19], the scientific collaboration network [135], corporate and governmental organizations [136], etc. exhibit hierarchical organization where small groups of nodes organize in a stratified manner into larger groups, over multiple scales. This definition of hierarchical structure, also used throughout this chapter, relates to that proposed by Clauset et al. [19].

Naturally, collective dynamics on scale-free [137–140] and hierarchical topologies [141–144, P2, P3] have been investigated intensively, but mostly separately, leaving sufficient room for further explorations concerning synchronization in networks simultaneously exhibiting the two topological properties mentioned

above. Notably, the coexistence of the generic feature of scale-free topology along with a hierarchical organization in many networks in nature and society is immensely intriguing [34]. Examples in this direction constitute the internet at the domain level, the world wide web of documents, the actor network, the semantic web viewed as a network of words, biochemical networks in the cell, etc. [34, 129].

This chapter is further organized as follows: In Sec. 8.3.1, we outline the rewiring mechanism adopted during the course of this chapter for constructing the networks studied here. Further, we discuss a few key characteristics of network topology (Sec. 3.2) and the relationships between them with the synchronizability of the rewired networks will be studied in this chapter. In Sec. 8.4, we utilize the MSF framework (Sec. 4.3.1) in exploring the synchronizability of the aforementioned network models (of DSF and PSF) after stochastically rewiring their edges. Further, we investigate the influence of rewiring on the topological properties of the resulting networks and, in turn, their relation to the synchronizability of the associated topologies. Finally, we present the conclusions of our work in Sec. 8.5.

8.3. Methods

8.3.1. Network Construction

Notable instances among models simultaneously incorporating the prominent topological features of scale-free behaviour and hierarchical organization under one roof are the deterministic scale-free (DSF, Sec. 3.3.2.1) [28], pseudofractal scale-free (PSF, Sec. 3.3.2.2) [29], Apollonian [66] and the hierarchical network model [34]. We specifically study DSF and PSF networks in this chapter, the topology of them developed over 2 generations is illustrated in Figures 3.1(a) and 3.1(b), respectively. Evidently, these models are completely deterministic, leading to a perfectly hierarchical assembly of the associated networks. However, it is most natural to assume that real-world topologies are neither completely deterministic, nor perfectly hierarchical. Thus, a realistic model of practical networked systems should feature an aspect of randomness, besides simultaneously manifesting not far from scale-free and hierarchical design. Henceforth, as a preliminary solution to this problem, we suggest in the following perfectly hierarchical networks (generated by the deterministic rules of the aforementioned models) with randomly rewired links as better representatives of associated connected architectures in the real-world. The mechanism used throughout this chapter for rewiring edges, while preserving the (scale-free) degree distribution of the otherwise perfectly hierarchical networks, is illustrated in Fig. 8.1.

The desired operational state in complex networks is often associated with the synchronized motion of its dynamical components [11]. In this chapter, we investigate the synchronizability of the proposed network models using the

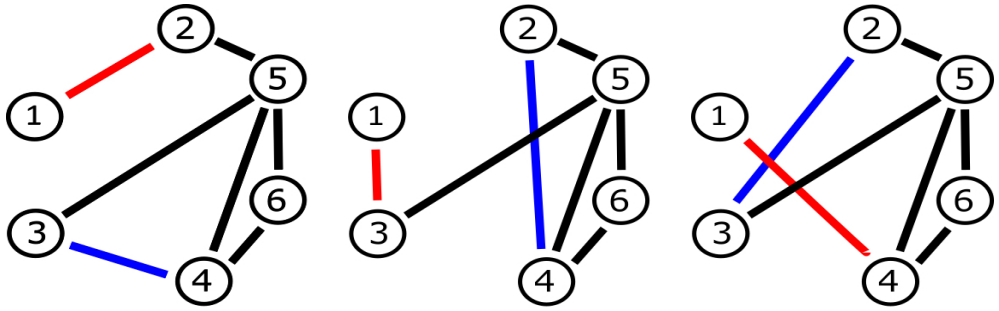

Figure 8.1.: (a) We randomly select two (distinct) edges of the network with the first edge (red) connecting nodes numbered 1 and 2 and the second edge (blue) connecting nodes numbered 3 and 4. We rewire (b) the first edge to connect nodes 1 and 3 and the second edge to connect nodes 2 and 4 (provided there does not already exist an edge between nodes 1 and 3 or between 2 and 4). Otherwise, we rewire (c) the first edge to connect nodes 1 and 4 and the second edge to connect nodes 2 and 3 (provided there does not already exist edges between the respective nodes as well). If the aforementioned steps fail, we choose a new pair of edges to rewire. Clearly, we preserve the scale-free degree distribution of the deterministic networks we start with, but successively loose the hierarchical structure while rewiring them. Also, note that we allow for a multiple selection of the same edge in subsequent rewiring steps.

master stability function (MSF) framework (Sec. 4.3.1). We recall that real-world topologies exhibiting the small-world property are known to facilitate network synchronization [9, 64] as well as to be more robust to random perturbations [9]. In this regard, the classical network model of Watts and Strogatz (Sec. 3.3.1.3) [17] is particularly notable for capturing the small-world property. In strong analogy with the present work, the Watts-Strogatz model generates graphs by randomly rewiring completely regular architectures (ring lattices), thus interpolating between absolutely regular and random graphs with the small-world property appearing for intermediate rewiring probability. However, MSF-based measurements of synchronizability of the Watts-Strogatz model surprisingly do not reveal exclusive features in the small-world regime [127]. In such networks, synchronizability is only enhanced for an initial increase of the number of rewired edges, which then saturates afterwards as further links are rewired. In fact, the synchronizabilities of the rewired networks (for a given number of rewired edges) are not much different from one another. On the other hand, networks resulting from rewiring hierarchical scale-free networks considered here exhibit both significantly enhanced as well as deteriorated synchronizability (compared to that of their completely deterministic counterparts).

In a related context, Donetti et al. [68] proposed *entangled networks*, constructed by starting with a random network of certain size and rewiring it using a modified simulated annealing-based approach, while keeping its average degree fixed. In contrast, we start with the deterministic networks of DSF and PSF and rewire them using a different mechanism (Fig. 8.1), where we instead maintain a fixed degree distribution. Further, the scheme of constructing entangled networks is aimed at achieving optimal synchronizability. However, we focus on exploring the synchronizability of an ensemble of rewired networks and, in turn, obtaining the 'optimal' synchronizability of the representative network among the different members of this ensemble. Further, Donetti et al. found that the topological features of average distance between nodes and betweenness centrality exhibit negative correlations with the synchronizability of entangled networks. Similarly, Dwivedi et al. [145] investigated the optimization of synchronizability in multiplex networks and demonstrated that a stronger interlayer connectivity as compared to the connections within each layer leads to better synchronizability. Moreover, they obtained results similar to those of Donetti et al. [68] where the latter have shown that entangled networks with more homogeneous degree distributions, distances between nodes and betweenness centrality distributions exhibit better synchronizability.

We also investigate the influence of rewiring on the topological properties of the resulting networks and in turn, their relation to the synchronizability of the associated topologies. For that purpose, we now briefly describe the previously deduced relationships between synchronizability and the topological properties of average path length (Sec. 3.2.2), maximum betweenness centrality (Sec. 3.2.3), average local clustering, global clustering (transitivity, Sec. 3.2.4) and assortativity (Sec. 3.2.5) of a network.

8.3.2. Network Properties and Synchronizability

The *average path length* $\mathcal{L}$ of a network is defined as the mean value of the shortest path length between all possible pairs of nodes (Sec. 3.2.2). Intuitively, a smaller average path length of a network should facilitate efficient communication between oscillators, culminating in improved synchronizability of the overall system [127].

The *betweenness centrality* bc_i of a node is related to the fraction of shortest paths between all pairs of nodes that pass through that node (Sec. 3.2.3). We study here the maximum betweenness centrality values bc_{max} of all nodes of a network realization, which have been argued to be inversely related to synchronizability [80].

The *average local clustering coefficient* $\mathcal{C}_i^L$ relates to the average (over all nodes of a network) of the probabilities of the existence of an edge between two randomly selected neighbours of a node (Sec. 3.2.4). Likewise, the *global clustering coefficient* $\mathcal{C}^G$ of a network (often also called network *transitivity*) is related to

the mean probability that two nodes with a common neighbour are themselves neighbours (Sec. 3.2.4). Larger clustering coefficients are generally associated with a reduced synchronizability of small-world and scale-free networks [61].

The *assortativity coefficient* r of a network quantifies the overall preference of any of its nodes to connect with other nodes having a similar degree (Sec. 3.2.5). Positive values of r indicate a tendency of nodes with a similar degree to connect, while negative values of r indicate links between nodes of different degree. A more negative degree correlation (i.e., an increase in *disassortativity*) has been shown to be associated with an enhancement in the overall synchronizability of scale-free networks [146].

8.4. Results

We consider two paradigmatic network topologies both simultaneously exhibiting scale-free degree distributions and hierarchical organization. In the one hand, we study a DSF network developed over 3 generations comprising $N = 81$ nodes and $E = 130$ edges. On the other hand, we investigate a 3-generation PSF network with $N = 123$ nodes and $E = 243$ edges. In both cases, we generate an ensemble of 10^4 networks by rewiring e (equivalently, a fraction $f = \frac{e}{E}$) pairs of edges of the completely deterministic networks, using the mechanism described in Fig. 8.1. Further, for a particular value of f, we compute the values of $\mathcal{L}$, bc_{max}, $\mathcal{C}^L$, $\mathcal{C}^G$, r and R of each network with e randomly rewired links of the ensemble and then estimate the expectation values $\langle\mathcal{L}\rangle$, $\langle bc_{max}\rangle$, $\langle\mathcal{C}^L\rangle$, $\langle\mathcal{C}^G\rangle$, $\langle r\rangle$ and $\langle R\rangle$ as the corresponding ensemble means.

We present the variation in the expected synchronizability $\langle R\rangle$ (solid line) with the fraction f of rewired edges of the DSF network in Fig. 8.2(a). We clearly observe that rewired versions of the otherwise completely DSF network exhibit significantly enhanced as well as deteriorated values of synchronizability (Fig. 8.2(a)). The dashed line represents the minimum R value over the ensemble of rewired networks for a given value of f. The corresponding topologies thus represent approximately 'optimally' synchronizable networks for the respective value of f. The fluctuations in the minimum R values may be attributed to the relatively small considered ensemble sizes (10^4), as compared with the much greater variety of possible rewired networks for a given value of f. Also, in the inset of Fig. 8.2(a), we observe a minimal value of $\langle R\rangle$ (highest average synchronizability) for f equal to $f^* = 0.046$ (6 rewired edges) of the 81-node network. As f is further increased beyond f^*, the value of $\langle R\rangle$ increases again, finally saturating at $\langle R\rangle \sim 185$ for $f \gtrsim 0.6$.

Figure 8.2(b) demonstrates that a similar (and even more pronounced) behaviour of average synchronizability is found in the PSF networks, for which we observe a minimal value of $\langle R\rangle$ for $f^* = 0.16$ (39 rewired edges). Moreover, we find similar results (presented in Appendix B) with regard to synchronizability of 4-generation DSF and PSF networks as well.

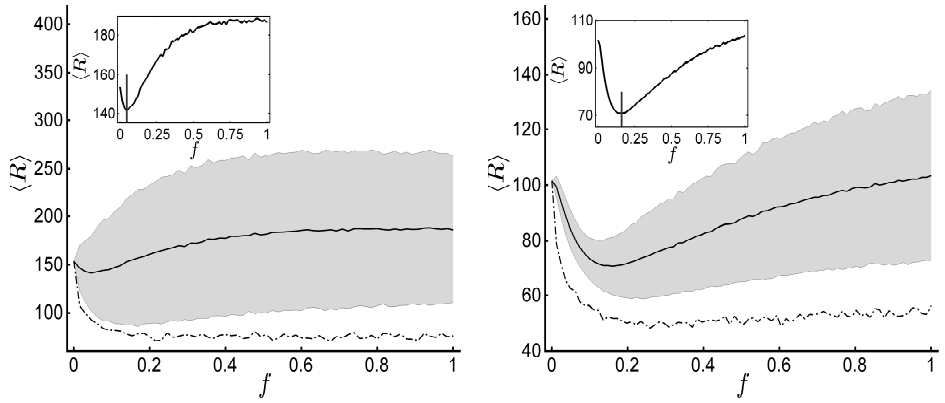

(a) (b)

Figure 8.2.: Relationship of expected synchronizability $\langle R \rangle$ (solid line) with the fraction f of rewired edges of the 3-generation (a) DSF and (b) PSF networks. The shaded areas are representative of the standard deviations (1σ) of the R values for the ensemble of rewired networks generated for computing $\langle R \rangle$ for any particular value of f. The dashed line represents the minimum R value over the ensemble of rewired networks for a given value of f. The inset magnifies the $\langle R \rangle$ values, where the vertical line marks the value of $f^* = 0.046$ (0.16) for the DSF (PSF) network. Note that we do not rewire e edges (for a given value of f) of the same realization, but generate ensembles of networks with e rewired edges (for the respective value of f). Therefore, one may obtain different values of f^* for different realizations, if they were rewired consecutively instead of the procedure as followed here.

Next, we investigate the relationships between f and the topological properties $\langle \mathcal{L} \rangle$, $\langle bc_{max} \rangle$, $\langle \mathcal{C}^L \rangle$ and $\langle \mathcal{C}^G \rangle$ of the associated ensemble of stochastically rewired DSF networks in Fig. 8.3. For $f < f^*$, the decrease in $\langle \mathcal{L} \rangle$ and the increase in $\langle bc_{max} \rangle$ conform to the decreasing trend of $\langle R \rangle$ (as per the earlier discussion in Sec. 8.3.2 on network properties and their expected relationship with synchronizability). The value of $\langle \mathcal{C}^L \rangle$ (as well as $\langle \mathcal{C}^G \rangle$) starts from zero and increases as more edges are rewired. This implies the formation of triangles in the network, which promotes communication between the oscillators, thereby enhancing synchronizability. However, for $f > f^*$, further decrease in $\langle \mathcal{L} \rangle$ and increase in $\langle bc_{max} \rangle$ should still improve the average synchronizability, which however only declines from thereon.

Thus, rewiring a few edges ($f < f^*$) alters the topological features of the ensemble of networks for better synchronizability. However, when more edges ($f > f^*$) are further rewired, it no longer affects on average the topological properties relevant for improving synchronizability, in fact, only undermines it. Hong et al. [80] have previously proposed maximum betweenness centrality as a

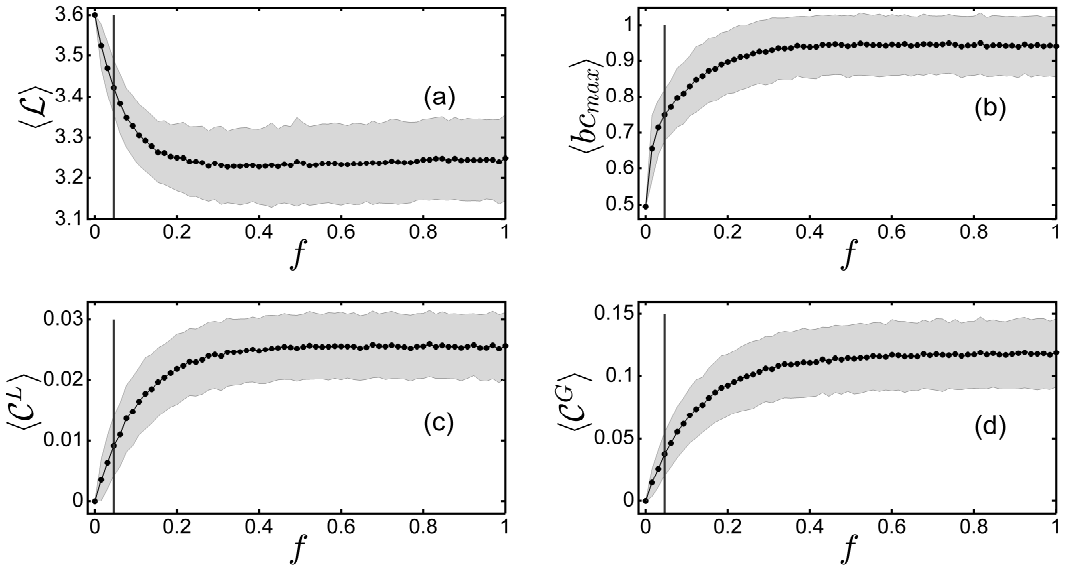

Figure 8.3.: Relationship between f and the topological properties (a) $\langle \mathcal{L} \rangle$, (b) $\langle bc_{max} \rangle$, (c) $\langle \mathcal{C}^L \rangle$, and (d) $\langle \mathcal{C}^G \rangle$ of the associated ensemble of randomly rewired DSF networks. The shaded areas are representative of the standard deviations (1σ) of the respective topological features of the ensemble of rewired networks (generated for a given value of f). The vertical lines indicate the location of f^*.

suitable indicator for predicting synchronizability of networks. They have shown that among various topological factors, such as, short characteristic path length or large heterogeneity of the degree distribution, it is a small value of the maximum betweenness centrality of a network that promotes synchronization [80]. However, this is not corroborated by our results in Fig. 8.3 where we do not observe a strong linear relationship between $\langle R \rangle$ and $\langle bc_{max} \rangle$, as also indicated by a correlation coefficient of 0.776. Similarly, a correlation coefficient of -0.681 rules out a systematic linear dependence between $\langle R \rangle$ and $\langle \mathcal{L} \rangle$. However, a correlation coefficient of 0.847 (0.889) between $\langle R \rangle$ and $\langle \mathcal{C}^L \rangle$ ($\langle \mathcal{C}^G \rangle$) indicates an appreciable underlying linear relationship. Further, for $f > f^*$, the correlation coefficient of 0.939 (0.970) between $\langle R \rangle$ and $\langle \mathcal{C}^L \rangle$ ($\langle \mathcal{C}^G \rangle$) underlines the above observation.

Analogously to Fig. 8.3, Fig. 8.4 again shows the relationships between f and the topological properties $\langle \mathcal{L} \rangle$, $\langle bc_{max} \rangle$, $\langle \mathcal{C}^L \rangle$ and $\langle \mathcal{C}^G \rangle$ of the associated ensemble of rewired PSF networks. In this case, we observe a clear relationship between $\langle R \rangle$ and $\langle \mathcal{L} \rangle$, further corroborated by a correlation coefficient of 0.987. On the other hand, a possible linear relationship between $\langle R \rangle$ and $\langle bc_{max} \rangle$, $\langle \mathcal{C}^L \rangle$ and $\langle \mathcal{C}^G \rangle$ is ruled out by correlation coefficients of -0.25, -0.175 and -0.373, respectively.

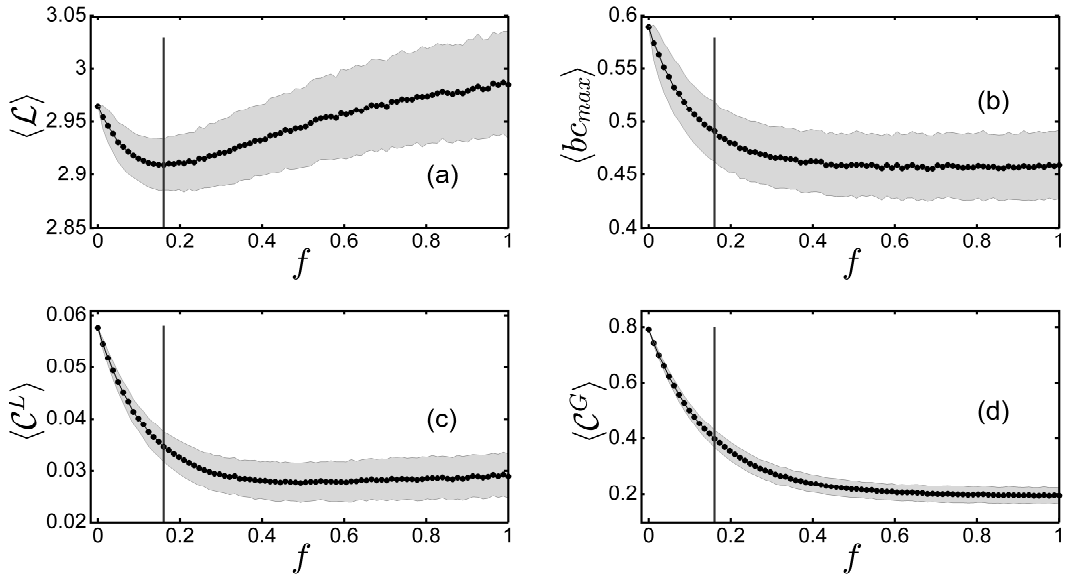

Figure 8.4.: Same as in Fig. 8.3, for randomly rewired PSF networks.

Taken together, we notice that the topological features of the ensembles of rewired DSF (Fig. 8.3) and PSF (Fig. 8.4) networks exhibit certain contrasting variations, as f is tuned from 0 to 1. Prior to saturation, the bc_{max} of the rewired DSF networks (Fig. 8.3(b)) initially increases with f, as opposed to a corresponding decrease in bc_{max} observed for the rewired PSF networks (Fig. 8.4(b)). On the contrary, both clustering coefficients $\langle \mathcal{C}^L \rangle$ and $\langle \mathcal{C}^G \rangle$ increase with f until saturation for rewired DSF networks (Figures 8.3(c) and 8.3(d)), which however display a decreasing trend in the case of rewired PSF networks (Figures 8.4(c) and 8.4(d)).

Jalan et al. [147] have recently studied the role of degree-degree correlations (assortativity, Sec. 3.2.5) in the cluster synchronizability of networks during the evolution of coupled chaotic dynamics on them. They have shown that an increased disassortativity relates to an increase or decrease in the cluster synchronizability of networks depending on their degree distribution and average connectivity, such that networks with heterogeneous degree distributions exhibit significant changes in cluster synchronizability in comparison to those with homogeneous degree distributions. For gathering similar insights, we now investigate the relationships between the assortativity ($\langle r \rangle$) and the synchronizability of the rewired DSF and PSF networks considered here (Fig. 8.5). Note that the degree distribution of the deterministic DSF and PSF networks is preserved during the process of rewiring, as also mentioned earlier. Clearly, the decrease in the degree

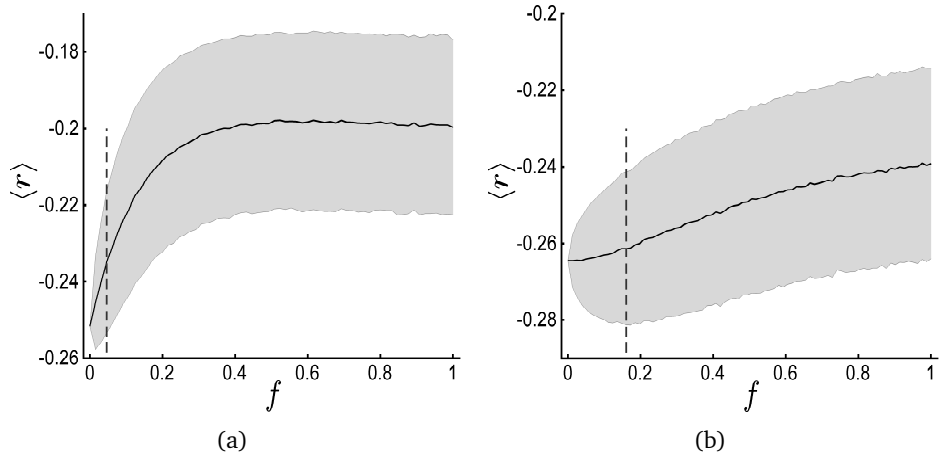

Figure 8.5.: Relationship between f and $\langle r \rangle$ of rewired (a) DSF and (b) PSF networks. The shaded areas are representative of the standard deviations (1σ) of r values of the ensemble of rewired networks (generated for a given value of f). The vertical lines indicate the location of f^*.

of disassortativity of the rewired DSF as well as PSF networks is accompanied by an improvement (decline) in their synchronizability for $f < f^*$ ($f > f^*$). However, we again do not observe any strict correlations between $\langle r \rangle$ and $\langle R \rangle$.

We now compare the synchronizability of rewired DSF and PSF networks with that of random scale-free networks generated using the classical BA model of growth and preferential attachment (Sec. 3.3.1.2). In this regard, we consider an ensemble of 100 such random scale-free networks of 81 nodes (123 nodes) each for comparison with rewired DSF (PSF) networks, respectively. While generating the BA networks, we incorporate the growing character of the network by starting with a small number of vertices and at every time step introducing a new vertex and linking it to 2 vertices already present in the system, until the network comprises 81 (123) nodes. Preferential attachment is incorporated by assuming that the probability Π_i that a new node will be connected to node i depends on the degree k_i of node i, such that $\Pi_i = \frac{k_i}{\sum_j k_j}$. The 81-node (123-node) BA networks have a total of 158 (242) edges in each realization. The $\langle R \rangle$ values of the considered ensemble of 81-node (123-node) BA networks turn out to be 36.74 (49.75), which is much smaller than the minimum R values among the ensembles of rewired DSF (PSF) networks for different f, presented in Fig. 8.2. Thus, random scale-free networks generated using the classical BA model appear to promote synchronizability better than randomly rewired DSF as well as PSF networks. We outline further investigations to unveil the reasons for this behaviour as a subject of future research.

In a similar spirit, we also investigate the synchronizability of an ensemble of 100 networks of 81 (123) nodes generated using the random configuration model [10]. We find that their $\langle R \rangle$ values of 175.71 (112.54) are larger than those of the rewired DSF (PSF) networks of 141.24 (70.71), even when their respective f^* fractions of edges are rewired. Also, the networks with the minimum R values within this ensemble of 81-node (123-node) networks generated using the random configuration model are 81.57 (65.93), which are again larger than the minimum values of 70.47 (48.41) among the R values of the entire ensemble of rewired DSF (PSF) networks, for all values of f. Thus, we conclude that the rewired versions of DSF and PSF networks generally exhibit better synchronizability than networks generated using the random configuration model.

Note that the above results apply to situations involving bounded MSFs (Sec. 4.3.1), i.e., where the MSF exhibits negative values within a range of the normalized coupling parameter [61]. Also, finite λ_N (the largest eigenvalue of the Laplacian matrix of the network) is related to the maximum degree of the network, while λ_2 (the first non-zero eigenvalue of the Laplacian matrix) relates to the connectivity [61]. Given that the degree distribution is preserved when rewiring the networks considered in this chapter, one does not expect significant variations in λ_N.

8.5. Conclusion

Many real-world complex networks simultaneously exhibit the generic feature of scale-free topology along with hierarchical organization. In this regard, two notable models which simultaneously capture the two different topological properties are the deterministic and pseudofractal scale-free networks. These models comprise completely deterministic processes underlying the formation of the respective networks. However, real-world networks are presumably neither completely deterministic, nor perfectly hierarchical. Thus, a practical model of such networks should feature an aspect of randomness, while exhibiting scale-free and hierarchical design. For this purpose, we suggested preserving the scale-free degree distribution of the deterministic networks we start with, while tweaking the hierarchical structure by rewiring them. Specifically, we hypothesized that perfectly hierarchical scale-free networks (generated by the deterministic rules of the aforementioned models) with randomly rewired links may provide more realistic representatives of associated real-world topologies than perfectly hierarchical ones.

The desired operational state in many complex systems often concurs with the synchronized motion of dynamical units coupled on a networked architecture. Consequently, we utilized the analytical framework of master stability function (MSF) in investigating the synchronizability of dynamical systems coupled on the proposed network structures. Interestingly, this revealed that the process of rewiring is capable of significantly enhancing as well as deteriorating the

synchronizability of the resulting networks. Importantly, when a certain critical fraction of edges of the otherwise completely deterministic networks was rewired, it optimized the average synchronizability of the resulting topologies. This observation is, however, different from *Braess's paradox* where the *addition* of edges undermines synchrony in complex oscillator networks [95]. We also investigated the influence of rewiring links on some key topological properties (average path length, maximum betweenness centrality, average local clustering coefficient, global clustering coefficient and assortativity coefficient) of the resulting networks and, in turn, their relation to the synchronizability of the associated topologies demonstrating distinct behaviours in these different models of hierarchical scale-free networks. We speculate that an interplay between the various topological properties of the networks, in particular, their average path lengths and clustering coefficients in a trade-off leads to an 'optimal' value of synchronizability when rewiring the respective networks.

In a related context, we recall that networks exhibiting the small-world property have been considered conducive for synchronization [9, 64]. However, MSF-based measurements of the synchronizability of Watts-Strogatz networks did not reveal exclusive features in the small-world regime [127]. Importantly, the critical fraction of rewired edges (for maximal synchronizability) in the hierarchical scale-free networks considered here, roughly corresponds to a similar value for typical Watt-Strogatz networks to exhibit small-world behaviour. Specifically, we also found that rewiring a few edges of the deterministic scale-free as well as pseudofractal scale-free networks generated a topology with significantly enhanced or 'optimal' synchronizability, which did not exhibit major improvements thereafter, as the fraction of rewired edges was further increased.

Chapter 9.

Intermittent Synchronization in Small-world Networks

9.1. Summary

The last few years have witnessed a considerable amount of research directed towards the existence and stability of synchronized dynamics on complex networks. Amongst various topologies, those with *small-world* (SW, Sec. 3.3.1.3) properties have been found to be quite conducive for the optimal manifestation of synchronized motion. In this chapter, however, we present a case which appears to contradict the aforementioned result. In particular, we investigate the phenomenon of *temporally intermittent* synchronized and desynchronized dynamics in Watts-Strogatz (WS) networks (Sec. 3.3.1.3) of chaotic Rössler oscillators. We consider topologies for which the master stability function (MSF, Sec. 4.3.1) predicts stable synchronized behaviour, as the link rewiring probability (β) of the WS model is tuned from 0 to 1. The MSF framework essentially utilizes the largest Lyapunov exponent transversal to the synchronization manifold in making stability considerations, thereby ignoring the other Lyapunov exponents. However, for an N-node (dimensional) networked dynamical system, we observe that the differences in its Lyapunov spectra (corresponding to the $N-1$ directions transversal to the synchronization manifold) are crucial, and serve as indicators of the presence of *intermittently synchronized* behaviour. In addition to the linear stability-based MSF analysis, we estimate the probability of the system to exhibit the intermittently synchronized state in terms of the fraction of state space volume shared by the respective state, as β is varied from 0 to 1. This probability becomes appreciably large in the SW regime, which is surprising, since this limit has been otherwise considered optimal for synchronized dynamics. Also, we do not notice much different likelihood of the system to exhibit persistent synchronized motion in the SW regime of the WS model, as compared to the likelihood observed for greater randomness ($\beta \sim 1$) in the corresponding model. Thus, we conclude that although the synchronized state does occur in SW networks, it is not associated with larger likelihoods of observation in the SW regime of the WS model. In contrast, a significant fraction of the state space in the SW limit is actually prone to intermittently synchronized dynamics. This chapter is based on

the associated publication P5 and the following sections will closely follow the respective publication.

9.2. Introduction

Synchronization of dynamical units coupled on complex networks has been recognized as one of the most significant forms of collective behaviour with implications in population dynamics [148–150], epidemiology [151, 152], neural networks [153–155], secure communications [156], power grids [13, 157, 158], etc. and is often critical to the overall functionality of relevant complex dynamical systems.

In the above context, *small-world* (SW, Sec. 3.3.1.3) properties of real-world networks have been found to be particularly conducive towards synchronization [9]. A notable model exhibiting the aforementioned topological structure is the Watts-Strogatz (WS) network (Sec. 3.3.1.3), which has been shown to exhibit more robust synchronization (of the dynamical elements coupled on them) in its small-world limit, as compared to its completely regular or random ones [9, 63, 127]. Such investigations usually consider the dynamical components (of the network) starting from asynchronous initial conditions, asymptotically reaching the synchronized state and thereby, maintaining synchronized operation. Interestingly however, there have also been reports of chaotic oscillator networks exhibiting dynamics which switches between synchronized and desynchronized behaviour in a *temporally intermittent* fashion [20, 159, 160].

Previous work in this direction, starting with that of Baker et al. [20], subsequently led to explorations of different aspects of *intermittent synchronization* in coupled dynamical systems [159–162]. The intermittency observed in these studies were mainly attributed to either *attractor bubbling* [160] or *on-off intermittency* [163]. Further, the intermittently synchronized dynamics arising out of coupled map networks has been labelled as *chaotic Griffiths phase*, and it has been shown that the number of positive Lyapunov exponents in this phase scales anomalously with the power of network size [164].

In this chapter, we study WS networks of chaotic Rössler oscillators, as its parameter of link rewiring probability (β) is tuned from 0 to 1. We consider a coupling regime for which the master stability function (MSF, Sec. 4.3.1) predicts stable synchronized behaviour. MSF essentially utilizes the largest transverse Lyapunov exponent (TLE) of the master stability equation (Eq. (4.5)) in making stability considerations, thereby ignoring the other Lyapunov exponents. We demonstrate in the following, that the largest TLE fails to capture the occurrence of intermittent bursts in a synchronized dynamics. Further, we show that the complete spectra of Lyapunov exponents emerge as a better indicator of the occurrence of such intermittency.

The aforementioned temporally intermittent synchronized dynamics is often undesirable as it hampers the sustained synchronized operation of the respective

system. Therefore, it is crucial to investigate the relationship between topological properties of networks and the possibility of encountering such dynamical behaviour. In this regard, we specifically study the variation of the fraction of state space volume shared by the intermittently synchronized dynamical behaviour with respect to changes in the network topology, as β is tuned from 0 to 1. In analogy with the interpretation of Wiley et al. [8] (discussed in Sec. 4.1.10), we construe this fraction as the probability of the system to exhibit intermittently synchronized dynamics. We thereafter make the surprising account that this probability becomes appreciably large in the SW limit of the WS model, as compared to its regular or random counterparts, suggesting that SW networks may be significantly more prone to such intermittently synchronized dynamics. Therefore, it becomes crucial to revisit the problem of synchronization in SW networks from the perspective of state space volumes and identify the reasons underlying the emergence of such intermittency in SW topologies, which are otherwise considered optimal for synchronized dynamics.

This chapter is further organized as follows: In Sec. 9.3, we outline the setting for observing intermittent synchronization in WS networks of chaotic Rössler oscillators. We further analyse our observations in Sections 9.3.1 and 9.3.2. Finally, we present the conclusions of our work in Sec. 9.4.

9.3. Results

We now demonstrate a scenario of observing intermittent synchronization in a SW network of N coupled Rössler oscillators, where the dynamics of node i (in correspondence with Eq. (5.2)) is given by

$$\begin{aligned}
\dot{x}_i^1 &= -x_i^2 - x_i^3 + \epsilon \sum_{j=1}^{N} A_{ij} \left(x_j^1 - x_i^1 \right), \\
\dot{x}_i^2 &= x_i^1 + a x_i^2, \\
\dot{x}_i^3 &= b + x_i^3 \left(x_i^1 - c \right).
\end{aligned} \tag{9.1}$$

The parameters a, b and c are chosen to be 0.2, 0.2 and 7.0, respectively such that each uncoupled Rössler oscillator (Eq. (5.7)) exhibits chaotic dynamics and the synchronous state corresponds to the case where all oscillators have identical dynamics (i.e., *complete synchronization*). Further, we resort to the WS model (outlined in Sec. 3.3.1.3) for constructing SW networks. In particular, we generate WS networks comprising $N = 100$ nodes for the simulations performed in the context of this chapter, where each node has $\langle k \rangle = 8$ nearest-neighbours (i.e., $\frac{\langle k \rangle}{2} = 4$ neighbours on each side).

To begin with, we invoke MSF (Sec. 4.3.1) to obtain the interval of coupling strength ϵ for which the completely synchronized state of the network (Eq. (9.1)) is locally stable. For the system (Eq. (9.1)) under investigation, the numerical

values of α_1 and α_2 turn out to be 0.1232 and 4.663 (see Sec. 4.3.1), respectively [123]. Figure 9.1 illustrates the range of coupling strength as a function of the link rewiring probability, for which the completely synchronized state is locally stable. We emphasize that this interval of coupling has been obtained by using the maximum TLE ($\Lambda_{max}(\alpha)$, Sec. 4.3.1) from the complete spectrum of Lyapunov exponents of the master stability equation (Eq. (4.5)) of the network (Eq. (9.1)).

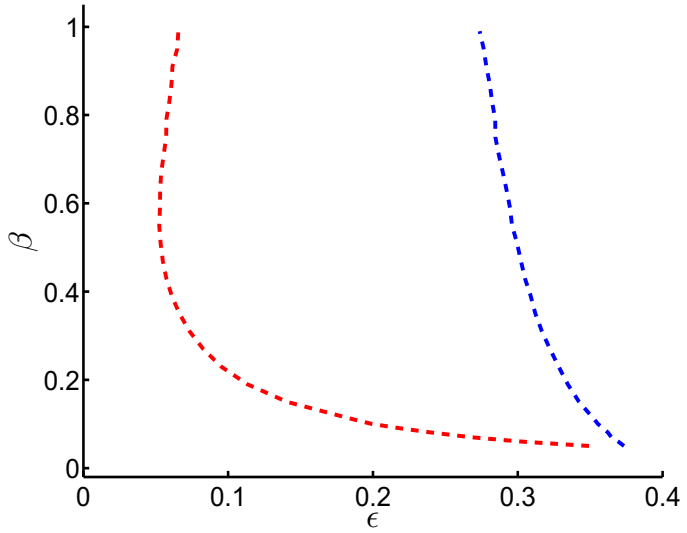

Figure 9.1.: Plot of minimum (ϵ_{min}, red) and maximum (ϵ_{max}, blue) values of coupling strength ϵ for which the completely synchronized state of the system (Eq. (9.1)) is locally stable, as a function of the link rewiring probability β of the WS model.

Now, we present a case where MSF predicts stable synchronized behaviour, but the actual dynamics can also be intermittent in time depending upon the choice of initial conditions. To capture the transition to synchronization, we compute the synchronization error Z_{sync} defined as

$$Z_{sync}(t) = \frac{1}{N}\sum_{i=1}^{N}\sum_{j=1}^{d}\left(x_i^j(t) - \langle x^j(t)\rangle\right)^2, \tag{9.2}$$

where $\langle x^j(t)\rangle = \frac{1}{N}\sum_{i=1}^{N} x_i^j(t)$. The above measure approaching towards zero is indicative of the onset of complete synchronization. We observe the transient behaviour of this quantity as the system evolves over time. To ensure reproducibility and avoid machine precision-related problems, we set a synchronization error threshold of $Z^*_{sync} = 10^{-4}$ as the value below which the system is considered to

have attained complete synchronization [4].

Fig. 9.2(a) clearly depicts the temporally intermittent nature of Z_{sync}. Notice that the system starts in the desynchronized state and with the progression of time, the synchronization error falls below Z^*_{sync} and stays below the threshold value for a while. However, it then abruptly makes a jump and crosses the threshold leading to desynchronization in the system, and such episodes ensue indefinitely and intermittently. Also, note that the coupling strength for this case is within the interval presented in Fig. 9.1, which predicts locally stable completely synchronized dynamics.

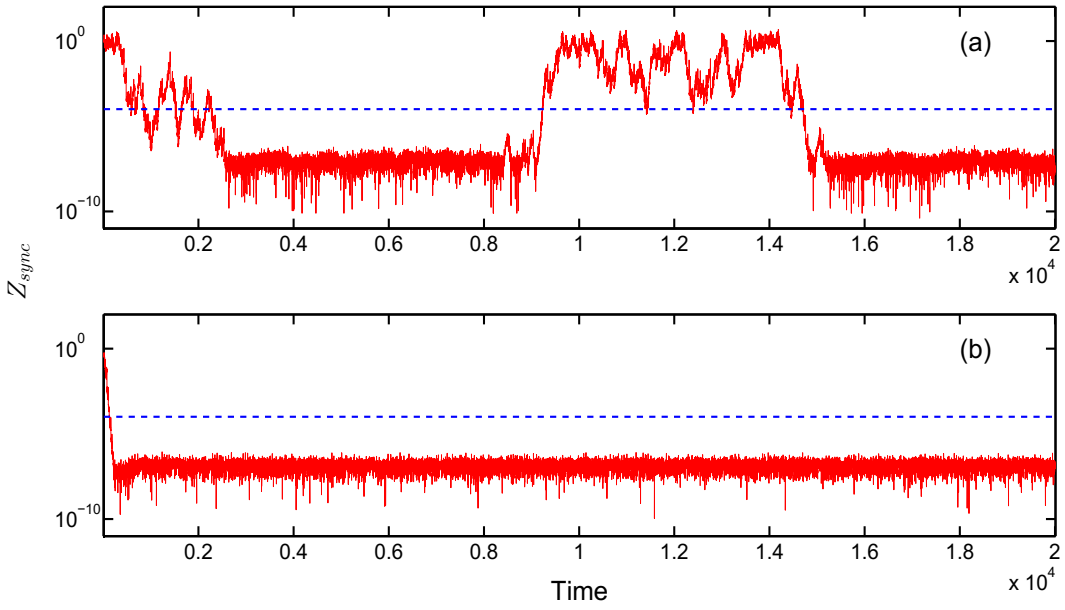

Figure 9.2.: The variation of synchronization error Z_{sync} over time (at $\epsilon = 0.28$) for the different link rewiring probabilities of (a) $\beta = 0.09$ and (b) $\beta = 0.47$ of the WS model.

We further characterize this intermittent behaviour in Sec. 9.3.1. Note that the manifestation of this behaviour depends on the choice of initial conditions, which will be further illustrated and explored in Sec. 9.3.2. Further, we extensively investigate the dependence of this intermittent behaviour on the degree of randomness (β) in the WS network. This reveals that intermittent synchronization manifests itself primarily in the range of $\beta \in (0.06,\ 0.2)$, which coincides with the SW limit [17]. For higher values of β, the system exhibits complete

[4] Note that the qualitative nature of the results presented here are independent of the numerical value selected for Z^*_{sync}.

synchronization at all times. For instance, Fig. 9.2(b) is representative of a case where synchronization is maintained at all times, after initial transients.

9.3.1. Lyapunov Spectrum Analysis

In the previous section, we established that despite linear stability analysis predicting stability of the completely synchronized state, the behaviour may turn out to be intermittently synchronized in time for a wide range of the network randomness parameter (β) of the WS network. In this section, we attempt to unravel the reason underlying the occurrence of intermittent synchronization using information from the whole Lyapunov spectrum of the master stability equation (Eq. (4.5)). Previous studies have identified the cause of intermittency in the synchronized state as local instabilities in the directions transversal to the synchronization manifold [12, 159, 160]. In this regard, Chaté [165] has shed light on the possible link between spatio-temporal intermittency and the complete Lyapunov spectrum. In strong analogy with the aforementioned work, we uncover in the following, the presence of a relation between the structure of the complete Lyapunov spectrum and the possibility of intermittent synchronization in the coupled dynamical system (Eq. (9.1)) under investigation.

The system (in Eq. (9.1)) has a $3 \times N$-dimensional state space and the synchronization manifold is 3-dimensional. Therefore, transverse to the synchronization manifold, there are $3 \times (N-1)$ perturbation directions which are further grouped into $N-1$, 3-dimensional sub-spaces [12]. We determine the maximum Lyapunov exponents from these $N-1$, 3-dimensional sub-spaces for different initial conditions and realizations of the network. Figure 9.3 illustrates the distribution of the $N-1$ maximum TLE values for four representative cases corresponding to complete and intermittent synchronization. Figures 9.3(a) and 9.3(b) represent the behaviour of the distribution of maximum TLE values for $\beta = 0.95$, which is outside the window of highest likelihood of intermittent synchronization (Fig. 9.4). For both cases, the distribution is far away from zero which clearly indicates either a stable (Fig. 9.3(a)) or an unstable (Fig. 9.3(b)) completely synchronized state. Further, Figures 9.3(c) and 9.3(d) for which intermittent synchronization is observed, correspond to the distributions obtained for $\beta = 0.08$ and $\beta = 0.1$, respectively. Notice that the distribution accumulates close to zero in Figures 9.3(c) and 9.3(d), which is a possible indicator of intermittency in the synchronized state.

The above feature of intermittent synchronization is reminiscent of spatio-temporal intermittency in spatially extended systems. The increase in densities of Lyapunov spectra near zero is similar to the signature of spatio-temporal intermittency in coupled map lattice models [165, 166]. Such trends were also clearly discerned in models of self-organized criticality [167], which exhibit characteristics of spatio-temporal intermittency [168]. Therefore, in summary,

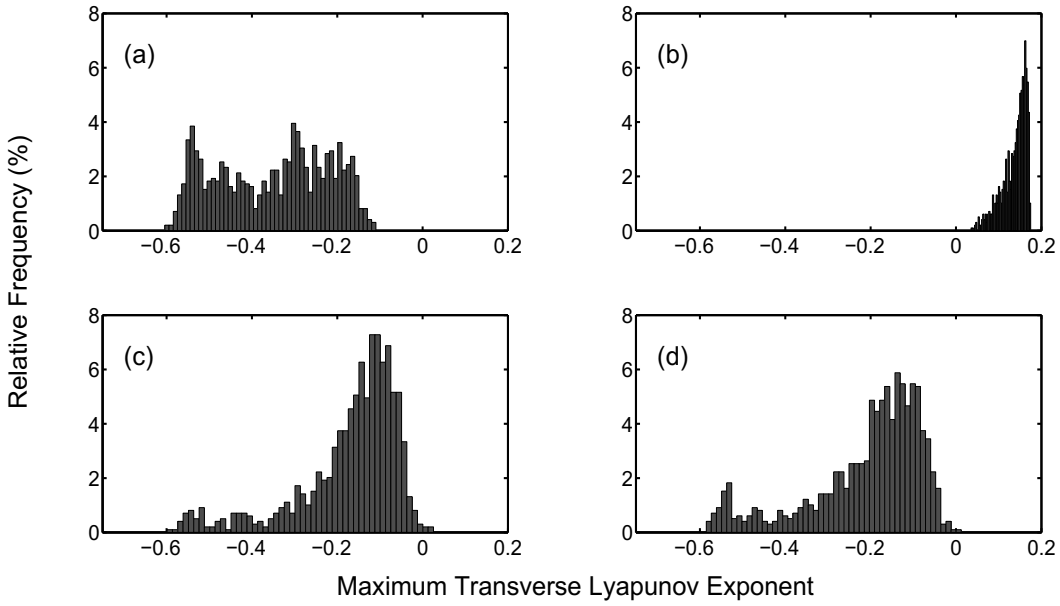

Figure 9.3.: Distribution of the maximum transverse Lyapunov exponent of the master stability equation (Eq. (4.5)) of the system (Eq. (9.1)). The relative frequencies (%) correspond to the percentage of maximum transverse Lyapunov exponent values lying within the respective bin of the histogram. (a) Link rewiring probability $\beta = 0.95$ of the WS model corresponding to a scenario where the completely synchronized state is stable, i.e., the coupling strength is chosen from within the stability interval illustrated in Fig. 9.1. (b) $\beta = 0.95$ corresponding to a scenario where the completely synchronized state is unstable, i.e., the coupling strength is chosen from outside the stability interval. (c) $\beta = 0.08$ and (d) $\beta = 0.1$ correspond to cases for which the system exhibits intermittent synchronization, although in both situations, the coupling strength is chosen to be the mean value from the stability interval of the completely synchronized state (i.e., lies within the stability interval illustrated in Fig. 9.1). The above results have been computed over an ensemble comprising 100 WS networks.

our results lend credence to the conjecture that intermittency in extended systems is signalled by a significant increase in exponents close to zero.

9.3.2. Probability of Intermittent Synchronization: A State Space Volume-based Perspective

In the previous section, we explored the existence of the intermittently synchronized state for a range of rewiring probability (β) of the WS network. However, in addition to the intermittently synchronized state, there are other coexisting dynamical regimes in the state space of the system (Eq. (9.1)). In this regard,

we now investigate the possibility of encountering these dynamical states in the aforementioned scenario. For this purpose, we consider the fraction of the state space volume shared by the intermittently synchronized (and other coexisting dynamical) state(s), which is representative of the likelihood of the respective state appearing in the evolution of the system, when started from a random initial condition. Note that this interpretation is in analogy with that of Wiley et al. [8] (discussed in Sec. 4.1.10), where these fractions are construed as the respective probabilities of the system to exhibit the corresponding dynamical states. In this section, we explore the variation of the aforementioned probabilities with changes in β.

We broadly classify the qualitatively different emergent collective behaviours observed here into four categories, namely, intermittently synchronized, completely synchronized, desynchronized and unbounded. To compute the fraction of state space volume shared by these states and hence the respective probabilities of their emergence, we first initialize all the nodes with random values of: $x \in [-15, 15]$, $y \in [-15, 15]$, $z \in [-5, 35]$. As mentioned earlier, there are

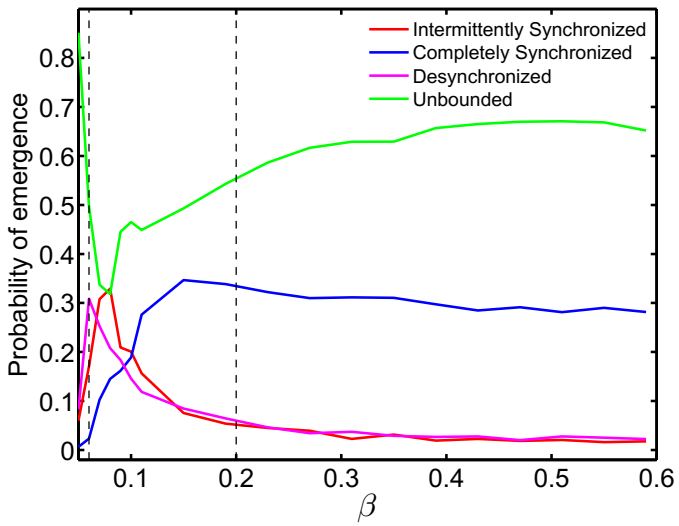

Figure 9.4.: Probability of emergence of the intermittently synchronized (red), completely synchronized (blue), desynchronized (magenta), and unbounded (green) states during the evolution of the system (Eq. (9.1)), as a function of the link rewiring probability β of the WS model. The above results have been computed over 100 initial conditions, drawn uniformly at random. The region bounded by the two vertical black dashed lines, represents the network regime (small-world) where the likelihood of intermittent synchronization becomes appreciably large. For each value of β, we sample over the coupling strength interval, bounded by ϵ_{min} and ϵ_{max}, where linear stability analysis predicts locally stable complete synchronization, as displayed in Fig. 9.1.

four possibilities: the system (i) synchronizes intermittently in time, (ii) exhibits complete synchronization, (iii) does not synchronize, and (iv) diverges. We thus estimate the probability of emergence of one of the four aforementioned dynamical states as the fraction of initial conditions that exhibit the respective state (post transients).

Figure 9.4 illustrates the variation in the probabilities of emergence of the respective dynamical states with changes in β. Note that the sum of these probabilities is always 1, indicative of the fact that the four dynamical states mentioned above, cover the overall state space of the system. Importantly, we observe that the probability of emergence of the intermittently synchronized state is most significant in the range $\beta \in (0.06,\, 0.2)$, which is marked by the two vertical black dashed lines. Given that the state space is shared by the aforementioned four different types of dynamical behaviour, one expects the system's response to be quite sensitive to external perturbations in the range $\beta \in (0.06,\, 0.2)$. Notice that the probability of exhibiting persistent completely synchronized dynamics, first increases monotonically with β and later decreases gradually for higher values of β. Also, note that the maximal values of the above probabilities corresponding to the intermittently synchronized and completely synchronized states do not coincide, but both appear inside the SW regime.

9.4. Conclusion

We have reported the existence of *intermittent synchronization* in Watts-Strogatz networks of chaotic Rössler oscillators. We found the existence of intermittent synchronization for network topologies for which the master stability function framework predicts the existence of a stable synchronized behaviour. Moreover, our primary finding is that intermittent synchronization is most pronounced in the much celebrated *small-world* limit (of the Watts-Strogatz model).

We also found that the complete Lyapunov spectrum contains consistent indicators to detect the presence of an intermittently synchronized regime. Further, we have computed the fraction of state space volume shared by all emergent behaviours, as the network rewiring parameter (β) of the WS model is varied. We have observed that the fraction of state space volume of intermittently synchronized behaviour, interpreted as the probability of its emergence, becomes appreciably large in the small-world regime, which is surprising, since this limit has been otherwise considered optimal for stable synchronized dynamics.

Chapter 10.

Conclusion and Outlook

Stability is crucial to the proper functionality of practical dynamical systems. Such systems often exhibit *multistability*, characterized by the coexistence of several possible final stable states. Also, many such complex systems involve large collections of dynamical units interacting with each other on *complex networks*. Further, real-world complex (networked) dynamical systems exhibiting multistability are prone to *large* perturbations or shocks, which drive the system to an alternative stable state. Thus, maintaining operation of such systems in a particular stable state (which in the case of a complex dynamical network, often concurs with the *synchronization* of its different dynamical components) in the face of random perturbations, is vital to their desired operation. Subsequently, the developments in this dissertation were largely motivated by the pervasiveness of multistability in complex (networked) dynamical systems and the associated need for suitable quantifiers of the respective stability of multiple *attractors* of such systems. Subsequently, a central focus of this dissertation was the investigation of stability of dynamical processes (particularly, synchronization) against random perturbations of complex (networked) dynamical systems. In particular, this endeavour comprised the development of a framework for the assessment of stability and resilience of multistable complex (networked) dynamical systems against large perturbations or shocks.

As expected, *linear stability*-based methods of assessment are too local to investigate the stability of a system against non-infinitesimal perturbations. Subsequently, Menck et al. [9] proposed the measure of *basin stability* (BS), quantified in a non-local and nonlinear fashion using the volume of the basin of attraction of a stable state as an answer to the question of *how stable* an attractor of a dynamical system is, in the face of random perturbations. However, a fundamental assertion in this dissertation was that the non-local stability of the different attractors of a multistable dynamical system is determined by the overall structure (besides the corresponding volume) of their respective basins of attraction. With this as an underpinning, we had set forth on an endeavour comprising the development of a framework for the assessment of stability of (multistable) complex (networked) dynamical systems, particularly in the event of random perturbations.

In Chapter 5, we proposed the framework of *multiple-node basin stability* (MNBS) for gauging the global stability and robustness of networked dynamical

systems in response to non-infinitesimal perturbations simultaneously affecting multiple nodes of the system [P1]. Subsequently, we studied the MNBS of the synchronized state in a deterministic scale-free network of Rössler oscillators and a conceptual model of the United Kingdom power grid with second-order Kuramoto-type nodal dynamics.

In the examples presented in Chapter 5, MNBS was applied to networks of identical oscillators. Thus, a logical extension of this work should constitute its application to probing multistability in networks of non-identical oscillators. Furthermore, MNBS can be applied to assessing the stability of interdependent networks of dynamical systems. Also, the framework of MNBS can be applied to revealing the underlying structure of a complex network by examining the responses of different sets of nodes or oscillators to localized perturbations.

In Chapter 6, we utilized the concept of *ecological resilience* in identifying the crucial aspects characterizing multistability and quantified the same. Subsequently, we proposed the measure of *integral stability* (IS) for holistically inferring stability of multistable dynamical systems [P2]. We demonstrated the potential of IS by using exemplary multistable dynamical systems such as the damped driven pendulum, a model of Amazonian rainforest and the Daisyworld model.

Immediate potential applications of IS constitute its extension to assessing multistability in networked dynamical systems. For example, the development of statistical measures similar to those of *single-node basin stability* (SNBS) and MNBS (Chapter 5) is a feasible direction. We emphasize that the calculation of IS (as well as BS) is computationally expensive. Subsequently, future studies should address the development of efficient computational strategies for calculating IS. In this context, any analytical framework supporting the estimation of IS from the dynamical equations of motion will be highly rewarding as well as may significantly reduce the associated computational costs.

The present architecture of IS is applicable to deterministic stationary dissipative dynamical systems. Although being faced with additional practical challenges, the development of a methodology for estimation of IS from time series data sets seems extremely promising. Corresponding in-depth investigations should be the subject of future studies. In this direction, the approach of Tanaka et al. [169] in identifying the separatrices in state space and the basins of attraction from time series data sets may be useful. Further, we identify the work of Abarbanel et al. [170] as an important cornerstone in calculating the local Lyapunov exponents from observed data sets.

In Chapter 7, we considered the viewpoint of engineering resilience in addressing the aforementioned problem of 'appropriately' quantifying multistability. More specifically, in the context of networked dynamical systems, we proposed the framework of *single-node recovery time* (SNRT) for obtaining an estimate of the relative time scales underlying the transient dynamics of the nodes of a network returning to its desired operational state, following a non-infinitesimal perturbation to the dynamical state of any particular node of the network [P3].

Subsequently, we demonstrated the potential of SNRT in deterministic and random (scale-free and Erdős-Rényi) networks of Rössler oscillators and the model of the power grid of the United Kingdom with second-order Kuramoto-type nodal dynamics.

We have presented the aforementioned framework of SNRT (and associated illustrations) in the special context of networks of identical oscillators with continuous-time dynamics exhibiting bistability on account of coexisting synchronized and desynchronized regimes. However, the framework is generally applicable to any networked (continuous- or discrete-time) dynamical system with non-identical nodes and multiple coexisting states. Thus, future work on SNRT could comprise its extension and application to networks of non-identical nodes and/or exhibiting more complex patterns of multistability. Further development on SNRT could comprise its generalization to a framework of *multiple-node recovery time*, in analogy with the concept of MNBS proposed in the context of basin stability (Chapter 5).

Regarding a potential field of application, we emphasize that time-delays arise frequently in the inherent dynamics of individual oscillators and in their interactions on complex networks [171]. Therefore, another interesting endeavour could constitute incorporating time-delays in networked dynamical systems and investigating their influence on SNRT (and global recovery time (GRT)) of the network. Finally, complex systems comprising oscillators coupled on prototypical network types such as Watts-Strogatz, multilayer, interdependent, etc. are open to applications of SNRT. These ventures could further unravel interesting relationships between SNRT and topological features of the aforementioned networks.

In Chapter 8, we studied the influence of rewiring edges on the synchronizability and topology of networks simultaneously exhibiting *hierarchical* organization and *scale-free* behaviour. Interestingly, this revealed that randomly rewired versions of such networks exhibit significantly enhanced as well as deteriorated synchronizability. Importantly, when a certain critical fraction of edges of the otherwise completely deterministic networks were rewired, it optimized the average synchronizability of the resulting topologies [P4].

The aforementioned results may have potential implications in the design of complex networks (simultaneously exhibiting hierarchical structure and scale-free behaviour) for better synchronizability. A more challenging problem is that of comparing real-world topologies with rewired versions of the deterministic scale-free hierarchical networks explored in Chapter 8, in ascertaining a possible deterministic backbone of certain practical networks and the proportions of randomness in the same. Any efforts in this direction could certainly provide deeper insights into the developmental processes and synchronizability of many practical networked dynamical systems simultaneously displaying hierarchical structure and scale-free behaviour.

In Chapter 9, we investigated the phenomenon of *temporally intermittent*

synchronized and desynchronized dynamics in Watts-Strogatz (WS) networks of chaotic Rössler oscillators. We specifically found that the likelihood of the system to exhibit the intermittently synchronized state becomes appreciably large in the *small-world* regime, which is surprising, since this limit has been otherwise considered optimal for synchronized dynamics [P5].

The above results bear potentially important implications in the design of topologies to ensure persistent synchronized operation of dynamical units coupled on them. Further, we recommend investigating the presence of the intermittently synchronized state when calculating BS-based measures in complex oscillator networks [9, 13, 107, 172, P1, P2, P3]. Also, it would be worthwhile investigating the variations in the distribution of the complete Lyapunov spectrum with changes in the link rewiring probability of the WS model. Finally, inquiries concerning the robustness of this enhanced intermittency in time-varying topologies could yield potentially interesting results.

Appendix

A. SNRT of Random Scale-free Networks of Rössler Oscillators

For illustrative purposes, we have also studied the distribution of SNRT values in an ensemble of 100 random BA scale-free networks, each comprising 243 Rössler oscillators. Subsequently, we have compared these results with those obtained for the ensemble of 81-node 100 random BA scale-free networks considered in Chapter 7 (Sec. 7.4.2). These results are very similar to the corresponding ones provided in Fig. 7.3 (for the ensemble of 81-node random scale-free networks), as shown in Fig. A.1. We clearly observe similar results for two different network sizes, and even for the different coupling strengths considered for the respective cases.

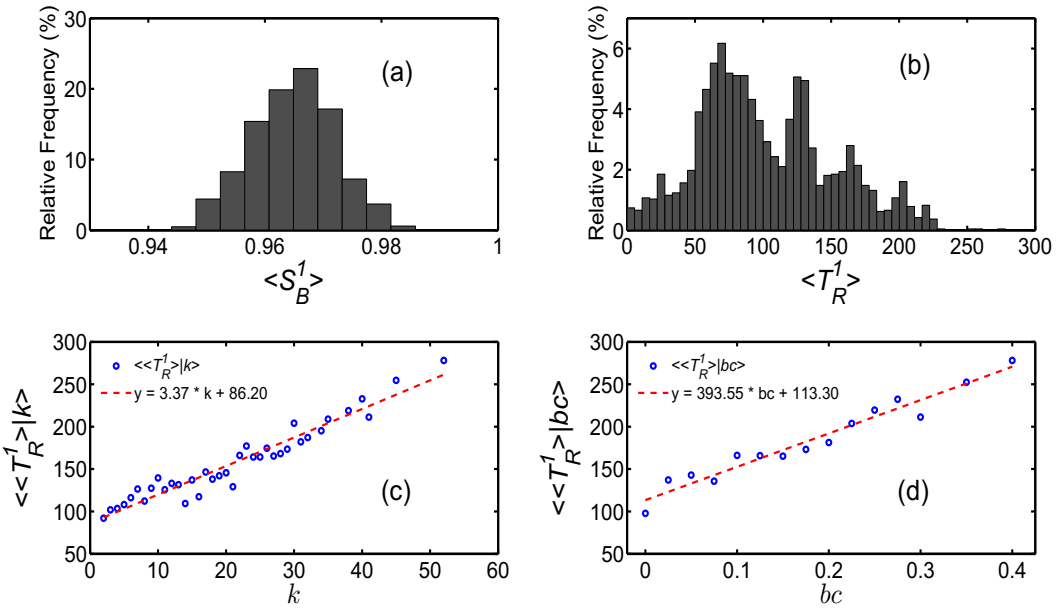

Figure A.1.: As in Fig. 7.3, for an ensemble of 100 random BA scale-free networks, each comprising 243 Rössler oscillators (for $\epsilon = 1.3$).

B. 4-generation DSF and PSF Networks

The original deterministic configurations of DSF and PSF networks studied in Chapter 8 restrict the network sizes to a few integer values (corresponding to the different generations of growth). As a result, this poses a major impediment to the systematic investigation of the variation of our results with respect to the sizes of the respective networks. Further, for a larger number of generations, the number of nodes and edges increase substantially, thus posing additional computational impediments to such an analysis. While the results presented in Chapter 8 (Sec. 8.4) exclusively focussed on rewired versions of 3-generation DSF and PSF networks, we here present additional results obtained for their 4-generation counterparts. In analogy with Fig. 8.2, Fig. B.1 shows the corresponding results regarding the relationship of the expected synchronizability $\langle R \rangle$ with the fraction f of rewired edges for 243-node (422 edges) DSF and 366-node (729 edges) PSF networks. For the 3-generation DSF (PSF) networks considered in Chapter 8, the values of f^* turn out to be 0.046 (0.16), while for the 4-generation networks they come out to be 0.057 (0.148), respectively. Considering these cases, we find that the value of f^* does not vary substantially with changes in the network size.

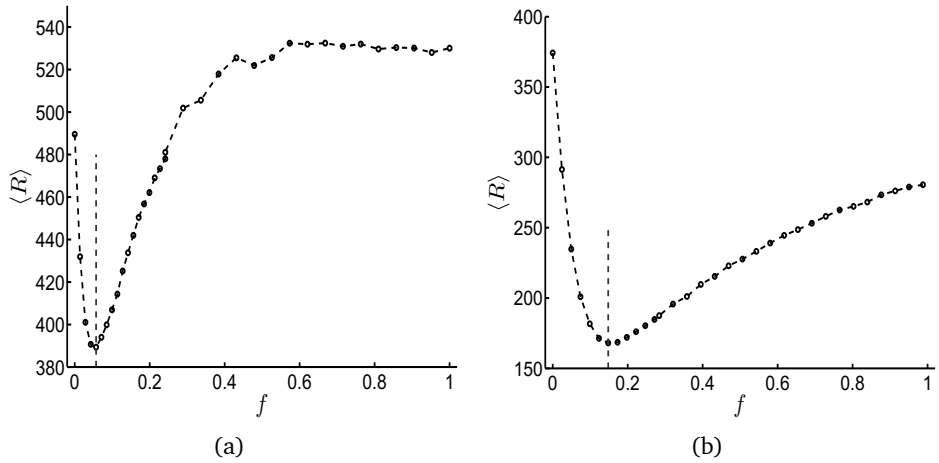

Figure B.1.: As in Fig. 8.2, but for 4-generation (a) DSF and (b) PSF networks.

Bibliography

[1] Guanrong Chen. “Stability of nonlinear systems”. In: *Encyclopedia of RF and Microwave Engineering* (2004).

[2] Simon A Levin, Stephen R Carpenter, H Charles J Godfray, Ann P Kinzig, Michel Loreau, Jonathan B Losos, Brian Walker, and David S Wilcove. *The Princeton Guide to Ecology*. Princeton University Press, New Jersey, 2009.

[3] Jan Machowski, Janusz Bialek, and Jim Bumby. *Power System Dynamics: Stability and Control*. John Wiley & Sons, Wiltshire, 2011.

[4] Ulrike Feudel. “Complex dynamics in multistable systems”. In: *International Journal of Bifurcation and Chaos* 18.06 (2008), pp. 1607–1626.

[5] Alexander N Pisarchik and Ulrike Feudel. “Control of multistability”. In: *Physics Reports* 540.4 (2014), pp. 167–218.

[6] Marina Hirota, Milena Holmgren, Egbert H Van Nes, and Marten Scheffer. “Global resilience of tropical forest and savanna to critical transitions”. In: *Science* 334.6053 (2011), pp. 232–235.

[7] Bert Wuyts, Alan R Champneys, and Joanna I House. “Amazonian forest-savanna bistability and human impact”. In: *Nature Communications* 8.15519 (2017).

[8] Daniel A Wiley, Steven H Strogatz, and Michelle Girvan. “The size of the sync basin”. In: *Chaos* 16.1 (2006), p. 015103.

[9] Peter J Menck, Jobst Heitzig, Norbert Marwan, and Jürgen Kurths. “How basin stability complements the linear-stability paradigm”. In: *Nature Physics* 9.2 (2013), pp. 89–92.

[10] Mark Newman. *Networks: An Introduction*. Oxford University Press, New York, 2010.

[11] Arkady Pikovsky, Michael Rosenblum, and Jürgen Kurths. *Synchronization: A Universal Concept in Nonlinear Sciences*. Vol. 12. Cambridge University Press, Cambridge, 2003.

[12] Louis M Pecora and Thomas L Carroll. “Master stability functions for synchronized coupled systems”. In: *Physical Review Letters* 80.10 (1998), p. 2109.

[13] Peter J Menck, Jobst Heitzig, Jürgen Kurths, and Hans Joachim Schellnhuber. "How dead ends undermine power grid stability". In: *Nature Communications* 5.3969 (2014).

[14] Brian Walker, Crawford S Holling, Stephen R Carpenter, and Ann Kinzig. "Resilience, adaptability and transformability in social–ecological systems". In: *Ecology and Society* 9.2 (2004), p. 5.

[15] Crawford S Holling. "Resilience and stability of ecological systems". In: *Annual Review of Ecology and Systematics* 4 (1973), pp. 1–23.

[16] Crawford Stanley Holling. *Engineering Resilience versus Ecological Resilience*. Engineering Within Ecological Constraints. National Academy Press, Washington DC, 1996.

[17] Duncan J Watts and Steven H Strogatz. "Collective dynamics of 'small-world' networks". In: *Nature* 393.6684 (1998), pp. 440–442.

[18] Albert-László Barabási and Réka Albert. "Emergence of scaling in random networks". In: *Science* 286.5439 (1999), pp. 509–512.

[19] Aaron Clauset, Cristopher Moore, and Mark EJ Newman. "Hierarchical structure and the prediction of missing links in networks". In: *Nature* 453.7191 (2008), pp. 98–101.

[20] Gregory L Baker, James A Blackburn, and HJT Smith. "Intermittent synchronization in a pair of coupled chaotic pendula". In: *Physical Review Letters* 81.3 (1998), p. 554.

[21] Yuri A Kuznetsov. *Elements of Applied Bifurcation Theory*. Vol. 112. Springer Science & Business Media, New York, 2013.

[22] Soumitro Banerjee. *Dynamics for Engineers*. John Wiley & Sons, West Sussex, 2005.

[23] Predrag Cvitanovic, Roberto Artuso, Ronnie Mainieri, Gregor Tanner, Gábor Vattay, Niall Whelan, and Andreas Wirzba. "Chaos: Classical and Quantum". In: *ChaosBook.org* (2005).

[24] Robert C Hilborn. *Chaos and Nonlinear Dynamics: An Introduction for Scientists and Engineers*. Oxford University Press, Oxford, 2000.

[25] Alain Barrat and Martin Weigt. "On the properties of small-world network models". In: *The European Physical Journal B* 13.3 (2000), pp. 547–560.

[26] Mark EJ Newman. "Assortative mixing in networks". In: *Physical Review Letters* 89.20 (2002), p. 208701.

[27] Paul Erdös and Alfréd Rényi. "On random graphs, I". In: *Publicationes Mathematicae (Debrecen)* 6 (1959), pp. 290–297.

[28] Albert-László Barabási, Erzsebet Ravasz, and Tamas Vicsek. "Deterministic scale-free networks". In: *Physica A: Statistical Mechanics and its Applications* 299.3 (2001), pp. 559–564.

[29] Sergey N Dorogovtsev, Alexander V Goltsev, and José Ferreira F Mendes. "Pseudofractal scale-free web". In: *Physical Review E* 65.6 (2002), p. 066122.

[30] Agata Fronczak, Piotr Fronczak, and Janusz A Hołyst. "Average path length in random networks". In: *Physical Review E* 70.5 (2004), p. 056110.

[31] Réka Albert and Albert-László Barabási. "Statistical mechanics of complex networks". In: *Reviews of Modern Physics* 74.1 (2002), p. 47.

[32] Béla Bollobás and Oliver M Riordan. "Mathematical results on scale-free random graphs". In: *Handbook of Graphs and Networks: From the Genome to the Internet* (2003), pp. 1–34.

[33] Kazumoto Iguchi and Hiroaki Yamada. "Exactly solvable scale-free network model". In: *Physical Review E* 71.3 (2005), p. 036144.

[34] Erzsébet Ravasz and Albert-László Barabási. "Hierarchical organization in complex networks". In: *Physical Review E* 67.2 (2003), p. 026112.

[35] Zhongzhi Zhang, Yuan Lin, Shuyang Gao, Shuigeng Zhou, and Jihong Guan. "Average distance in a hierarchical scale-free network: an exact solution". In: *Journal of Statistical Mechanics: Theory and Experiment* 2009.10 (2009), P10022.

[36] Aleksandr Mikhailovich Lyapunov. "The general problem of the stability of motion". In: *International Journal of Control* 55.3 (1992), pp. 531–534.

[37] Steven H Strogatz. *Nonlinear Dynamics And Chaos: With Applications To Physics, Biology, Chemistry, and Engineering*. Westview Press, Massachusetts, 2014.

[38] Fred Attneave. "Multistability in perception." In: *Scientific American* 225.6 (1971), pp. 62–71.

[39] FT Arecchi and F Lisi. "Hopping mechanism generating 1/f noise in nonlinear systems". In: *Physical Review Letters* 49.2 (1982), p. 94.

[40] FT Arecchi, R Meucci, G Puccioni, and J Tredicce. "Experimental evidence of subharmonic bifurcations, multistability, and turbulence in a Q-switched gas laser". In: *Physical Review Letters* 49.17 (1982), p. 1217.

[41] JA Scott Kelso. "Multistability and metastability: understanding dynamic coordination in the brain". In: *Philosophical Transactions of the Royal Society of London B: Biological Sciences* 367.1591 (2012), pp. 906–918.

[42] Robert M May. "Thresholds and breakpoints in ecosystems with a multiplicity of stable states". In: *Nature* 269.5628 (1977), pp. 471–477.

[43] Alexander Robinson, Reinhard Calov, and Andrey Ganopolski. "Multistability and critical thresholds of the Greenland ice sheet". In: *Nature Climate Change* 2.6 (2012), pp. 429–432.

[44] Amitabh Joshi and Min Xiao. “Optical multistability in three-level atoms inside an optical ring cavity”. In: *Physical Review Letters* 91.14 (2003), p. 143904.

[45] Ekkehard Ullner, Aneta Koseska, Jürgen Kurths, Evgenii Volkov, Holger Kantz, and Jordi García-Ojalvo. “Multistability of synthetic genetic networks with repressive cell-to-cell communication”. In: *Physical Review E* 78.3 (2008), p. 031904.

[46] Michael F Crowley and Irving R Epstein. “Experimental and theoretical studies of a coupled chemical oscillator: phase death, multistability and in-phase and out-of-phase entrainment”. In: *The Journal of Physical Chemistry* 93.6 (1989), pp. 2496–2502.

[47] John Milnor. “On the concept of attractor”. In: *Communications in Mathematical Physics* 99.2 (1985), pp. 177–195.

[48] Michael Evans and Timothy Swartz. *Approximating Integrals via Monte Carlo and Deterministic Methods*. Vol. 20. Oxford University Press, Oxford, 2000.

[49] John von Neumann. “Various Techniques Used in Connection With Random Digits”. In: *J. Res. Nat. Bur. Stand.* 12 (1951), pp. 36–38.

[50] Stuart L Pimm. “The complexity and stability of ecosystems”. In: *Nature* 307.5949 (1984), pp. 321–326.

[51] Carl Folke, Steve Carpenter, Brian Walker, Marten Scheffer, Thomas Elmqvist, Lance Gunderson, and Crawford Stanley Holling. “Regime shifts, resilience, and biodiversity in ecosystem management”. In: *Annual Review of Ecology, Evolution, and Systematics* 35 (2004).

[52] Lance H Gunderson. “Ecological resilience–in theory and application”. In: *Annual Review of Ecology and Systematics* 31 (2000), pp. 425–439.

[53] Beatrix E Beisner, Daniel T Haydon, and Kim Cuddington. “Alternative stable states in ecology”. In: *Frontiers in Ecology and the Environment* 1.7 (2003), pp. 376–382.

[54] Thomas Leuteritz and Hamid Ekbia. “Not all roads lead to resilience: a complex systems approach to the comparative analysis of tortoises in arid ecosystems”. In: *Ecology and Society* 13.1 (2008).

[55] Yoshiki Kuramoto. “Self-entrainment of a population of coupled nonlinear oscillators”. In: *International Symposium on Mathematical Problems in Theoretical Physics*. Springer. 1975, pp. 420–422.

[56] Steven H Strogatz and Renato E Mirollo. “Stability of incoherence in a population of coupled oscillators”. In: *Journal of Statistical Physics* 63.3 (1991), pp. 613–635.

[57] Louis M Pecora and Thomas L Carroll. “Synchronization in chaotic systems”. In: *Physical Review Letters* 64.8 (1990), p. 821.

[58] Michael G Rosenblum, Arkady S Pikovsky, and Jürgen Kurths. “Phase synchronization of chaotic oscillators”. In: *Physical Review Letters* 76.11 (1996), p. 1804.

[59] Tomislav Stankovski, Valentina Ticcinelli, Peter VE McClintock, and Aneta Stefanovska. “Neural Cross-Frequency Coupling Functions”. In: *Frontiers in Systems Neuroscience* 11 (2017), p. 33.

[60] Mark EJ Newman. “The structure and function of complex networks”. In: *SIAM Review* 45.2 (2003), pp. 167–256.

[61] Alex Arenas, Albert Díaz-Guilera, Jürgen Kurths, Yamir Moreno, and Changsong Zhou. “Synchronization in complex networks”. In: *Physics Reports* 469.3 (2008), pp. 93–153.

[62] Ankit Agarwal, Norbert Marwan, Maheswaran Rathinasamy, Bruno Merz, and Jürgen Kurths. “Multi-scale event synchronization analysis for unravelling climate processes: a wavelet-based approach”. In: *Nonlinear Processes in Geophysics* 24.4 (2017), p. 599.

[63] Mauricio Barahona and Louis M Pecora. “Synchronization in small-world systems”. In: *Physical Review Letters* 89.5 (2002), p. 054101.

[64] Takashi Nishikawa, Adilson E Motter, Ying-Cheng Lai, and Frank C Hoppensteadt. “Heterogeneity in oscillator networks: Are smaller worlds easier to synchronize?” In: *Physical Review Letters* 91.1 (2003), p. 014101.

[65] Adilson E Motter, CS Zhou, and Jürgen Kurths. “Enhancing complex-network synchronization”. In: *EPL (Europhysics Letters)* 69.3 (2005), p. 334.

[66] José S Andrade Jr, Hans J Herrmann, Roberto FS Andrade, and Luciano R Da Silva. “Apollonian networks: Simultaneously scale-free, small world, Euclidean, space filling, and with matching graphs”. In: *Physical Review Letters* 94.1 (2005), p. 018702.

[67] Adilson E Motter, Changsong Zhou, and Jürgen Kurths. “Network synchronization, diffusion, and the paradox of heterogeneity”. In: *Physical Review E* 71.1 (2005), p. 016116.

[68] Luca Donetti, Pablo I Hurtado, and Miguel A Munoz. “Entangled networks, synchronization, and optimal network topology”. In: *Physical Review Letters* 95.18 (2005), p. 188701.

[69] Stefano Boccaletti, Vito Latora, Yamir Moreno, Martin Chavez, and D-U Hwang. “Complex networks: Structure and dynamics”. In: *Physics Reports* 424.4 (2006), pp. 175–308.

[70] Takashi Nishikawa and Adilson E Motter. “Synchronization is optimal in nondiagonalizable networks”. In: *Physical Review E* 73.6 (2006), p. 065106.

[71] Takashi Nishikawa and Adilson E Motter. “Maximum performance at minimum cost in network synchronization”. In: *Physica D* 224.1 (2006), pp. 77–89.

[72] Chuan-Yang Yin, Wen-Xu Wang, Guanrong Chen, and Bing-Hong Wang. “Decoupling process for better synchronizability on scale-free networks”. In: *Physical Review E* 74.4 (2006), p. 047102.

[73] Zhisheng Duan, Guanrong Chen, and Lin Huang. “Complex network synchronizability: Analysis and control”. In: *Physical Review E* 76.5 (2007), p. 056103.

[74] Adilson E Motter. “Bounding network spectra for network design”. In: *New Journal of Physics* 9.6 (2007), p. 182.

[75] Yuying Gu and Jitao Sun. “Altering synchronizability by adding and deleting edges for scale-free networks”. In: *Physica A* 388.15 (2009), pp. 3261–3267.

[76] Takashi Nishikawa and Adilson E Motter. “Network synchronization landscape reveals compensatory structures, quantization, and the positive effect of negative interactions”. In: *Proceedings of the National Academy of Sciences* 107.23 (2010), pp. 10342–10347.

[77] Ali Ajdari Rad, Mahdi Jalili, and Martin Hasler. “Efficient rewirings for enhancing synchronizability of dynamical networks”. In: *Chaos* 18.3 (2008), p. 037104.

[78] Majid Dadashi, Iman Barjasteh, and Mahdi Jalili. “Rewiring dynamical networks with prescribed degree distribution for enhancing synchronizability”. In: *Chaos* 20.4 (2010), p. 043119.

[79] Mahdi Jalili. “Enhancing synchronizability of diffusively coupled dynamical networks: a survey”. In: *IEEE Transactions on Neural Networks and Learning Systems* 24.7 (2013), pp. 1009–1022.

[80] H Hong, Beom Jun Kim, MY Choi, and Hyunggyu Park. “Factors that predict better synchronizability on complex networks”. In: *Physical Review E* 69.6 (2004), p. 067105.

[81] Steven H Strogatz. “Exploring complex networks”. In: *Nature* 410.6825 (2001), pp. 268–276.

[82] Kunihiko Kaneko. “Clustering, coding, switching, hierarchical ordering, and control in a network of chaotic elements”. In: *Physica D: Nonlinear Phenomena* 41.2 (1990), pp. 137–172.

[83] Mark R Tinsley, Simbarashe Nkomo, and Kenneth Showalter. “Chimera and phase-cluster states in populations of coupled chemical oscillators”. In: *Nature Physics* 8.9 (2012), pp. 662–665.

[84] Iryna Omelchenko, Astero Provata, Johanne Hizanidis, Eckehard Schöll, and Philipp Hövel. “Robustness of chimera states for coupled FitzHugh-Nagumo oscillators”. In: *Physical Review E* 91.2 (2015), p. 022917.

[85] Mercedes Pascual and Jennifer A Dunne. *Ecological Networks: Linking Structure to Dynamics in Food Webs*. Oxford University Press, New York, 2005.

[86] Adilson E Motter and Ying-Cheng Lai. “Cascade-based attacks on complex networks”. In: *Physical Review E* 66.6 (2002), p. 065102.

[87] Premysl Jiruska, Marco De Curtis, and John GR Jefferys. *Modern Concepts of Focal Epileptic Networks*. Vol. 114. Elsevier, Massachusetts, 2014.

[88] Jianxi Gao, Xueming Liu, Daqing Li, and Shlomo Havlin. “Recent Progress on the Resilience of Complex Networks”. In: *Energies* 8.10 (2015), pp. 12187–12210.

[89] Reuven Cohen, Keren Erez, Daniel Ben-Avraham, and Shlomo Havlin. “Resilience of the Internet to random breakdowns”. In: *Physical Review Letters* 85.21 (2000), p. 4626.

[90] Jianxi Gao, Baruch Barzel, and Albert-László Barabási. “Universal resilience patterns in complex networks”. In: *Nature* 530.7590 (2016), pp. 307–312.

[91] Alexander Radebach, Reik V Donner, Jakob Runge, Jonathan F Donges, and Jürgen Kurths. “Disentangling different types of El Niño episodes by evolving climate network analysis”. In: *Physical Review E* 88.5 (2013), p. 052807.

[92] Jonathan F Donges, Jobst Heitzig, Reik V Donner, and Jürgen Kurths. “Analytical framework for recurrence network analysis of time series”. In: *Physical Review E* 85.4 (2012), p. 046105.

[93] Otto E Rössler. “An equation for continuous chaos”. In: *Physics Letters A* 57.5 (1976), pp. 397–398.

[94] Martin Rohden, Andreas Sorge, Marc Timme, and Dirk Witthaut. “Self-organized synchronization in decentralized power grids”. In: *Physical Review Letters* 109.6 (2012), p. 064101.

[95] Dirk Witthaut and Marc Timme. “Braess’s paradox in oscillator networks, desynchronization and power outage”. In: *New Journal of Physics* 14.8 (2012), p. 083036.

[96] Francisco A Rodrigues, Thomas K DM Peron, Peng Ji, and Jürgen Kurths. “The Kuramoto model in complex networks”. In: *Physics Reports* 610 (2016), pp. 1–98.

[97] Debsankha Manik, Dirk Witthaut, Benjamin Schäfer, Moritz Matthiae, Andreas Sorge, Martin Rohden, Eleni Katifori, and Marc Timme. “Supply networks: Instabilities without overload”. In: *The European Physical Journal Special Topics* 223.12 (2014), pp. 2527–2547.

[98] Jie Sun, Erik M Bollt, and Takashi Nishikawa. “Master stability functions for coupled nearly identical dynamical systems”. In: *EPL (Europhysics Letters)* 85.6 (2009), p. 60011.

[99] Vladimir V Klinshov, Vladimir I Nekorkin, and Jürgen Kurths. “Stability threshold approach for complex dynamical systems”. In: *New Journal of Physics* 18.1 (2015), p. 013004.

[100] Henry DI Abarbanel, Reggie Brown, and Matthew B Kennel. “Variation of Lyapunov exponents on a strange attractor”. In: *Journal of Nonlinear Science* 1.2 (1991), pp. 175–199.

[101] Leonel Da Silveira Lobo Sternberg. “Savanna–forest hysteresis in the tropics”. In: *Global Ecology and Biogeography* 10.4 (2001), pp. 369–378.

[102] Andrew J Watson and James E Lovelock. “Biological homeostasis of the global environment: the parable of Daisyworld”. In: *Tellus B* 35.4 (1983), pp. 284–289.

[103] Andrew J Wood, Graeme J Ackland, James G Dyke, Hywel TP Williams, and Timothy M Lenton. “Daisyworld: A review”. In: *Reviews of Geophysics* 46.1 (2008).

[104] RS MacKay and J-A Sepulchre. “Multistability in networks of weakly coupled bistable units”. In: *Physica D: Nonlinear Phenomena* 82.3 (1995), pp. 243–254.

[105] Artur C Fassoni and Hyun M Yang. “An ecological resilience perspective on cancer: insights from a toy model”. In: *Ecological Complexity* 30 (2017), pp. 34–46.

[106] Sergey N Dorogovtsev and Jose FF Mendes. “Evolution of networks”. In: *Advances in Physics* 51.4 (2002), pp. 1079–1187.

[107] Frank Hellmann, Paul Schultz, Carsten Grabow, Jobst Heitzig, and Jürgen Kurths. “Survivability of Deterministic Dynamical Systems”. In: *Scientific Reports* 6.29654 (2016).

[108] Alexander Zumdieck, Marc Timme, Theo Geisel, and Fred Wolf. “Long chaotic transients in complex networks”. In: *Physical Review Letters* 93.24 (2004), p. 244103.

[109] Marc Timme, Fred Wolf, and Theo Geisel. “Topological speed limits to network synchronization”. In: *Physical Review Letters* 92.7 (2004), p. 074101.

[110] Marc Timme, Theo Geisel, and Fred Wolf. “Speed of synchronization in complex networks of neural oscillators: analytic results based on random matrix theory”. In: *Chaos* 16.1 (2006), p. 015108.

[111] GX Qi, HB Huang, L Chen, HJ Wang, and CK Shen. “Fast synchronization in neuronal networks”. In: *EPL (Europhysics Letters)* 82.3 (2008), p. 38003.

[112] GX Qi, HB Huang, CK Shen, HJ Wang, and L Chen. “Predicting the synchronization time in coupled-map networks”. In: *Physical Review E* 77.5 (2008), p. 056205.

[113] Seung-Woo Son, Hawoong Jeong, and Hyunsuk Hong. “Relaxation of synchronization on complex networks”. In: *Physical Review E* 78.1 (2008), p. 016106.

[114] Rüdiger Zillmer, Nicolas Brunel, and David Hansel. “Very long transients, irregular firing, and chaotic dynamics in networks of randomly connected inhibitory integrate-and-fire neurons”. In: *Physical Review E* 79.3 (2009), p. 031909.

[115] Adrián E Granada and Hanspeter Herzel. “How to achieve fast entrainment? The timescale to synchronization”. In: *PLoS One* 4.9 (2009), e7057.

[116] Carsten Grabow, Steven M Hill, Stefan Grosskinsky, and Marc Timme. “Do small worlds synchronize fastest?” In: *EPL (Europhysics Letters)* 90.4 (2010), p. 48002.

[117] Carsten Grabow, Stefan Grosskinsky, and Marc Timme. “Speed of complex network synchronization”. In: *The European Physical Journal B* 84.4 (2011), pp. 613–626.

[118] Sheng-Jun Wang, Ru-Hai Du, Tao Jin, Xing-Sen Wu, and Shi-Xian Qu. “Synchronous slowing down in coupled logistic maps via random network topology”. In: *Scientific Reports* 6.23448 (2016).

[119] Tim Kittel, Jobst Heitzig, Kevin Webster, and Juergen Kurths. “Timing of transients: quantifying reaching times and transient behavior in complex systems”. In: *New Journal of Physics* 19.8 (2017).

[120] Pascal Fries. “A mechanism for cognitive dynamics: neuronal communication through neuronal coherence”. In: *Trends in Cognitive Sciences* 9.10 (2005), pp. 474–480.

[121] Juergen Fell and Nikolai Axmacher. “The role of phase synchronization in memory processes”. In: *Nature Reviews Neuroscience* 12.2 (2011), pp. 105–118.

[122] Lance H Gunderson, Craig Reece Allen, and Crawford S Holling. *Foundations of Ecological Resilience*. Island Press, Washington, 2012.

[123] Liang Huang, Qingfei Chen, Ying-Cheng Lai, and Louis M Pecora. “Generic behavior of master-stability functions in coupled nonlinear dynamical systems”. In: *Physical Review E* 80.3 (2009), p. 036204.

[124] Petter Holme, Beom Jun Kim, Chang No Yoon, and Seung Kee Han. “Attack vulnerability of complex networks”. In: *Physical Review E* 65.5 (2002), p. 056109.

[125] Luis F Lago-Fernández, Ramón Huerta, Fernando Corbacho, and Juan A Sigüenza. “Fast response and temporal coherent oscillations in small-world networks”. In: *Physical Review Letters* 84.12 (2000), p. 2758.

[126] Prashant M Gade and Chin-Kun Hu. “Synchronous chaos in coupled map lattices with small-world interactions”. In: *Physical Review E* 62.5 (2000), p. 6409.

[127] Hyunsuk Hong, Moo-Young Choi, and Beom Jun Kim. “Synchronization on small-world networks”. In: *Physical Review E* 65.2 (2002), p. 026139.

[128] Xiao Fan Wang and Guanrong Chen. “Synchronization in small-world dynamical networks”. In: *International Journal of Bifurcation and Chaos* 12.01 (2002), pp. 187–192.

[129] Erzsébet Ravasz, Anna Lisa Somera, Dale A Mongru, Zoltán N Oltvai, and A-L Barabási. “Hierarchical organization of modularity in metabolic networks”. In: *Science* 297.5586 (2002), pp. 1551–1555.

[130] Michalis Faloutsos, Petros Faloutsos, and Christos Faloutsos. “On power-law relationships of the internet topology”. In: *ACM SIGCOMM Computer Communication Review*. Vol. 29. 4. ACM. 1999, pp. 251–262.

[131] Hawoong Jeong, Bálint Tombor, Réka Albert, Zoltan N Oltvai, and A-L Barabási. “The large-scale organization of metabolic networks”. In: *Nature* 407.6804 (2000), pp. 651–654.

[132] Hawoong Jeong, Sean P Mason, A-L Barabási, and Zoltan N Oltvai. “Lethality and centrality in protein networks”. In: *Nature* 411.6833 (2001), pp. 41–42.

[133] Réka Albert and Albert-László Barabási. “Topology of evolving networks: local events and universality”. In: *Physical Review Letters* 85.24 (2000), p. 5234.

[134] Fredrik Liljeros, Christofer R Edling, Luis A Nunes Amaral, H Eugene Stanley, and Yvonne Åberg. “The web of human sexual contacts”. In: *Nature* 411.6840 (2001), pp. 907–908.

[135] Huawei Shen, Xueqi Cheng, Kai Cai, and Mao-Bin Hu. “Detect overlapping and hierarchical community structure in networks”. In: *Physica A* 388.8 (2009), pp. 1706–1712.

[136] Haiyuan Yu and Mark Gerstein. “Genomic analysis of the hierarchical structure of regulatory networks”. In: *Proceedings of the National Academy of Sciences* 103.40 (2006), pp. 14724–14731.

[137] Jürgen Jost and Maliackal Poulo Joy. “Spectral properties and synchronization in coupled map lattices”. In: *Physical Review E* 65.1 (2001), p. 016201.

[138] Xiao Fan Wang and Guanrong Chen. “Synchronization in scale-free dynamical networks: robustness and fragility”. In: *IEEE Transactions on Circuits and Systems I: Fundamental Theory and Applications* 49.1 (2002), pp. 54–62.

[139] Xiao Fan Wang. “Complex networks: topology, dynamics and synchronization”. In: *International Journal of Bifurcation and Chaos* 12.05 (2002), pp. 885–916.

[140] Pedro G Lind, Jason AC Gallas, and Hans J Herrmann. “Coherence in scale-free networks of chaotic maps”. In: *Physical Review E* 70.5 (2004), p. 056207.

[141] Alex Arenas, Albert Díaz-Guilera, and Conrad J Pérez-Vicente. “Synchronization reveals topological scales in complex networks”. In: *Physical Review Letters* 96.11 (2006), p. 114102.

[142] A Díaz-Guilera. “Dynamics towards synchronization in hierarchical networks”. In: *Journal of Physics A* 41.22 (2008), p. 224007.

[143] Per Sebastian Skardal and Juan G Restrepo. “Hierarchical synchrony of phase oscillators in modular networks”. In: *Physical Review E* 85.1 (2012), p. 016208.

[144] Paul Schultz, Thomas Peron, Deniz Eroglu, Thomas Stemler, Gonzalo Marcelo Ramírez Ávila, Francisco A Rodrigues, and Jürgen Kurths. “Tweaking synchronization by connectivity modifications”. In: *Physical Review E* 93.6 (2016), p. 062211.

[145] Sanjiv K Dwivedi, Camellia Sarkar, and Sarika Jalan. “Optimization of synchronizability in multiplex networks”. In: *EPL (Europhysics Letters)* 111.1 (2015), p. 10005.

[146] Mario di Bernardo, Franco Garofalo, and Francesco Sorrentino. “Effects of degree correlation on the synchronization of networks of oscillators”. In: *International Journal of Bifurcation and Chaos* 17.10 (2007), pp. 3499–3506.

[147] Sarika Jalan, Anil Kumar, Alexey Zaikin, and Jürgen Kurths. “Interplay of degree correlations and cluster synchronization”. In: *Physical Review E* 94.6 (2016), p. 062202.

[148] Bernd Blasius, Amit Huppert, and Lewi Stone. “Complex dynamics and phase synchronization in spatially extended ecological systems”. In: *Nature* 399.6734 (1999), p. 354.

[149] Eric Post and Mads C Forchhammer. “Synchronization of animal population dynamics by large-scale climate”. In: *Nature* 420.6912 (2002), p. 168.

[150] Anshul Choudhary and Sudeshna Sinha. “Balance of interactions determines optimal survival in multi-species communities”. In: *PloS one* 10.12 (2015), e0145278.

[151] David JD Earn, Pejman Rohani, and Bryan T Grenfell. “Persistence, chaos and synchrony in ecology and epidemiology”. In: *Proceedings of the Royal Society of London B: Biological Sciences* 265.1390 (1998), pp. 7–10.

[152] Claudio Juan Tessone, Massimo Cencini, and Alessandro Torcini. “Synchronization of extended chaotic systems with long-range interactions: an analogy to Levy-flight spreading of epidemics”. In: *Physical Review Letters* 97.22 (2006), p. 224101.

[153] David P Rosin, Damien Rontani, Daniel J Gauthier, and Eckehard Schöll. “Control of synchronization patterns in neural-like Boolean networks”. In: *Physical Review Letters* 110.10 (2013), p. 104102.

[154] Rachel Mislovaty, Einat Klein, Ido Kanter, and Wolfgang Kinzel. “Public channel cryptography by synchronization of neural networks and chaotic maps”. In: *Physical Review Letters* 91.11 (2003), p. 118701.

[155] Valentin P Zhigulin, Mikhail I Rabinovich, Ramon Huerta, and Henry DI Abarbanel. “Robustness and enhancement of neural synchronization by activity-dependent coupling”. In: *Physical Review E* 67.2 (2003), p. 021901.

[156] Chai Wah Wu and Leon O Chua. “A simple way to synchronize chaotic systems with applications to secure communication systems”. In: *International Journal of Bifurcation and Chaos* 3.06 (1993), pp. 1619–1627.

[157] Florian Dörfler, Michael Chertkov, and Francesco Bullo. “Synchronization in complex oscillator networks and smart grids”. In: *Proceedings of the National Academy of Sciences* 110.6 (2013), pp. 2005–2010.

[158] Adilson E Motter, Seth A Myers, Marian Anghel, and Takashi Nishikawa. “Spontaneous synchrony in power-grid networks”. In: *Nature Physics* 9.3 (2013), pp. 191–197.

[159] Sunghwan Rim, Myung-Woon Kim, Dong-Uk Hwang, Young-Jai Park, and Chil-Min Kim. “Reconsideration of intermittent synchronization in coupled chaotic pendula”. In: *Physical Review E* 64.6 (2001), p. 060101.

[160] Daniel J Gauthier and Joshua C Bienfang. “Intermittent loss of synchronization in coupled chaotic oscillators: Toward a new criterion for high-quality synchronization”. In: *Physical Review Letters* 77.9 (1996), p. 1751.

[161] James A Blackburn, Gregory L Baker, and HJT Smith. “Intermittent synchronization of resistively coupled chaotic Josephson junctions”. In: *Physical Review B* 62.9 (2000), p. 5931.

[162] IM Kyprianidis, Ch K Volos, SG Stavrinides, IN Stouboulos, and AN Anagnostopoulos. “On–off intermittent synchronization between two bidirectionally coupled double scroll circuits”. In: *Communications in Nonlinear Science and Numerical Simulation* 15.8 (2010), pp. 2192–2200.

[163] Young Hun Yu, Keumcheol Kwak, and Tong Kun Lim. “On-off intermittency in an experimental synchronization process”. In: *Physics Letters A* 198.1 (1995), pp. 34–38.

[164] Kenji Shinoda and Kunihiko Kaneko. “Chaotic Griffiths Phase with Anomalous Lyapunov Spectra in Coupled Map Networks”. In: *Physical Review Letters* 117.25 (2016), p. 254101.

[165] H Chaté. “Lyapunov analysis of spatiotemporal intermittency”. In: *EPL (Europhysics Letters)* 21.4 (1993), p. 419.

[166] Kunihiko Kaneko. “Spatiotemporal intermittency in coupled map lattices”. In: *Progress of Theoretical Physics* 74.5 (1985), pp. 1033–1044.

[167] G Ananthakrishna and MS Bharathi. “Dynamical approach to the spatiotemporal aspects of the Portevin–Le Chatelier effect: chaos, turbulence, and band propagation”. In: *Physical Review E* 70.2 (2004), p. 026111.

[168] Ayşe Erzan and Sudeshna Sinha. “Spatiotemporal intermittency on the sandpile”. In: *Physical Review Letters* 66.21 (1991), p. 2750.

[169] Martin L Tanaka and Shane D Ross. “Separatrices and basins of stability from time series data: an application to biodynamics”. In: *Nonlinear Dynamics* 58.1 (2009), pp. 1–21.

[170] Henry DI Abarbanel, Reggie Brown, and Matthew B Kennel. “Local Lyapunov exponents computed from observed data”. In: *Journal of Nonlinear Science* 2.3 (1992), pp. 343–365.

[171] Muthusamy Lakshmanan and Dharmapuri Vijayan Senthilkumar. *Dynamics of Nonlinear Time-Delay Systems*. Springer Science & Business Media, Berlin Heidelberg, 2011.

[172] Paul Schultz, Peter J Menck, Jobst Heitzig, and Jürgen Kurths. “Potentials and limits to basin stability estimation”. In: *New Journal of Physics* 19.2 (2017), p. 023005.

Selbständigkeitserklärung

Ich erkläre, dass ich die Dissertation selbständig und nur unter Verwendung der von mir gemäß § 7 Abs. 3 der Promotionsordnung der Mathematisch-Naturwissenschaftlichen Fakultät, veröffentlicht im Amtlichen Mitteilungsblatt der Humboldt-Universität zu Berlin Nr. 126/2014 am 18.11.2014 angegebenen Hilfsmittel angefertigt habe.

Berlin, den 16. März 2018 Chiranjit Mitra